MICROPHASE AND MACROPHASE SEPARATION IN BINARY AND TERNARY BLOCK COPOLYMER BLENDS

MICHAL BANASZAK

ISBN 0-315-73367-5

MICROPHASE AND MACROPHASE SEPARATION IN BINARY AND TERNARY BLOCK COPOLYMER BLENDS

By

©Michał Banaszak

M. Sc., A. Mickiewicz University, Poznań, Poland

A THESIS SUBMITTED TO THE SCHOOL OF GRADUATE STUDIES IN PARTIAL FULFILLMENT OF THE REQUIREMENTS FOR THE DEGREE OF DOCTOR OF PHILOSOPHY

DEPARTMENT OF PHYSICS

MEMORIAL UNIVERSITY OF NEWFOUNDLAND

DECEMBER 1991

ST. JOHN'S NEWFOUNDLAND

Abstract

In this thesis we investigate some properties of microphase separated copolymer blends by means of the theory of polymer mixtures developed by K.M. Hong and J. Noolandi, carrying out numerical self-consistent calculations for copolymer solvent blends and modifying a fourth order expansion of the free energy for copolymer/homopolymer blends. In all cases we restrict attention to the lamellar structure.

Using the numerical self-consistent calculations we carry out systematic studies for copolymer/selective solvent blends in both the weak and strong segregation regimes. Comparison with earlier results of Whitmore and Noolandi for copolymer/neutral solvent blends is provided.

We also study the lamellar structure of binary *A-b-B/A* and ternary *A-b-B/A/B* copolymer/homopolymer blends near the microphase separation transition. The approach we have developed in this case combines perturbative solutions to the modified diffusion equation with a model for the total A and B polymer density profiles. As test of this procedure we have compared numerical self-consistent calculations for binary copolymer/selective solvent blends with the modification of fourth order expansion introduced in this thesis. We have used the procedure to calculate the domain and subdomain thicknesses, the interfacial width, swelling of the copolymers by the homopolymers, and individual polymer density profiles, and their dependence on the copolymer and homopolymer degrees of polymerization, overall composition, and Flory interaction parameter. The results are compared with three sets of experiments on copolymer/homopolymer blends. They are consistent with the picture that added homopolymers tend to penetrate within the copolymers and swell them laterally, and that the degree to which this

occurs depends on the relative molecular weights of the copolymers and homopolymers, as indicated in experiments of Hashimoto and coworkers and others. The tendency of added homopolymers to cause an increase or decrease in the domain thickness correlates with their tendency to stabilize or destabilize the microphase.

Finally we construct phase diagrams of ternary, *A-b-B/A/B*, copolymer/homopolymer blends. This work is an extension of earlier research by Whitmore and Noolandi for binary and ternary blends. The approach, again, uses a perturbative solution to the modified diffusion equation to calculate the polymer distribution functions, but it employs only one wavenumber in the fourth order expansion of the free energy, significantly simplifying the numerical calculations. The main results of these calculations are phase diagrams for a variety of model systems containing symmetric and asymmetric copolymers mixed with homopolymers of varying molecular weights, and for a *PS-b-PI/PS/PI* mixture. We also compare induced microphase formation in ternary and binary blends.

Table of Contents

List of Tables

List of Figures

Acknowledgements

It is a great pleasure to thank all those who contributed to this dissertation. I wish to thank my thesis supervisor, Dr. Mark Whitmore, for his knowledgeable and skillful direction of my research, constant encouragement, preparation of an interesting research programme, and extremely helpful assistance in completing this thesis. I also thank him for all the big and the small favours which added up to creation of a mutual understanding going beyond formal duties.

I am indebted to Dr. John Whitehead for sharing many new and challenging scientific ideas during the course of my graduate studies, for his remarkable service as Graduate Officer in the Department of Physics, and for guidance as a member of my Supervisory Committee. I also wish to thank Dr. M.R. Morrow for his participation in the same Committee.

I thank Dr. Michael Coombes for many enlightening discussions, sharing his knowledge and expertise in polymer physics, and also for many informal discussions which helped me to understand the Canadian and Newfoundland culture.

Mr. Jeff Vavasour, working in Dr. Whitmore's research group, helped me immensely by his great abilities in dealing with numerical problems and his willingness to share his "know-how". Thanks, Jeff.

I thank Drs. J. Noolandi, K.M. Hong and L. Marks for the initial version of the self-consistent programme.

I gratefully acknowledge the financial assistance provided by the School of Graduate Studies and Department of Physics in the form of graduate fellowships.

I extend sincere thanks to my family and friends for their interest, support, and

encouragement.

I thank Dr. Bogdan Mróz, Dr. André Roberge, Dr. Maciek Skierski, Mr. Bojiong Yuan, and Dr. Jurek Żuk for sharing their knowledge and helping in many ways during my stay in St. John's.

Dziekuję wszystkim, którzy przyczynili się do powstania tej pracy: przyjaciołom, znajomym oraz swoim nauczycielom w Polsce, w szczególności Panu Profesorowi Tadeuszowi Lulkowi oraz Profesorowi Rufinowi Makarewiczowi.

Serdecznie dziękuję swoim Rodzicom oraz Rodzeństwu, Tomkowi, Agnieszce i Mikołajowi, za ciągłe wsparcie, troskę, modlitwę, pamięć i życzliwość.

Dorocie dziekuję za wszystkie dni, które wspólnie przeżyliśmy na Nowej Funlandii i za wszystkie następne, które mamy zamiar ze sobą spędzić w Polsce oraz w innych miejscach na kuli ziemskiej.

Chapter 1

Introduction

1.1 Motivation of Work

The search for new polymeric materials is one of the most fascinating undertakings in contemporary science. Instead of developing entirely new polymeric materials, the polymer scientists and technologists usually mix different polymers to form a polymer blend or, alternatively, chemically bond two (or more) kinds of polymer chains which are, otherwise, immiscible [1]. In fact, most of the commercially applicable polymeric materials are polymer blends. Physical properties of those blends are, therefore, of great importance. Knowledge of phase behaviour and structure, in particular, can be beneficial in producing the new materials. One may argue that development of physical theories capable of meaningful predictions of polymer blend properties is necessary in order to efficiently explore different possibilities. We hope that the following dissertation contributes to this development.

Polymers are molecules consisting of large numbers ($\sim 10^2 - 10^5$) of identical units called *monomers*. These molecules can be described by chemical formulas which give the patterns of chemical bonds and atoms. The polymer molecules can be looked on as chains which, in general, exhibit a rich architecture. The simplest architecture is, of course, a linear one but also others can exist, e.g. grafted polymers and star polymers as discussed in references [2, 3, 4]. Our interest, however, will be limited to linear polymers. A linear polymer of type p can be characterized by the number of monomer units, Z_p,

referred to as the degree of polymerization. Throughout the thesis we neglect the effects of polydispersity, i.e., we assume that all the chains of one species have exactly the same degree of polymerization.

Further complexity can arise from the fact that polymer chains can be composed of two (or more) kinds of monomers. Copolymers are molecules consisting of two, or more [5], species of monomers. We limit, again, ourselves to linear copolymers, i.e., excluding grafted copolymers and star copolymers [2]. Linear copolymers can be further classified as either random, alternating or block copolymers. We, furthermore, concentrate on block copolymers with two kinds of monomers and only two distinct blocks, e.g. polystyrene and polybutadiene, which are referred to as *diblock copolymers*. The total number of monomers of a diblock copolymer of type c, denoted by Z_c is, once again, called the degree of polymerization. The number of monomers of type A forming one block is denoted by Z_{cA} and the number of monomers of type B forming the other block is denoted by Z_{cB}.

Equilibrium properties of diblock copolymers, homopolymers and copolymer/homopolymer blends are very interesting. Even if we restrict ourselves to linear chains composed of two different types of monomeric units, there is a multitude of possible phases. A sample of diblock copolymers can exist in either an ordered or disordered phase. The order-disorder transition is called the *microphase separation transition, MST*. The ordered phase is referred to as a *microphase* and can occur as a 3-dimensional array of spheres or an ordered bicontinuous "double diamond" structure, a 2-dimensional array of cylinders or a 1-dimensional lamellar structure [6, 7, 8]. The equilibrium morphology of the microphase depends mainly on relative volume fraction of the two components f_A and $f_B = 1 - f_A$. If those fractions are approximately equal then an alternating array of lamellae is the equilibrium structure. In fact experimental studies show that lamellar morphology appears for $0.35 \lesssim f_A \lesssim 0.65$, cylindrical structure is formed for $0.20 \lesssim f_A \lesssim 0.35$

and for $0.65 \lesssim f_A \lesssim 0.80$, spherical structure is stable below 20 % and above 80 %, whereas the recently found ordered bicontinuous "double diamond" structure is stable in a narrow range of composition, between cylindrical and lamellar morphologies [6, 7]. We concentrate exclusively on lamellar structures in this thesis. The layer thickness is of the order of the radius of gyration of the copolymer coil, i.e., about 10^1–10^2 nm.

Microphase separation occurs because of the repulsive net interactions between monomers of different species. The interactions are generally modelled by a contact repulsion via the Flory interaction parameter χ between A and B monomers. This parameter was first introduced by Flory [9] and can be defined as the energy of formation of a A-B contact multiplied by the lattice coordination number, i.e., the number of nearest neighbours. It depends, in general, on composition, degrees of polymerization and temperature [10] as described in sections 2.4 and 4.4. For simplicity, we assume that it depends on temperature only, but we do not specify the functional form of this dependence. It might, however, be worth mentioning here that usually the χ parameter is found to have an inverse temperature dependence [10]:

$$\chi(T) = A + \frac{B}{T}, \tag{1.1}$$

where A and B are constants, and $B > 0$ so that a decrease in the temperature, T, causes an increase in χ. In general, increasing χ for a system with given molecular weights and concentrations strengthens the tendency to phase separate.

For a symmetric diblock copolymer ($Z_{cA} = Z_{cB} = \frac{1}{2}Z_c$) with equal monomer volumes and Kuhn lengths (effective step lengths per monomer), Leibler [11] showed, in RPA (mean field) approximation, that microphase separation occurs if

$$\chi Z_c \geq 10.5. \tag{1.2}$$

If χZ_c is only slightly greater than 10.5 then the interface between microdomains is diffuse and the amplitude of the density variation of each component is very small. We refer to

this situation as the ***weak segregation limit.*** If, on the other hand, the product χZ_c is much greater than 10.5, the interfaces between microdomains are very narrow and the density variations are the maximum possible. This is the ***strong segregation limit.*** Besides the weak and strong segregation limits, we often use the more general concepts of the weak and strong segregation regimes. The weak segregation regime refers not only to the weak segregation limit but also to systems with less diffuse interfaces, not necessarily very close to the MST. Similarly, the strong segregation regime refers to strongly segregated systems, i.e., with a narrow interface but not necessarily in the strong segregation limit.

Mixtures of copolymers and homopolymers (or solvent) can exhibit this rich variety of morphologies as well as additional phase behaviour. A ternary blend consisting of diblock copolymers, *A-b-B*, homopolymers hH and homopolymers hD is denoted by *A-b-B/H/D*. In this dissertation we will consider binary *A-b-B/A* and ternary *A-b-B/A/B* blends in which the homopolymer(s) are the same chemical species as a corresponding block of the copolymer. This blend consists of blocks which we denote cA and cB, and homopolymers which we denote hA and hB. The effective repulsion between A and B monomers leads to the segregation phenomena. A mixture of two homopolymers hA and hB separates into A-rich and B-rich phases if the interaction parameter χ is big enough. This phenomenon is called ***macrophase separation.*** In particular, for a mixture of two homopolymers with equal monomer volumes, volume fractions, Kuhn lengths and degrees of polymerization, $Z_{hA} = Z_{hB} = Z_h$, macrophase separation occurs if [12]

$$\chi Z_h \geq 2. \tag{1.3}$$

In copolymer/homopolymer blends both macrophase separation and microphase separation occur. Each of the macrophases can be ordered or disordered. For a pure copolymer *A-b-B*, on the other hand, macrophase separation is not possible because of the chemical joints connecting block A and block B.

Prediction of phase behaviour and structure of copolymer/homopolymer blends, with the goal of meeting specific requirements, is our objective of this work. In this thesis we attempt to show how some physical characteristics, e.g. domain and subdomain thicknesses, of those blends can, indeed, be influenced by varying compositions, degrees of polymerization and the temperature.

Additional motivation for this work is provided by the existence of a number of experimental studies of these blends, e.g. Hashimoto et al. [13, 14, 15], Winey [16, 17], Quan et al. [18], and Owens et al. [19, 20, 21], so that our theoretical results can be related to the experimental data. This is done especially in our systematic studies of the lamellar structure of copolymer/homopolymer blends, chapter 4 of this thesis. We have also been motivated by experimental work of Russel et al. [23, 24] who studied interfacial properties of copolymers, and also by Han et al. [25, 26]. In undertaking this research, we have been encouraged by the success of earlier theories in providing a description of the behaviour of copolymer blends, e.g. Hong and Noolandi [27, 28], Whitmore and Noolandi [29, 30, 31] and Vilgis and Noolandi [32]. In particular, Noolandi and Hong [33] show that increasing the solvent concentration in copolymer/nonselective solvent blends causes the domain thickness to decrease. This theoretical result is in agreement with experimental work of Shibayama et al. [34]. Whitmore and Noolandi also show that the nonselective solvent is distributed almost uniformly throughout the macrophase separated blend. This uniformity is the basis of the dilution approximation as elucidated in section 3.1. The next success of the theory is the prediction that high molecular weight homopolymers induce microphase separation for binary copolymer/homopolymer blends. This effect has been observed experimentally as well, e.g. by Owens et al. [21]. The references [27, 29] provide a method of a unified treatment of both microphase and macrophase separation, and construction of phase diagrams of binary copolymer/homopolymer blends, which exhibit the same topology as the ones described in experimental work of Zin and Roe [35, 36].

Whitmore and Noolandi have also predicted a faster than Gaussian, and faster than in the strong segregation regime, scaling of the layer thickness, as a function of copolymer degree of polymerization, near the MST. This, again, agrees with experimental work of Almdal et al. [37], as discussed in subsection 3.2.1. It is known that block copolymers can act as surfactants, reducing the interfacial tension of two incompatible homopolymers at their interfaces [38, 39]. Theoretical calculations of interfacial tension as a function of copolymer and homopolymer degrees of polymerization, performed by Noolandi and Hong [28] for *PS-b-PDB/PS/PBD* blend, yield qualitative agreement with experimental work of Gaillard et al. [39]. Subsequent work of Vilgis and Noolandi [32], aiming at the search of universal compatibilizer, extends the preceding theory to a more general case of *X-b-Y/A/B* blend with a solvent.

Our work on ternary phase diagrams is a natural extension of an earlier paper by Whitmore and Noolandi [29] on binary phase diagrams, while our copolymer/selective solvent model calculations originated directly from their copolymer/nonselective solvent paper [30].

1.2 Projects

This dissertation consists of three related projects aiming at accounting for the detailed lamellar structure and phase behaviour of both binary *A-b-B/A* and ternary *A-b-B/A/B* systems. In the remainder of this section, those projects are briefly outlined. Detailed descriptions of the individual projects are included in appropriate chapters, as described in section 1.4. Throughout this thesis we differentiate between *model* and *real system* calculations. The former are performed for ideal systems with the same Kuhn lengths, equal densities and convenient χ parameters for all components, while the latter are based on realistic values of those quantities.

1.2.1 Lamellar Structure of Copolymer/Selective Solvent Blends

The first project deals with the investigation of copolymer/selective solvent blends and applies the theory of Hong and Noolandi [30, 33, 52] which involves the self-consistent solution of a system of integro-differential equations. Power laws are extracted and density profiles are calculated. Comparison with copolymer/nonselective solvent blends of reference [30], and systematic studies are provided.

1.2.2 Lamellar Structure of Copolymer/Homopolymer Blends

An analogous self-consistent approach for copolymer/homopolymer blends has not been developed yet. We have decided, however, to treat copolymer/homopolymer blends by using and modifying a fourth order expansion and minimization of the free energy, rather than to develop the self-consistent approach, because the former is more efficient numerically and, in our opinion, gives, in many cases, better physical insight.

The second and the third projects are based on our extension of the Hong and Noolandi formalism and contain most of the results of this thesis. These two projects

are based on using the perturbative solution of the diffusion equation, the resulting fourth order expansion of the free energy, inclusion of incompressibility following Ohta and Kawasaki [40] and minimization of the free energy. This expansion is presented in section 2.3.

In this, the second project, the lamellar structure of binary and ternary copolymer/homopolymer blends is explored. The free energy, Δf, is evaluated by including summation over many wavevectors in the fourth order expansion. Furthermore, systematic studies on model systems are carried out and extensive comparison with experimental data of Hashimoto et al. [13, 14, 15], Winey [16], and Quan et al. [18], is provided. This approach is tested by performing numerical self-consistent model calculation as set forth in the first project.

1.2.3 Phase Behaviour of Ternary Copolymer/Homopolymer Blends

In the third project we calculate phase diagrams for ternary *A-b-B/A/B* blends using the fourth order approximation developed in this dissertation. For simplicity we, again, assume the lamellar structure, throughout, and calculate the free energy up to the fourth order using only one wavenumber in the expansion. This is probably the simplest way to calculate the free energy over the full range of compositions which accounts for both macrophase and microphase separation. Also in this project, we investigate the phenomenon of induced microphase separation for *ternary* copolymer/homopolymer blends.

1.3 Short Review of Relevant Theories

For homopolymer/solvent and homopolymer/homopolymer systems, the lattice model was developed by Flory and Huggins, summarized in reference [9], and referred to as the Flory-Huggins theory. In this theory, the entropy of mixing, ΔS_M, was evaluated by generalization of the lattice model calculations for ideal binary fluids. Furthermore, the heat of mixing, ΔH_M was postulated in a simple form as being proportional to the product of concentrations of the two components. The free energy of mixing is further calculated, in a standard way, as $\Delta F_M = \Delta H_M - T\Delta S_M$. This relatively simple model proved to be a useful tool in dealing with the polymer blends [1, 9], e.g. for constructing phase diagrams of binary and ternary polymer mixtures.

Edwards was the first to apply the functional integral methods to polymer physics [41, 42]. He investigated the effect of finite monomer size (excluded volume problem [9]) on the configurational statistical mechanics of polymer chains. Using functional integrals over chain configurations and self-consistent mean field theory, he succeeded in obtaining the realistic scaling behaviour of the end-to-end distance of a polymer as a function of the degree of polymerization, Z_p [41]. Those power laws were known from earlier Flory work who derived them by phenomenological arguments [9]. In reference [42], Edwards derived, using the self-consistent theory, the equation of state of a polymer mixture in terms of the excluded volume parameter, v, defined in reference [42], for intermediate (semi-dilute) concentrations of polymer in solution. He also showed that his approach fails to yield the equation of state in dilute and dense (concentrated) solutions. Edwards and Dolan investigated the statistical mechanics, in particular the density profiles, of polymer chains end-grafted at a plane surface [43, 44]. Edwards' work influenced to a great degree the mean field theories of Helfand et al. [45]–[51], Hong and Noolandi [27, 33, 52], and all other workers discussed in this section.

Meier in his pioneering works [53, 54] contributed greatly to the initial development of copolymer theories. He proposed an expression for the free energy of the microphase separated copolymer state with respect to the homogeneous and amorphous melt. The postulated free energy included three different terms:

1. a change in the heat of mixing, ΔH_M, analogous to the Flory expression for ΔH_M [9],

2. a loss of entropy related to the localization of A-b-B joints at the interface,

3. a loss of entropy related to the localization of A- and B-blocks in the respective subdomains, which was calculated by solving diffusion-type equation with appropriate boundary conditions.

This approach worked well in the strong segregation regime (because only in this regime both interfaces and subdomains are sharply localized) and was successful in predicting the scaling behaviour of the domain thickness as a function of molecular weight (degree of polymerization). It is worth noting that Meier did not use mean field or self-consistency in his calculations.

Freed and coworkers have extensively applied the functional integral methods to polymer physics, using the powerful techniques of the field theory, e.g. the renormalization group calculations, as summarized in reference [55]. The renormalization group theory of polymer excluded volume was developed by Freed and coworkers in references [56]–[58]. Excluded volume interactions were incorporated in terms of the continuous chain formalism as in Edwards' work [41, 42], and also as in this thesis. The alternatives to the continuous chain formalism include lattice calculations and Flory theories, all elucidated in Freed's book [55]. In this monograph he also discusses the concept of "coarse graining", i.e., averaging polymer characteristics over distances much larger than monomer

sizes but smaller than the overall polymer lengths, which is equivalent to introducing a "cut-off" associated with the inverse of some characteristic length. In this thesis all the expressions should be interpreted in the "coarse grained" sense, in particular the delta functions appearing in the expression for densities, eq. 2.4. "Coarse graining" allows us to introduce the bulk densities and to calculate the equilibrium density profiles of bulk polymers modelled as a collection of flexible chains.

The first mean field theory of block copolymers applying the functional integral method, with Wiener measure as statistical weight for the chain configurations, was proposed by Helfand [47]. By using the saddle point approximation and putting into execution the Feynman-Kac theorem [47], he succeeded in deriving a system of self-consistent equations and solving it numerically. Helfand started with the assumption that the system was compressible with a compressibility coefficient, κ. But then he assumed that this coefficient vanishes, $\kappa \rightarrow 0$, which translated into employing an undetermined function $w_\xi(\mathbf{r})$ (which corresponds to $\eta(\mathbf{r})$ in this thesis) and using the incompressibility condition. Helfand and Wassermann were able to calculate the free energy and density profiles for different morphologies (lamellae [46, 48], cylinders [49], spheres [50]) and for varying domain thicknesses, and were, therefore, able to predict both the equilibrium domain thickness and the equilibrium structure for a given set of bulk densities, Kuhn lengths, the interaction parameter, the copolymer degree of polymerization and the relative volume fraction of one type of monomer, denoted f_A (for A monomers) in notation of this thesis. They simplified their formalism by using what they called "a narrow interphase approximation" [48] which worked well in the strong segregation regime. The phase diagram for a microphase separated styrene-butadiene copolymer, *PS-b-PBD*, as a function of f_{PS} with realistic Kuhn lengths and densities, was presented in reference [51] showing that the layers were stable from $f_{PS} \simeq 0.33$ to $f_{PS} \simeq 0.66$, the cylinders from $f_{PS} \simeq 0.17$ to 0.83 excluding the region "taken" by lamellae, and the spheres formed an

equilibrium structure if $f_{PS} \lesssim 0.17$ or $f_{PS} \gtrsim 0.83$. The boundaries between different morphologies have been found to be independent of χ parameter. These findings generally agree with the experimental data for strongly segregated copolymers [7]. Also scaling behaviour of domain thickness, d, as a function of copolymer molecular weight (copolymer degree of polymerization, Z_c) agreed with the experiment [48].

Shortly after that, Leibler [11] presented a complementary approach for the weak segregation regime which also applied to the diblock copolymer melts above the MST. He employed a Landau-type [59] analysis and random phase approximation (RPA) [12] to calculate the free energy up to the fourth order using for an order parameter the thermal equilibrium monomer density profile minus the density profile in the homogeneous system. He started with calculating correlation functions for a homogeneous melt composed of ideal noninteracting copolymer Gaussian coils. Then the incompressibility and the interactions (via the Flory interaction χ parameter) were incorporated, and by applying the RPA [12], the two, three and four point density correlation functions were calculated. By performing the standard Legendre transformation, as thoroughly described in reference [60], Leibler obtained the vertex functions which were the coefficients in the fourth order expansion of the free energy. The Fourier transforms of density-density correlation functions for the homogeneous melt were peaked about the value of the wavevector corresponding to the copolymer radius of gyration. As the MST was approached the correlation function maximum value ("peak") grew bigger, finally diverging for some wavevector, k^*, which indicates that the homogenenous phase becomes unstable with respect to the inhomogeneous one. This is the MST spinodal. The calculated correlation functions were compared with the results of many SAXS experiments, e.g. Hashimoto [10], yielding good agreement.

The Leibler theory predicted the existence of three ordered structures: spheres, cylinders, and lamellae. It assumed that k^* remained also the dominant mode below the MST in the ordered phase. It also kept only some wavevectors $\boldsymbol{k}_n$, i.e., those with length k^* in the Fourier expansion of the equilibrium monomer density profile, i.e.,

$$\phi_{cA}(\boldsymbol{r}) \sim \sum_n a_n \cos(\boldsymbol{r} \cdot \boldsymbol{k}_n), \tag{1.4}$$

where $|\boldsymbol{k}_n| = k^*$. In this thesis we refer to this condition, expressed by eq. 1.4, as the *one wavenumber approximation*. However, this approach predicted unrealistic boundaries between those structures. In particular the spherical structure was stable only in a very narrow strip near the order-disorder transition. The boundaries depended on χ even in the strongly segregated regime, the equilibrium morphology of the ordered structure in the immediate vicinity of order-disorder transition was spherical except for the perfectly symmetric case with $f_A = 0.5$, and for low enough temperature (high enough χ) the equilibrium structure was lamellar for all f_A. These discrepancies might be attributable, at least partially, to the fourth order expansion of the free energy which caused a truncation error by neglecting the higher order terms, the one wavenumber approximation and the mean field theory itself.

Fredrickson and Helfand [61] investigated the possibility that the discrepancies may be due to the very nature of mean field theory which neglects the fluctuations by including only the dominant part in the thermodynamic partition function. They modified Leibler's approach by employing the Hartree approximation as described by Brazovskii in reference [62]. In this way the fluctuations were taken into account, but still with fourth order expansion and one wavenumber approximation. It was found that, for copolymer degree of polymerization going to infinity, the mean field theory expressions were recovered. But for finite degree of polymerization some interesting predictions were made. In particular, it was found that, unlike Leibler's phase diagram, a direct transition from the

disordered melt to the lamellar structure was possible (so called "window" was opened), for f_A close, but not necessarily equal, to 0.5, with qualitative agreement with the experiment [7], and the MST itself was shifted towards lower temperatures. In general, however, this phase diagram represented the experimental reality only slightly more faithfully than the Leibler's one did. The strip of the spherical structure, introduced in the discussion of Leibler's phase diagram, was still present, and disappeared for low enough temperatures (high enough χ). Furthermore, for $Z_c = 10^9$, the lamellar "window" was tiny (for $0.49 \lesssim f_A \lesssim 0.51$) and there was, again, a very narrow strip of spherical structure. For $Z_c = 10^4$, on the other hand, the lamellar "window" was broader (for $0.40 \lesssim f_A \lesssim 0.60$), but, surprisingly, the spherical morphology disappeared completely from the phase diagram. One might speculate that these discrepancies are due to the one wavenumber nature and fourth order approximation of both approaches. This is, indeed, suggested by very recent results of Whitmore and Vavasour [63] who by means of mean field numerical self-consistent approach constructed phase diagrams of copolymer/neutral solvent blend. The structure of those phase diagrams looks more reasonable. In this thesis we use a mean field theory so that the fluctuations are not included.

In a recent communication, Olvera de la Cruz [64] modified the Fredrickson and Helfand approach by taking into consideration higher harmonics (two wavenumbers in Fourier expansion) of the equilibrium monomer density profile. The shifting of the wavevector corresponding to the maximum scattering in the isotropic state was investigated for three structures: $3D$ hexagonal lattice, $2D$ hexagonal packed cylinders and bcc. It was predicted by Leibler theory that k^* was independent of temperature. Olvera de la Cruz found that k^* contracted for bcc structure, while it stretched for the other two structures (in the isotropic state near the MST) compared with the Leibler's mean field result. Olvera de la Cruz [64] also questioned the validity of the lamellar "window", claiming that lamellar structure is not always the equilibrium structure in the vicinity of

$f_A = 0.5$ as previously thought, but the $3D$ hexagonal lattice.

The theoretical method of this thesis is based on the mean field theory introduced by Hong and Noolandi [27, 33, 52], and is fully discussed in chapter 2. To date it has been applied to copolymer/solvent and copolymer/homopolymer blends, in the weak and the strong segregation regimes in references [27, 29, 30, 33, 52]. For copolymer/solvent blends, the numerical solutions to the numerical self-consistent equations of the theory [30, 33] are the primary application of this approach. There is no theory of copolymer *blends* which incorporates fluctuations.

Sufficiently accurate numerical solutions can be particularly difficult to obtain in the weak segregation regime, where the free energy, relative to the homogeneous phase, is very small. Therefore Hong and Noolandi developed a complementary approach for this regime, employing a perturbative solution to the modified diffusion equations and a resulting fourth order expansion of the free energy. This is also discussed in chapter 2. For copolymer/homopolymer blends, *A-b-B/A/B*, we develop here a new fourth order expansion of the free energy which differs from the general expression for copolymer blends, presented in reference [27]. We expand the free energy using the total A-monomer (or equivalently B-monomer) density, while general expression contains all individual components, distinguishing copolymer blocks and homopolymers composed of the same type of monomer. The basis of our approach is the existence of only two different mean field potentials, $\omega_\alpha(\mathbf{r})$ and $\omega_\beta(\mathbf{r})$, as elucidated in section 2.3. The expression for the free energy of a homogeneous polymer blend in the formalism of Hong and Noolandi, which we rederive and use, is the same as that in the Flory-Huggins theory (eq. 2.87).

In reference [30] a theoretical study of the lamellar structure of diblock copolymers blended with neutral (nonselective) solvent was presented. Our first project, in fact, complements this work by replacing the neutral solvent with selective solvent in model calculations. In real system calculations, however, the correspondence between the work

of Whitmore and Noolandi and our work is more subtle. Reference [29] contains the comprehensive discussion of phase diagrams of binary copolymer/homopolymer blends. Our work on ternary phase diagrams is, to a large extent, a continuation and an extension of this work. In reference [31] the authors discuss the formation of micelles in copolymer/homopolymer blends. In order to restrict attention to systems with relatively simple phase diagrams we use their model in our last project to avoid regions where such micelles can be formed.

1.4 Content of the Thesis

The thesis is organized as follows. The general theory is introduced in Chapter 2 for both fourth order expansion mean field approach and for numerical self-consistent calculations. This presentation is an original extension of the Hong and Noolandi theory.

Chapter 3 contains the copolymer/selective solvent numerical self-consistent calculations and presentation of results.

Chapter 4 covers the discussion of the lamellar structure of copolymer/homopolymer blends in the weak segregation regime. This constitutes the second project and has been submitted to publication as reference [65].

Copolymer/homopolymer ternary phase diagrams are calculated and described in chapter 5. This is the third project and has been accepted for publication in *Macromolecules* [66]. Theory of chapter 5 is also used in chapter 4.

Chapter 6 summarizes with conclusions drawn from all three projects.

Chapter 2

Theory

2.1 General

This section is meant as an introduction to the Hong and Noolandi formalism which is the cornerstone of our theory. The method is essentially that of Hong and Noolandi [27, 52] but with the incompressibility incorporated following Ohta and Kawasaki [40]. This theory models an arbitrary mixture of amorphous copolymers, homopolymers and solvents using a general expression for the partition function for such a mixture. Amorphous polymers are modelled as systems of Gaussian chains, and a great number of successful theoretical models was based on this very basic assumption, e.g. Edwards [41, 42], Helfand et al. [45]–[51], Olvera de la Cruz et al. [2, 64], Leibler [11], Kawasaki et al. [67, 68], Hong and Noolandi [27, 33, 52], Whitmore and Noolandi [29, 30], Shull et al. [69, 70], Fredrickson and Helfand [61].

Real polymer (homopolymer or one of the blocks of a diblock) chain can be modelled as random walk of Z_p successive steps. Its radius of gyration, R_g, can be expressed as $R_g = (Z_p b_p^2/6)^{\frac{1}{2}}$, where b_p is referred to as the Kuhn length. This polymer chain can be further replaced with the equivalent Gaussian chain which is defined by the transformation:

$$Z_p \rightarrow Z_p/s \qquad b_p \rightarrow b_p s^{\frac{1}{2}}. \tag{2.1}$$

As s goes to zero then the chain is replaced by a space curve parameterized by continuous parameter τ ranging from 0 to Z_p. Gaussian chain is an idealization of a real polymer

chain as defined and fully described in reference [55]. All possible polymer configurations are denoted by the dot notation, $\mathbf{r}_p(\cdot)$, and a functional integral $\int \delta\mathbf{r}(\cdot)P[\mathbf{r}_p(\cdot)]$ can be defined, where

$$P[\mathbf{r}_p(\cdot)] \propto \exp[-\frac{3}{2b_p^2}\int_0^{Z_p} d\tau \dot{\mathbf{r}}_p^2(\tau)], \tag{2.2}$$

is the Wiener measure, b_p is the Kuhn length and $\dot{\mathbf{r}}(\tau)$ is the derivative with respect to τ. Formal definition of the functional integral requires discretization of the space curve and evaluation of the appropriate limit. In practical calculations, however, this limit is not directly evaluated. Instead the Feynman-Kac theorem, which relates this integral to the diffusion equation, is used.

Physically, a homopolymer p is characterized by a degree of polymerization Z_p, Kuhn statistical length b_p, and bulk density ρ_{op} expressed in number of monomers per unit volume. A diblock copolymer, A-b-B, similarly, can be described by the degrees of polymerization of each block, Z_{cA} and Z_{cB}, Kuhn statistical lengths of each block b_{cA} and b_{cB}, and bulk densities ρ_{ocA} and ρ_{ocB}. The equilibrium thermodynamic properties of a copolymer/homopolymer blend can be calculated from the partition function.

We consider a volume V containing $\tilde{N}_c$ copolymer molecules with block degrees of polymerizations Z_{cA} and Z_{cB}, $\tilde{N}_{hA}$ homopolymer molecules of type A with degree of polymerization Z_{hA}, $\tilde{N}_{hB}$ homopolymer molecules of type B with degree of polymerization Z_{hB}, and $\tilde{N}_s$ solvent molecules. We associate with each component, p, a Kuhn statistical length b_p, and bulk density ρ_{op}, in units of monomers per unit volume. Generally, $p = hA$, hB, cA, cB, and s, with the understanding that we do not have to specify a Kuhn length for the solvent. In this thesis we assume that the Kuhn lengths and the bulk densities of each homopolymer are the same as those of the corresponding block of the copolymer.

The equilibrium thermodynamic properties of the blend can be calculated from the

partition function. Assuming the blend to be incompressible, it can be written

$$\begin{aligned}
\mathbf{Z} \;=\; & \prod_{\kappa}^{c} \frac{\mathcal{Z}_{\kappa}^{\tilde{N}_{\kappa}}}{\tilde{N}_{\kappa}!} \int \prod_{i=1}^{\tilde{N}_s} d\boldsymbol{r}_{si} \times \\
& \int \prod_{i=1}^{\tilde{N}_{hA}} \delta \boldsymbol{r}_i(\cdot) P_{hA}[\boldsymbol{r}_i(\cdot)] \times \\
& \int \prod_{j=1}^{\tilde{N}_{hB}} \delta \boldsymbol{r}_j(\cdot) P_{hB}[\boldsymbol{r}_j(\cdot)] \times \\
& \int \prod_{k=1}^{\tilde{N}_c} \delta \boldsymbol{r}_{Ak}(\cdot) \delta \boldsymbol{r}_{Bk}(\cdot) P_{cA}[\boldsymbol{r}_{Ak}(\cdot)] P_{cB}[\boldsymbol{r}_{Bk}(\cdot)] \times \\
& \delta[\boldsymbol{r}_{Ak}(Z_{cA}) - \boldsymbol{r}_{Bk}(Z_{cB})] \times \\
& \prod_{\boldsymbol{r}} \delta(1 - \sum_{p} \frac{\hat{\rho}_p(\boldsymbol{r})}{\rho_{op}}) \times \\
& \exp[-\beta \hat{V}], \qquad (2.3)
\end{aligned}$$

where $\mathcal{Z}_\kappa$ is the contribution to the partition function from the kinetic energy of a molecule of type κ. The c over the product sign indicates, that for that product, the copolymer is to be treated as a single component. Otherwise the four weight functions are assumed to be of the standard Wiener form with the four polymer densities given by

$$\begin{aligned}
\hat{\rho}_p(\boldsymbol{r}) \;&=\; \hat{\rho}_p(\boldsymbol{r}, \{\boldsymbol{r}_{pi}\}) \\
&=\; \sum_{i=1}^{\tilde{N}_p} \int_0^{Z_p} d\tau \delta(\boldsymbol{r} - \boldsymbol{r}_{pi}(\tau)), \qquad (2.4)
\end{aligned}$$

while the solvent density is

$$\hat{\rho}_s(\boldsymbol{r}) = \sum_{i=1}^{\tilde{N}_s} \delta(\boldsymbol{r} - \boldsymbol{r}_{si}). \qquad (2.5)$$

The partition function is defined using the functional integrals over all configurations, where the expression $\delta[\boldsymbol{r}_{Ak}(Z_{cA}) - \boldsymbol{r}_{Bk}(Z_{cB})]$ accounts for the connectivity of the copolymer diblocks and $\prod_{\boldsymbol{r}} \delta[1 - \sum_p \hat{\rho}_p(\boldsymbol{r})/\rho_{op}]$ in equation 2.3 ensures incompressibility. This way of incorporating incompressibility into the partition function follows Ohta and Kawasaki

[40], and is different from the Hong and Noolandi approach, who used the incompressibility condition as a constraint in minimizing the free energy functional, $\mathcal{F}$, given in their formalism by eq. 2.22. In their presentation, $\eta(\mathbf{r})$ appears as a Lagrange multiplier. Both approaches give the same result, but the Ohta and Kawasaki one has, in our opinion, a conceptual advantage of including the incompressibility from the very start. In the notation of this thesis δ followed by a bracket denotes Dirac delta, while followed by $\mathbf{r}$ is a part of the functional integral (measure) symbol.

The interaction energy is a functional of the densities $\hat{\rho}_p(\mathbf{r})$. It is convenient to express it in units of $k_BT = \beta$, and model it via two-body interactions, $W_{pp'}(\mathbf{r} - \mathbf{r}')$, i.e.,

$$\beta\hat{V}[\{\hat{\rho}_p(\cdot)\}] = \frac{1}{2}\sum_{pp'}\int d\mathbf{r}\, d\mathbf{r}'\hat{\rho}_p(\mathbf{r})W_{pp'}(\mathbf{r}-\mathbf{r}')\hat{\rho}_{p'}(\mathbf{r}'). \tag{2.6}$$

Using the identity

$$\begin{aligned}&\prod_{\mathbf{r}}\delta(1-\sum_p\frac{\hat{\rho}_p(\mathbf{r})}{\rho_{op}})\exp[-\beta\hat{V}] = \\ &\int\{\prod_p\delta\rho_p(\cdot)\,\delta\left(\rho_p(\cdot)-\hat{\rho}_p(\cdot)\right)\}\left(\prod_{\mathbf{r}}\delta(1-\sum_p\frac{\rho_p(\mathbf{r})}{\rho_{op}})\exp[-W]\right)\end{aligned} \tag{2.7}$$

with

$$W[\{\rho_p(\cdot)\}] = \frac{1}{2}\sum_{pp'}\int d\mathbf{r}\, d\mathbf{r}'\rho_p(\mathbf{r})W_{pp'}(\mathbf{r}-\mathbf{r}')\rho_{p'}(\mathbf{r}'), \tag{2.8}$$

and substituting the integral representation of the delta functionals

$$\delta\left(\rho_p(\cdot)-\hat{\rho}_p(\cdot)\right) = \mathcal{N}_1\int\delta\omega_p(\cdot)\exp\left[\int d\mathbf{r}\,\omega_p(\mathbf{r})\left(\rho_p(\cdot)-\hat{\rho}_p(\cdot)\right)\right], \tag{2.9}$$

and

$$\begin{aligned}\prod_{\mathbf{r}}\delta(1-\sum_p\frac{\rho_p(\mathbf{r})}{\rho_{op}}) \;&=\; \mathcal{N}_2\int\delta\eta(\cdot)\times \\ &\exp\left[\int d\mathbf{r}\,\eta(\mathbf{r})(1-\sum_p\frac{\rho_p(\mathbf{r})}{\rho_{op}})\right],\end{aligned} \tag{2.10}$$

where $\mathcal{N}_1$ and $\mathcal{N}_2$ are normalizations, we can write the partition function, eq. 2.3, as

$$\begin{aligned}
\mathbf{Z} \;= \mathcal{N} \; & \prod_{\kappa}^{c} \frac{Z_{\kappa}^{\tilde{N}_{\kappa}}}{\tilde{N}_{\kappa}!} \times \\
& \int \delta\rho_{hA}(\cdot)\delta\rho_{hB}(\cdot)\delta\rho_{cA}(\cdot)\delta\rho_{cB}(\cdot)\delta\rho_{s}(\cdot) \times \\
& \int \delta\omega_{hA}(\cdot)\delta\omega_{hB}(\cdot)\delta\omega_{cA}(\cdot)\delta\omega_{cB}(\cdot)\delta\omega_{s}(\cdot)\delta\eta(\cdot) \times \\
& Q_{c}^{\tilde{N}_{c}} Q_{hA}^{\tilde{N}_{hA}} Q_{hB}^{\tilde{N}_{hB}} Q_{s}^{\tilde{N}_{s}} \times \\
& \exp[\int d\boldsymbol{r}\,\eta(\boldsymbol{r})(1 - \sum_{p} \frac{\rho_{p}(\boldsymbol{r})}{\rho_{op}})] \times \\
& \exp[\sum_{p} \int d\boldsymbol{r}\,\omega_{p}(\boldsymbol{r})\rho_{p}(\boldsymbol{r}) - W[\rho_{p}(\cdot)]]
\end{aligned} \tag{2.11}$$

where $\mathcal{N}$ is a normalization. For homopolymers ($p = hA$ or hB),

$$Q_{p}^{\tilde{N}_{p}} = \int \prod_{i=1}^{\tilde{N}_{p}} \delta\boldsymbol{r}_{i}(\cdot) P_{p}[\boldsymbol{r}_{i}(\cdot)] \exp[-\int d\boldsymbol{r}\,\omega_{p}(\boldsymbol{r})\hat{\rho}_{p}(\boldsymbol{r})], \tag{2.12}$$

where $\hat{\rho}_{p}(\boldsymbol{r})$ is related to $\boldsymbol{r}_{i}(\cdot)$ by eq. 2.4. Equation 2.12 implies

$$Q_{p} = \int \delta\boldsymbol{r}(\cdot) P_{p}[\boldsymbol{r}(\cdot)] \exp[-\int_{0}^{Z_{p}} \omega_{p}(\boldsymbol{r}_{p}(\tau))d\tau]. \tag{2.13}$$

For copolymers,

$$\begin{aligned}
Q_{c} \;= \; & \int \delta\boldsymbol{r}_{A}(\cdot)\delta\boldsymbol{r}_{B}(\cdot) P_{cA}[\boldsymbol{r}_{A}(\cdot)] P_{cB}[\boldsymbol{r}_{B}(\cdot)] \times \\
& \delta[\boldsymbol{r}_{A}(Z_{cA}) - \boldsymbol{r}_{B}(Z_{cB})] \times \\
& \exp[-\int_{0}^{Z_{cA}} \omega_{cA}(\boldsymbol{r}_{A}(\tau))d\tau - \int_{0}^{Z_{cB}} \omega_{cB}(\boldsymbol{r}_{B}(\tau))d\tau].
\end{aligned} \tag{2.14}$$

whereas the corresponding expression for the solvent, s, is

$$Q_{s} = \int d\boldsymbol{r} \exp(-\omega_{s}(\boldsymbol{r})). \tag{2.15}$$

These functionals, for polymers but not for solvent, can be expressed in terms of four propagators $Q_{p}(\boldsymbol{r}, \tau|\boldsymbol{r}')$, with $p = hA, hB, cA$ and cB, all of which satisfy the modified diffusion equation [27],

$$[-\frac{b_{p}^{2}}{6}\nabla^{2} + \omega_{p}(\boldsymbol{r})]Q_{p}(\boldsymbol{r}, \tau|\boldsymbol{r}') = -\frac{1}{Z_{p}}\frac{\partial}{\partial\tau}Q_{p}(\boldsymbol{r}, \tau|\boldsymbol{r}'), \tag{2.16}$$

with initial condition

$$Q_p(\mathbf{r}, 0|\mathbf{r}') = \delta(\mathbf{r} - \mathbf{r}'). \tag{2.17}$$

With these we have explicitly

$$Q_p = \int d\mathbf{r}\, d\mathbf{r}' Q_p(\mathbf{r}, 1|\mathbf{r}') \tag{2.18}$$

for homopolymers, and

$$Q_c = \int d\mathbf{r}\, d\mathbf{r}'\, d\mathbf{r}'' Q_{cA}(\mathbf{r}'', 1|\mathbf{r}) Q_{cB}(\mathbf{r}'', 1|\mathbf{r}') \tag{2.19}$$

for copolymers. In equation 2.13, τ ranges from 0 to Z_p whereas in eq. 2.18 the maximum τ is equal to 1. This is because in the modified diffusion equation, eq. 2.16, τ has been rescaled by factor $1/Z_p$. Using the Stirling approximation, the partition function, eq. 2.11 can be written as

$$\mathbf{Z} = \mathcal{N} \int [\prod_p \delta\rho_p(\cdot)\delta\omega_p(\cdot)]\delta\eta(\cdot) \exp\{-\mathcal{F}_T[\{\rho_p(\cdot)\}, \{\omega_p(\cdot)\}, \eta(\cdot)]\}, \tag{2.20}$$

where $\mathcal{F}_T(\{\rho_p(\cdot)\}, \{\omega_p(\cdot)\}, \eta(\cdot))$ is the free energy functional, (in units of k_BT), given by

$$\mathcal{F}_T[\{\rho_p(\cdot)\}, \{\omega_p(\cdot)\}, \eta(\cdot)] = \mathcal{F}[\{\rho_p(\cdot)\}, \{\omega_p(\cdot)\}] + \mathcal{G}[\{\rho_p(\cdot)\}, \eta(\cdot)], \tag{2.21}$$

with

$$\begin{aligned} \mathcal{F}[\{\rho_p(\cdot)\}, \{\omega_p(\cdot)\}] &= W[\{\rho_p(\cdot)\}] - \sum_p \int d\mathbf{r}\, \omega_p(\mathbf{r})\rho_p(\mathbf{r}) + \\ &\sum_\kappa^c \tilde{N}_\kappa (\ln \frac{\tilde{N}_\kappa}{Z_\kappa Q_\kappa} - 1), \end{aligned} \tag{2.22}$$

$$\mathcal{G}[\{\rho_p(\cdot)\}, \{\eta(\cdot)\}] = \int d\mathbf{r}\, \eta(\mathbf{r}) (\sum_p \frac{\rho_p(\mathbf{r})}{\rho_{op}} - 1). \tag{2.23}$$

We next need expressions for thermal average density distribution of each component. Using the partition function, eq. 2.3, we can express this for e.g. homopolymer hA very

generally as

$$\begin{aligned}\langle\hat{\rho}_{hA}(\mathbf{r})\rangle \;=\; & \frac{1}{\mathbf{Z}}\prod_{\kappa}^{c}\frac{\mathcal{Z}_{\kappa}^{\tilde{N}_{\kappa}}}{\tilde{N}_{\kappa}!}\int\prod_{i=1}^{\tilde{N}_s}d\mathbf{r}_{si}\times \\ & \int\prod_{i=1}^{\tilde{N}_{hA}}\delta\mathbf{r}_i(\cdot)P_{hA}[\mathbf{r}_i(\cdot)]\hat{\rho}_{hA}(\mathbf{r},\{\mathbf{r}_i(\cdot)\})\times \\ & \int\prod_{j=1}^{\tilde{N}_{hB}}\delta\mathbf{r}_j(\cdot)P_{hB}[\mathbf{r}_j(\cdot)]\times \\ & \int\prod_{k=1}^{\tilde{N}_c}\delta\mathbf{r}_{Ak}(\cdot)\delta\mathbf{r}_{Bk}(\cdot)P_{cA}[\mathbf{r}_{Ak}(\cdot)]P_{cB}[\mathbf{r}_{Bk}(\cdot)]\times \\ & \delta[\mathbf{r}_{Ak}(Z_{cA})-\mathbf{r}_{Bk}(Z_{cB})]\times \\ & \prod_{\mathbf{r}'}\delta(1-\sum_{p}\frac{\hat{\rho}_p(\mathbf{r}')}{\rho_{op}})\times \\ & \exp[-\beta\hat{V}] \end{aligned} \tag{2.24}$$

The functional integrals here are the same as in the partition function, eq. 2.3, except for the presence of the $\hat{\rho}_{hA}(\mathbf{r},\{\mathbf{r}_i(\cdot)\})$. Therefore we can introduce changes of variables as we did for $\mathbf{Z}$. The only difference is that $Q_{hA}^{\tilde{N}_{hA}}$ is replaced with

$$\int\prod_{i=1}^{\tilde{N}_{hA}}\delta\mathbf{r}_i(\cdot)P_{hA}[\mathbf{r}_i(\cdot)]\hat{\rho}_{hA}(\mathbf{r})\exp[-\int d\mathbf{r}'\omega_{hA}(\mathbf{r}')\hat{\rho}_{hA}(\mathbf{r}')] \tag{2.25}$$

which is seen to be equal to

$$-\frac{\delta}{\delta\omega_{hA}(\mathbf{r})}Q_{hA}^{\tilde{N}_{hA}}. \tag{2.26}$$

Proof:

$$\begin{aligned} & \int\prod_{i=1}^{\tilde{N}_{hA}}\delta\mathbf{r}_i(\cdot)P_{hA}[\mathbf{r}_i(\cdot)]\hat{\rho}_{hA}(\mathbf{r})\exp[-\int d\mathbf{r}'\omega_{hA}(\mathbf{r}')\hat{\rho}_{hA}(\mathbf{r}')] = \\ & -\int\prod_{i=1}^{\tilde{N}_{hA}}\delta\mathbf{r}_i(\cdot)P_{hA}[\mathbf{r}_i(\cdot)]\frac{\delta}{\delta\omega_{hA}(\mathbf{r})}\exp[-\int d\mathbf{r}'\omega_{hA}(\mathbf{r}')\hat{\rho}_{hA}(\mathbf{r}')] = \\ & -\frac{\delta}{\delta\omega_{hA}(\mathbf{r})}\int\prod_{i=1}^{\tilde{N}_{hA}}\delta\mathbf{r}_i(\cdot)P_{hA}[\mathbf{r}_i(\cdot)]\exp[-\int d\mathbf{r}'\omega_{hA}(\mathbf{r}')\hat{\rho}_{hA}(\mathbf{r}')] = \\ & -\frac{\delta}{\delta\omega_{hA}(\mathbf{r})}Q_{hA}^{\tilde{N}_{hA}}. \end{aligned} \tag{2.27}$$

We thus have, for homopolymer hA,

$$\langle\hat{\rho}_{hA}(\mathbf{r})\rangle = \frac{\mathcal{N}}{\mathbf{Z}}\int[\prod_{p'}\delta\rho_{p'}(\cdot)\delta\omega_{p'}(\cdot)]\delta\eta(\cdot)\frac{\tilde{N}_{hA}}{Q_{hA}}\frac{\delta Q_{hA}}{\delta\omega_{hA}(\mathbf{r})}\times \exp\{-\mathcal{F}_T[\{\rho_p(\cdot)\},\{\omega_p(\cdot)\},\eta(\cdot)]\}, \tag{2.28}$$

and a similar expression for homopolymer hB, with hA replaced by hB. For copolymer cA we obtain

$$\langle\hat{\rho}_{cA}(\mathbf{r})\rangle = \frac{\mathcal{N}}{\mathbf{Z}}\int[\prod_{p'}\delta\rho_{p'}(\cdot)\delta\omega_{p'}(\cdot)]\delta\eta(\cdot)\frac{\tilde{N}_{cA}}{Q_c}\frac{\delta Q_c}{\delta\omega_{cA}(\mathbf{r})}\times \exp\{-\mathcal{F}_T[\{\rho_p(\cdot)\},\{\omega_p(\cdot)\},\eta(\cdot)]\}, \tag{2.29}$$

with analogous expression of copolymer cB, and finally for the solvent s

$$\langle\hat{\rho}_s(\mathbf{r})\rangle = \frac{\mathcal{N}}{\mathbf{Z}}\int[\prod_{p'}\delta\rho_{p'}(\cdot)\delta\omega_{p'}(\cdot)]\delta\eta(\cdot)\frac{\tilde{N}_s}{Q_s}\frac{\delta Q_s}{\delta\omega_s(\mathbf{r})}\times \exp\{-\mathcal{F}_T[\{\rho_p(\cdot)\},\{\omega_p(\cdot)\},\eta(\cdot)]\}. \tag{2.30}$$

In fact all five densities can be expressed as

$$\langle\hat{\rho}_p(\mathbf{r})\rangle = \frac{\mathcal{N}}{\mathbf{Z}}\int[\prod_{p'}\delta\rho_{p'}(\cdot)\delta\omega_{p'}(\cdot)]\delta\eta(\cdot)\frac{\tilde{N}_\kappa}{Q_\kappa}\frac{\delta Q_\kappa}{\delta\omega_p(\mathbf{r})}\times \exp\{-\mathcal{F}_T[\{\rho_p(\cdot)\},\{\omega_p(\cdot)\},\eta(\cdot)]\}. \tag{2.31}$$

where $\kappa = p$ if $p = hA$, hB or s, or $\kappa = c$ if $p = cA$ or cB.

Exact evaluation of integrals such as eq. 2.31, as well as the calculation of the partition function, eq. 2.11, is beyond our current capability. In this thesis we use the saddle point approximation which amounts to taking into account the dominant part in the partition function. Thermal averages are approximated by their values at this saddle point; eq. 2.31 becomes

$$\langle\hat{\rho}_p(\mathbf{r})\rangle \to -\frac{\tilde{N}_\kappa}{Q_\kappa}\frac{\delta Q_\kappa}{\delta\omega_p(\mathbf{r})}\Big|_{sp}. \tag{2.32}$$

To find the saddle point we need to minimize $\mathcal{F}_T$ with respect to each $\rho_p(\mathbf{r})$, $\omega_p(\mathbf{r})$ and $\eta(\mathbf{r})$ subject to constraints of constant particle numbers

$$\int d\mathbf{r}\, \rho_p(\mathbf{r}) = N_p. \tag{2.33}$$

This minimization yields

$$\frac{\delta W}{\delta \rho_p(\mathbf{r})} - \omega_p(\mathbf{r}) + \lambda_p + \frac{\eta(\mathbf{r})}{\rho_{op}} = 0, \tag{2.34}$$

$$-\rho_p(\mathbf{r}) - \frac{\bar{N}_\kappa}{Q_\kappa}\frac{\delta Q_\kappa}{\delta \omega_p(\mathbf{r})} = 0, \tag{2.35}$$

$$\sum_p \frac{\rho_p(\mathbf{r})}{\rho_{op}} = 1, \tag{2.36}$$

where λ_p are the Lagrange multipliers associated with eq. 2.33. The last of these equations, arising from the incompressibility, makes $\mathcal{G} = 0$ at the saddle point, and hence the saddle point approximation to the free energy is

$$F \to \mathcal{F}[\{\rho_p(\cdot)\}, \{\omega_p(\cdot)\}]|_{sp}. \tag{2.37}$$

In the *mean field approximation* used in this paper, we use two different approaches to calculate the free energy, each incorporating the saddle point technique:

1. Direct numerical solution of the system of equations, eq 2.16–2.19, 2.32 and 2.34–2.36. This leads to a system of integro-differential equations to be solved self-consistently to give the equilibrium density distribution of each component $\langle\hat{\rho}_p(\mathbf{r})\rangle$, conjugate field $\omega_p(\mathbf{r})$, and free energy $\mathcal{F}$. This is explained in section 2.2.

2. Minimization of a fourth order approximation (Landau-Ginzburg expansion) of the free energy, $\mathcal{F}$, as elucidated in section 2.3 and developed in chapters 4 and 5, using many wavenumber and one wavenumber expansions, respectively. It is worth commenting here that this method is, in general, less accurate than the self-consistent approach due to the truncation error.

2.2 Numerical Self-consistent Formalism for Block Copolymer/Solvent Blends

In this section we sketch the derivation of a set of self-consistent equations for diblock copolymer/solvent blends following the presentation contained in papers of Hong and Noolandi [33] and Whitmore and Noolandi [30]. A volume V containing $\tilde{N}_c$ copolymer molecules with block degrees of polymerizations Z_{cA} and Z_{cB} and $N_s = \tilde{N}_s$ solvent molecules is considered. The system is illustrated schematically in Figure 2.1.

The two-body interaction energy, eq. 2.8 is expanded, in this approach, to account for the finite range of the interaction yielding a gradient expansion

$$\begin{aligned} W[\{\rho_p(\cdot)\}] \;=\; & \frac{1}{2}\sum_p W_{pp}\rho_{op}N_p + \\ & U_{AB}\int d\mathbf{r}\,\rho_{cA}(\mathbf{r})\rho_{cB}(\mathbf{r}) - U_{AB}\frac{\sigma^2}{6}\int d\mathbf{r}\,\nabla\rho_{cA}(\mathbf{r})\cdot\nabla\rho_{cB}(\mathbf{r}) + \\ & U_{AS}\int d\mathbf{r}\,\rho_{cA}(\mathbf{r})\rho_s(\mathbf{r}) - U_{AS}\frac{\sigma^2}{6}\int d\mathbf{r}\,\nabla\rho_{cA}(\mathbf{r})\cdot\nabla\rho_s(\mathbf{r}) + \\ & U_{BS}\int d\mathbf{r}\,\rho_{cB}(\mathbf{r})\rho_s(\mathbf{r}) - U_{BS}\frac{\sigma^2}{6}\int d\mathbf{r}\,\nabla\rho_{cB}(\mathbf{r})\cdot\nabla\rho_s(\mathbf{r}), \end{aligned} \tag{2.38}$$

where

$$W_{pp} = \int d\mathbf{r}\,W_{pp}(\mathbf{r}), \tag{2.39}$$

and

$$U_{pp'} = \int d\mathbf{r}\,U_{pp'}(\mathbf{r}), \tag{2.40}$$

with

$$U_{pp'}(\mathbf{r}) = W_{pp'}(\mathbf{r}) - \frac{1}{2\rho_{op}\rho_{op'}}(W_{pp}(\mathbf{r})\rho_{op}{}^2 + W_{p'p'}(\mathbf{r})\rho_{op'}{}^2). \tag{2.41}$$

In principle the Flory interaction parameter is defined as

$$\chi_{pp'} = \frac{\rho_{op}\rho_{op'}}{\rho_{os}}U_{pp'}. \tag{2.42}$$

Since the interaction $W_{pp'}$ is expressed in units of k_BT, the eq. 2.41 would imply that χ is inversely proportional to temperature. In practice, however, this is not the case.

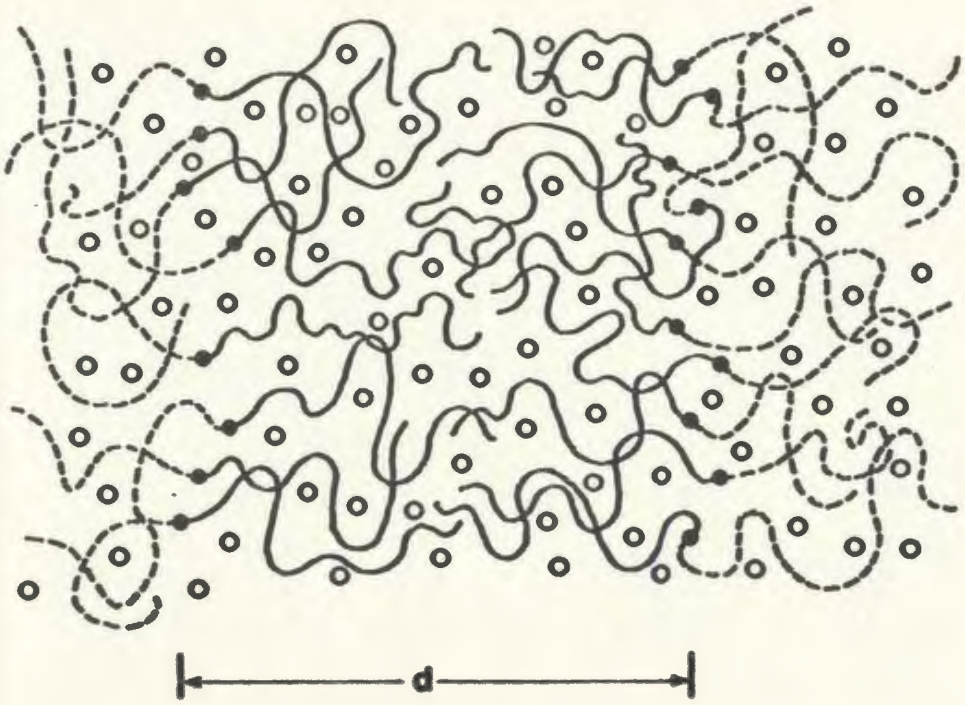

Figure 2.1: Schematic picture of copolymer solvent/system. Lamellar structure is assumed and the domain thickness is *d*. Solvent is denoted by open circles [30].

It has the form of eq 1.1 and we make no attempt to calculate this or account for the dependence of $\chi_{pp'}$ on volume fractions and degrees of polymerization. Further discussion of χ parameter is presented in sections 2.4 and 4.4. Equation 2.38 includes gradient terms representing finite range potentials, modelled approximately by the finite range parameter σ; we take $\sigma = \bar{b}$, i.e., the average of the Kuhn lengths, equal for all interactions. In some cases we take $\sigma = 0$. We define the local and average volume fractions of each of the three components, $p = cA$, cB or s,

$$\phi_p(\mathbf{r}) = \frac{\langle \rho_p(\mathbf{r}) \rangle}{\rho_{op}}, \tag{2.43}$$

and

$$\overline{\phi}_p = \frac{N_p}{V \rho_{op}}, \tag{2.44}$$

as well as the overall copolymer volume fraction

$$\overline{\phi}_c = \overline{\phi}_{cA} + \overline{\phi}_{cB}. \tag{2.45}$$

The free energy can be written as

$$F = F_{hom} + \Delta F, \tag{2.46}$$

where F_{hom} is the free energy of the homogeneous bulk phase of the *A-b-B/s* blend, and ΔF is due to inhomogeneities. If we choose $\omega_p(\mathbf{r}) = 0$ for the homogenous melt then

$$\begin{aligned} F_{hom} \;=\; & \frac{1}{2}\sum_p W_{pp}\rho_{op}N_p + \\ & U_{AB}\int d\mathbf{r}\,\rho_{cA}(\mathbf{r})\rho_{cB}(\mathbf{r}) - U_{AB}\frac{\sigma^2}{6}\int d\mathbf{r}\,\nabla\rho_{cA}(\mathbf{r})\cdot\nabla\rho_{cB}(\mathbf{r}) + \\ & U_{AS}\int d\mathbf{r}\,\rho_{cA}(\mathbf{r})\rho_s(\mathbf{r}) - U_{AS}\frac{\sigma^2}{6}\int d\mathbf{r}\,\nabla\rho_{cA}(\mathbf{r})\cdot\nabla\rho_s(\mathbf{r}) + \\ & U_{BS}\int d\mathbf{r}\,\rho_{cB}(\mathbf{r})\rho_s(\mathbf{r}) - U_{BS}\frac{\sigma^2}{6}\int d\mathbf{r}\,\nabla\rho_{cB}(\mathbf{r})\cdot\nabla\rho_s(\mathbf{r}) + \\ & \sum_\kappa^c \tilde{N}_\kappa(\ln\frac{\tilde{N}_\kappa}{Z_\kappa V} - 1). \end{aligned} \tag{2.47}$$

The system can form an infinite periodic microphase, described by a set of lattice vectors $\mathbf{R_n}$ and associated unit cell of volume Ω. In this thesis we assume the structure is lamellar with a domain thickness (lattice parameter) d, which requires that the copolymers are approximately symmetric.

We need to calculate the density profiles and free energy per unit volume for a given domain thickness d. It is convenient to calculate the reduced free energy per unit volume relative to a uniform melt, which can be expressed

$$\begin{aligned}\frac{\Delta F}{\rho_{os}V} &= \frac{1}{\Omega}\int_{\Omega} d\mathbf{r}\{\chi_{SA}[\phi_s(\mathbf{r})\phi_{cA}(\mathbf{r}) - \overline{\phi}_s\overline{\phi}_{cA} - \frac{\sigma^2}{6}\nabla\phi_s(\mathbf{r})\cdot\nabla\phi_{cA}(\mathbf{r})] \\ &+\chi_{SB}[\phi_s(\mathbf{r})\phi_{cB}(\mathbf{r}) - \overline{\phi}_s\overline{\phi}_{cB} - \frac{\sigma^2}{6}\nabla\phi_s(\mathbf{r})\cdot\nabla\phi_{cB}(\mathbf{r})] \\ &+\chi_{AB}[\phi_{cA}(\mathbf{r})\phi_{cB}(\mathbf{r}) - \overline{\phi}_{cA}\overline{\phi}_{cB} - \frac{\sigma^2}{6}\nabla\phi_{cA}(\mathbf{r})\cdot\nabla\phi_{cB}(\mathbf{r})] \\ &+\phi_s(\mathbf{r})\ln(\frac{\phi_s(\mathbf{r})}{\overline{\phi}_s}) - \frac{\rho_{oA}}{\rho_{os}}\omega_{cA}(\mathbf{r})\phi_{cA}(\mathbf{r}) - \frac{\rho_{oB}}{\rho_{os}}\omega_{cB}(\mathbf{r})\phi_{cB}(\mathbf{r})\} \\ &-\frac{\overline{\phi}_c}{r_{cA}+r_{cB}}\ln(\frac{Q_c}{V}).\end{aligned} \tag{2.48}$$

The equilibrium local volume fraction of component p at $\mathbf{r}$ is denoted by $\phi_p(\mathbf{r})$, and $\omega_{cA}(\mathbf{r})$ and $\omega_{cB}(\mathbf{r})$ are the saddle point potentials. The potential $\omega_s(\mathbf{r})$ has been eliminated by using equation,

$$\omega_s(\mathbf{r}) = \ln(\overline{\phi}_s/\phi_s(\mathbf{r})), \tag{2.49}$$

derived from eq. 2.30, 2.32 and 2.43. The first terms in eq. 2.48 represent the interaction energy of the components, calculated using generalized Flory parameters $\chi_{pp'}$, defined using the solvent for the reference density. Also appearing in eq. 2.48 are r_{cA} and r_{cB}, defined by

$$r_p = Z_p\frac{\rho_{os}}{\rho_{op}}, \tag{2.50}$$

with $p = cA$ or cB. Let us recall, eq. 2.36, that

$$\phi_{cA}(\mathbf{r}) + \phi_{cB}(\mathbf{r}) + \phi_s(\mathbf{r}) = 1, \tag{2.51}$$

everywhere throughout the system.

The three density profiles, as well as the other terms in the free energy, are calculated by solving diffusion equations for the polymer distribution functions. The two functions which are needed, $Q_{cA}(\mathbf{r},\tau|\mathbf{r}')$ and $Q_{cB}(\mathbf{r},\tau|\mathbf{r}')$, satisfy the modified diffusion equation, eq. 2.16. In the periodic system,

$$\begin{aligned} \phi_p(\mathbf{r}) &= \phi_p(\mathbf{r}+\mathbf{R_n}), \\ \omega_p(\mathbf{r}) &= \omega_p(\mathbf{r}+\mathbf{R_n}), \\ Q_p(\mathbf{r},\tau|\mathbf{r}') &= Q_p(\mathbf{r}+\mathbf{R_n},\tau|\mathbf{r}'+\mathbf{R_n}). \end{aligned} \tag{2.52}$$

To take advantage of this periodicity it is convenient to define

$$\overline{Q}_p(\mathbf{r},\tau|\mathbf{r}') = \sum_n Q_p(\mathbf{r}+\mathbf{R_n},\tau|\mathbf{r}'), \tag{2.53}$$

which satisfies

$$\overline{Q}_p(\mathbf{r},\tau|\mathbf{r}') = \overline{Q}_p(\mathbf{r}+\mathbf{R_n},\tau|\mathbf{r}'). \tag{2.54}$$

The $\overline{Q}_p$ satisfy the same diffusion equations as the Q_p, but are subject to the initial condition

$$\overline{Q}_p(\mathbf{r},0|\mathbf{r}') = \sum_n \delta(\mathbf{r}-\mathbf{r}'-\mathbf{R_n}). \tag{2.55}$$

From the $\overline{Q}_p$ the related functions q_p are constructed by integrating over one unit cell

$$q_p(\mathbf{r},\tau) = \int_\Omega d\mathbf{r}'\overline{Q}_p(\mathbf{r},\tau|\mathbf{r}'). \tag{2.56}$$

These quantities also satisfy the diffusion equation, but are subject to the initial condition

$$q_p(\mathbf{r},0) = 1. \tag{2.57}$$

It is sufficient to solve for $\overline{Q}_p$ and q_p in one unit cell. Performing functional derivative of Q_c with respect to $\omega_{cA}(\mathbf{r})$ as presented by Helfand in reference [47], the $\phi_p(\mathbf{r})$ are

constructed via eq. 2.35,

$$\phi_{cA}(\mathbf{r}) = \frac{\overline{\phi}_{cA}}{Q_c} \int_0^1 dt\, q_{cA}(\mathbf{r},\tau) \int_\Omega d\mathbf{r}'\, \overline{Q}_{cA}(\mathbf{r}, 1-t|\mathbf{r}') q_{cB}(\mathbf{r},1), \tag{2.58}$$

for component cA, and a corresponding expression for $\phi_{cB}(\mathbf{r})$. The quantity Q_c/V, which also appears in eq. 2.48 for the free energy, is given by

$$\frac{Q_c}{V} = \frac{1}{\Omega} \int_\Omega d\mathbf{r}\, q_{cA}(\mathbf{r},1) q_{cB}(\mathbf{r},1). \tag{2.59}$$

The potentials ω_p are needed to solve the diffusion equations. They are derived from eq. 2.34, resulting in

$$\begin{aligned} \omega_{cA}(\mathbf{r}) \;=\; & \frac{\rho_{os}}{\rho_{oA}} \{ \ln(\frac{\overline{\phi}_s}{\phi_s(\mathbf{r})}) \\ & + (\chi_{AB} - \chi_{SB})[\phi_{cB}(\mathbf{r}) - \overline{\phi}_{cB} + \frac{\sigma^2}{6} \nabla^2 \phi_{cB}(\mathbf{r})] \\ & + \chi_{AS} \{ \left[\phi_s(\mathbf{r}) - \overline{\phi}_s\right] - \left[\phi_{cA}(\mathbf{r}) - \overline{\phi}_{cA}\right] \\ & + \frac{\sigma^2}{6} \left[\nabla^2 \phi_s(\mathbf{r}) - \nabla^2 \phi_{cA}(\mathbf{r})\right] \} \}, \end{aligned} \tag{2.60}$$

for ω_{cA}, and by a similar expression for ω_{cB}. Lagrange multipliers, λ_p appearing in 2.34, are eliminated by evaluating the saddle point equation 2.34 for the homogenous melt, and by using the presence of the solvent we replace $\omega_s(\mathbf{r})$ by $\ln(\overline{\phi}_s/\phi_s(\mathbf{r}))$, eq. 2.49, and eliminate $\eta(\mathbf{r})$.

Eq 2.58, and 2.60 with analogous equations for $\phi_{cB}(\mathbf{r})$ and $\omega_{cB}(\mathbf{r})$, with the diffusion equation, eq. 2.16, for both cA and cB, constitute the system of equations which can be solved self-consistently. The numerical self-consistent procedure to determine the equilibrium values of $\omega_{cA}(\mathbf{r})$, $\omega_{cB}(\mathbf{r})$, $\phi_{cA}(\mathbf{r})$ and $\phi_{cB}(\mathbf{r})$ (solvent density $\phi_s(\mathbf{r})$ can be calculated from the incompressibility condition, eq. 2.51) is described in the subsequent section 3.2.

2.3 Fourth Order Mean Field Expansion of the Free Energy

In this section we derive the basic expressions we use for the free energy of copolymer/homopolymer blends. We specialize to the case of *A-b-B* copolymer and *A* and *B* homopolymers. The expressions reduce to binary blends in the limit of vanishing homopolymer *B* volume fraction.

A basic assumption we make is that all *A-B* interactions are the same irrespective of whether the interacting monomers belong to homopolymers or copolymers. This assumption allows us to combine $\phi_{hA}(\mathbf{r})$ and $\phi_{cA}(\mathbf{r})$ into total *A*-monomer density profile, $\phi_{\alpha}(\mathbf{r})$. In analogous manner, total *B*-monomer density profile can be obtained. Furthermore, this enables us to reduce the number of mean field potential from four (hA, cA, hB and cB), in the Hong and Noolandi theory, to two (A and B, or equivalently in the notation of this thesis, α and β). Setting, also, the finite range parameter equal to zero, $\sigma = 0$, the interaction energy can be expressed

$$\begin{aligned} W(\{\rho_p(\cdot)\}) \;=\; & \frac{1}{2}\sum_p W_{pp}\rho_{op}N_p + \\ & U_{AB}\int d\mathbf{r}\,\rho_{hA}(\mathbf{r})\rho_{hB}(\mathbf{r}) + U_{AB}\int d\mathbf{r}\,\rho_{hA}(\mathbf{r})\rho_{cB}(\mathbf{r}) + \\ & U_{AB}\int d\mathbf{r}\,\rho_{cA}(\mathbf{r})\rho_{hB}(\mathbf{r}) + U_{AB}\int d\mathbf{r}\,\rho_{cA}(\mathbf{r})\rho_{cB}(\mathbf{r}) \end{aligned} \tag{2.61}$$

Writing out eq. 2.34 explicitly for this case:

$$U_{AB}[(\rho_{hB}(\mathbf{r}) + \rho_{cB}(\mathbf{r}))] - \omega_{hA}(\mathbf{r}) + \lambda_{hA} + \frac{\eta(\mathbf{r})}{\rho_{oA}} = 0 \tag{2.62}$$

$$U_{AB}[(\rho_{hA}(\mathbf{r}) + \rho_{cA}(\mathbf{r}))] - \omega_{hB}(\mathbf{r}) + \lambda_{hB} + \frac{\eta(\mathbf{r})}{\rho_{oB}} = 0 \tag{2.63}$$

$$U_{AB}[(\rho_{hB}(\mathbf{r}) + \rho_{cB}(\mathbf{r}))] - \omega_{cA}(\mathbf{r}) + \lambda_{cA} + \frac{\eta(\mathbf{r})}{\rho_{oA}} = 0 \tag{2.64}$$

$$U_{AB}[(\rho_{hA}(\mathbf{r}) + \rho_{cA}(\mathbf{r}))] - \omega_{cB}(\mathbf{r}) + \lambda_{cB} + \frac{\eta(\mathbf{r})}{\rho_{oB}} = 0 \tag{2.65}$$

and subtracting eq. 2.62 from eq. 2.64, we find

$$\omega_{hA}(\mathbf{r}) - \lambda_{hA} = \omega_{cA}(\mathbf{r}) - \lambda_{cA}. \tag{2.66}$$

However, the overall level of each potential $\omega_p(\mathbf{r})$ is arbitrary. For this section it is convenient to choose them so that

$$\int d\mathbf{r}\omega_p(\mathbf{r}) = 0. \tag{2.67}$$

Integrating both sides of eq. 2.66 and using eq. 2.67, we obtain

$$\lambda_{hA} = \lambda_{cA} \tag{2.68}$$

Thus, at the saddle point,

$$\omega_{hA}(\mathbf{r}) = \omega_{cA}(\mathbf{r}) \equiv \omega_\alpha(\mathbf{r}). \tag{2.69}$$

Similarly,

$$\omega_{hB}(\mathbf{r}) = \omega_{cB}(\mathbf{r}) \equiv \omega_\beta(\mathbf{r}). \tag{2.70}$$

Thus at the saddle point, we have two distinct potentials, $\omega_\alpha(\mathbf{r})$ and $\omega_\beta(\mathbf{r})$. This is a useful result enabling us to modify the Hong and Noolandi approach as subsequently presented in this section. We next rescale the mean field potentials, the Kuhn statistical lengths, and the degrees of polymerization, in order to use the explicit solutions to the diffusion equation developed by Hong and Noolandi [27]:

$$\hat{\omega}_p(\mathbf{r}) = \frac{\rho_{op}}{\rho_o}\omega_p(\mathbf{r}), \tag{2.71}$$

$$\hat{b}_p^2 = \frac{\rho_{oA}}{\rho_o}b_{hA}^2, \tag{2.72}$$

$$\tau_{hA} = \frac{\rho_o}{\rho_{oA}}Z_{hA}, \tag{2.73}$$

$$\tau_{hB} = \frac{\rho_o}{\rho_{oB}}Z_{hB}, \tag{2.74}$$

$$\tau_{cA} = \frac{\rho_o}{\rho_{oA}}Z_{cA}, \tag{2.75}$$

$$\tau_{cB} = \frac{\rho_o}{\rho_{oB}}Z_{cB}, \tag{2.76}$$

$$\tau_c = \tau_{cA} + \tau_{cB}, \tag{2.77}$$

where ρ_o is an arbitrary reference density. Equation 2.32 can be rewritten as

$$\phi_p(\boldsymbol{r}) = -V\frac{\overline{\phi}_p}{r_p}\frac{\delta}{\delta\hat{\omega}_p(\boldsymbol{r})}\ln\frac{Q_\kappa}{V}. \tag{2.78}$$

The modified diffusion equation becomes

$$[-\frac{\hat{b}_p^2}{6}\nabla^2 + \tilde{\omega}_p(\boldsymbol{r})]Q_p(\boldsymbol{r},\tau|\boldsymbol{r}') = -\frac{1}{r_p}\frac{\partial}{\partial\tau}Q_p(\boldsymbol{r},\tau|\boldsymbol{r}'). \tag{2.79}$$

It is more convenient to work with the Fourier transforms:

$$\phi_p(\boldsymbol{r}) = \int\frac{d\boldsymbol{k}}{(2\pi)^3}\exp[i\boldsymbol{k}\cdot\boldsymbol{r}]\tilde{\phi}_p(\boldsymbol{k}), \tag{2.80}$$

and

$$\hat{\omega}_p(\boldsymbol{r}) = \int\frac{d\boldsymbol{k}}{(2\pi)^3}\exp[i\boldsymbol{k}\cdot\boldsymbol{r}]\tilde{\omega}_p(\boldsymbol{k}), \tag{2.81}$$

Equation 2.78 can be transformed to

$$\tilde{\phi}_p(\boldsymbol{k}) = -\frac{\overline{\phi}_p}{r_p}\frac{\delta}{\delta\tilde{\omega}_p(-\boldsymbol{k})}\ln\frac{Q_\kappa}{V} \quad \text{for } \boldsymbol{k}\neq 0, \tag{2.82}$$

$$\tilde{\phi}_p(\boldsymbol{k}=0) = \frac{N_p}{\rho_{op}}, \tag{2.83}$$

We use these results to calculate the saddle point approximation for the free energy, eq. 2.22. We, again, write the free energy as

$$F = F_{hom} + \Delta F, \tag{2.84}$$

where F_{hom} is the free energy of the homogeneous bulk phase of the *A-b-B/A/B* blend, and ΔF is due to inhomogeneities. For the homogeneous phase $\tilde{\phi}_p(\boldsymbol{k}) = 0$ for $\boldsymbol{k}\neq 0$ and $\tilde{\omega}_p(\boldsymbol{k}) = 0$ for all $\boldsymbol{k}$, and therefore $Q_\kappa = V$ for all κ . Thus

$$F_{hom} = \frac{1}{2}\sum_p W_{pp}\rho_{op}N_p + \rho_{oA}\rho_{oB}U_{AB}[\overline{\phi}_{hA}+\overline{\phi}_{cA}][\overline{\phi}_{hB}+\overline{\phi}_{cB}] + \sum_\kappa^C \tilde{N}_\kappa(\ln\frac{\tilde{N}_\kappa}{\mathcal{Z}_\kappa V} - 1). \tag{2.85}$$

We can subtract from this the free energy of a fully demixed system, F_{ref}. Dividing by the total volume V and the reference density ρ_o used above we are left with the free energy density of a uniform, homogeneous blend relative to fully demixed, homogeneous systems:

$$f_{hom} \equiv \frac{F_{hom} - F_{ref}}{V\rho_o} \tag{2.86}$$

$$= \sum_{\kappa}^{c} \frac{\overline{\phi}_\kappa}{r_\kappa} \ln \overline{\phi}_\kappa + \chi \overline{\phi}_\alpha \overline{\phi}_\beta. \tag{2.87}$$

Here we have identified $U_{AB}\rho_{oA}\rho_{oB}/\rho_o$ as the Flory interaction parameter $\chi \equiv \chi_{AB}$, and $\overline{\phi}_\alpha$ and $\overline{\phi}_\beta$ are the average volume fractions of A and B in the system, $\overline{\phi}_\alpha = \overline{\phi}_{cA} + \overline{\phi}_{hA}$, and $\overline{\phi}_\beta = \overline{\phi}_{cB} + \overline{\phi}_{hB}$.

The remaining free energy density is that of a microphase separated system relative to the homogeneous blend. It can be written:

$$\begin{aligned} \Delta f &\equiv \frac{\Delta F}{V\rho_o} \\ &= \frac{1}{V}\int' \frac{d\boldsymbol{k}}{(2\pi)^3} \chi [\tilde{\phi}_{hA}(\boldsymbol{k}) + \tilde{\phi}_{cA}(\boldsymbol{k})][\tilde{\phi}_{hB}(-\boldsymbol{k}) + \tilde{\phi}_{cB}(-\boldsymbol{k})] - \\ &\quad \frac{1}{V}\int' \frac{d\boldsymbol{k}}{(2\pi)^3} \sum_p \tilde{\phi}_p(\boldsymbol{k}) \tilde{\omega}_p(-\boldsymbol{k}) - \sum_{\kappa}^{c} \frac{\overline{\phi}_\kappa}{r_\kappa} \ln \frac{Q_\kappa}{V}, \end{aligned} \tag{2.88}$$

and the "prime" on the integration symbol means to exclude $\boldsymbol{k} = 0$. Introduce the local volume fractions A and B at each point:

$$\phi_\alpha(\boldsymbol{r}) = \phi_{hA}(\boldsymbol{r}) + \phi_{cA}(\boldsymbol{r}), \tag{2.89}$$

and

$$\phi_\beta(\boldsymbol{r}) = \phi_{hB}(\boldsymbol{r}) + \phi_{cB}(\boldsymbol{r}), \tag{2.90}$$

which because of incompressibility satisfy $\phi_\alpha(\boldsymbol{r}) + \phi_\beta(\boldsymbol{r}) = 1$. In Fourier space they satisfy

$$\tilde{\phi}_\beta(\boldsymbol{k}) = -\tilde{\phi}_\alpha(\boldsymbol{k}) \qquad \text{for } \boldsymbol{k} \neq 0. \tag{2.91}$$

Equation 2.88 can be transformed to

$$\begin{aligned}\Delta f &= \frac{1}{V}\int' \frac{d\boldsymbol{k}}{(2\pi)^3}\chi\tilde{\phi}_\alpha(\boldsymbol{k})\tilde{\phi}_\beta(\boldsymbol{k}) - \\ &\quad \frac{1}{V}\int' \frac{d\boldsymbol{k}}{(2\pi)^3}[\tilde{\phi}_\alpha(\boldsymbol{k})\tilde{\omega}_\alpha(-\boldsymbol{k}) + \tilde{\phi}_\beta(\boldsymbol{k})\tilde{\omega}_\beta(-\boldsymbol{k})] - \\ &\quad \sum_\kappa^c \frac{\overline{\phi}_\kappa}{r_\kappa}\ln\frac{Q_\kappa}{V}. \end{aligned} \tag{2.92}$$

At this point we further approximate our expressions, by using a fourth order expansion of the free energy, which is based on an iterative solution of the modified diffusion equation [27]. This restricts work to regions where Δf is small, i.e., weak segregation limit. To facilitate the fourth order expansion, we need an expansion parameter, and we choose, $\psi_\alpha(\boldsymbol{r}) = \phi_\alpha(\boldsymbol{r}) - \overline{\phi}_\alpha$, as one, which is small near the MST. In Fourier space we have

$$\tilde{\psi}_\alpha(\boldsymbol{k}) = \tilde{\phi}_\alpha(\boldsymbol{k}) = -\tilde{\psi}_\beta(\boldsymbol{k}) = -\tilde{\psi}_\beta(\boldsymbol{k}) \quad \text{for } \boldsymbol{k} \neq 0, \tag{2.93}$$

where $\tilde{\psi}_\beta(\boldsymbol{k})$ is the Fourier transform of $\psi_\beta(\boldsymbol{r}) = \phi_\beta(\boldsymbol{r}) - \overline{\phi}_\beta$. Our goal, at this stage, is to present our derivation of the free energy expansion, Δf, up to the fourth order, using $\tilde{\phi}_\alpha(\boldsymbol{k}) \equiv \tilde{\psi}_\alpha(\boldsymbol{k})$ as an expansion parameter. This expansion itself differs from the general Hong and Noolandi expression which contains contributions from all components, i.e., hA, cA, hB and cB (for this case) [27]. For any potential $\tilde{\omega}$, not just at the saddle point, the solution of the modified diffusion equation can be given as an expansion in the $\tilde{\omega}$, which can be integrated to evaluate eq. 2.18 and 2.19 yielding

$$\begin{aligned}\frac{Q_\kappa}{V} &= 1 + \frac{(-r_\kappa)^2}{2!V}g^\kappa_{ij}\tilde{\omega}_i\tilde{\omega}_j + \\ &\quad \frac{(-r_\kappa)^3}{3!V}g^\kappa_{ijk}\tilde{\omega}_i\tilde{\omega}_j\tilde{\omega}_k + \\ &\quad \frac{(-r_\kappa)^4}{4!V}g^\kappa_{ijkl}\tilde{\omega}_i\tilde{\omega}_j\tilde{\omega}_k\tilde{\omega}_l + \cdots, \end{aligned} \tag{2.94}$$

where $i \equiv (i, \boldsymbol{k}_i)$, $\tilde{\omega}_i \equiv \tilde{\omega}_i(\boldsymbol{k}_i)$, and summation over subscripts and integration over wavevectors are implied by repeated indices. Functions $g^\kappa_{ijk\cdots l}$, given in Appendix A,

have the following form:

$$g^{\kappa}_{ijk\cdots l} = (2\pi)^3 \delta(\boldsymbol{k}_i + \boldsymbol{k}_j + \boldsymbol{k}_k + \cdots + \boldsymbol{k}_l) g^{(n)}_{\kappa,ijk\cdots l}(\boldsymbol{k}_i, \boldsymbol{k}_j, \boldsymbol{k}_k, \cdots, \boldsymbol{k}_l),$$

with $\kappa = hA, hB$ or C, and with $i = hA, hB, cA$, and cB,

$$\begin{aligned}
g^{(n)}_{hA,ijk\cdots l} \quad &\text{may be different from zero if} \quad i = j = k = \cdots = l = hA, \\
g^{(n)}_{hB,ijk\cdots l} \quad &\text{may be different from zero if} \quad i = j = k = \cdots = l = hB, \\
g^{(n)}_{c,ijk\cdots l} \quad &\text{may be different from zero if} \quad i = cA \text{ or } i = cB, \\
&\text{and} \qquad\qquad\qquad\quad j = cA \text{ or } j = cB, \\
&\text{and} \qquad\qquad\qquad\quad k = cA \text{ or } k = cB, \\
& \qquad\qquad\qquad\qquad\quad \cdots \\
&\text{and} \qquad\qquad\qquad\quad l = cA \text{ or } l = cB.
\end{aligned}$$

This means, as shown below in eq. 2.95, that $g^{(n)}_{hA,ijk\cdots l}$ couples only to $\omega_{hA}(\boldsymbol{k})$, $g^{(n)}_{hB,ijk\cdots l}$ to $\omega_{hB}(\boldsymbol{k})$, and $g^{(n)}_{c,ijk\cdots l}$ to both $\omega_{cA}(\boldsymbol{k})$ and $\omega_{cB}(\boldsymbol{k})$. The superscript n signifies an n^{th} order term in the solution of the diffusion equation.

In our calculations we expand the logarithm of Q_κ/V and truncate the series:

$$\begin{aligned}
\ln \frac{Q_\kappa}{V} \cong\ & \frac{(-\tau_\kappa)^2}{2!V} g^{\kappa}_{ij} \tilde{\omega}_i \tilde{\omega}_j + \\
& \frac{(-\tau_\kappa)^3}{3!V} g^{\kappa}_{ijk} \tilde{\omega}_i \tilde{\omega}_j \tilde{\omega}_k + \\
& \frac{(-\tau_\kappa)^4}{4!V} g^{\kappa}_{ijkl} \tilde{\omega}_i \tilde{\omega}_j \tilde{\omega}_k \tilde{\omega}_l + \\
& -\frac{(-\tau_\kappa)^4}{2(2!)^2 V^2} (g^{\kappa}_{ij} \tilde{\omega}_i \tilde{\omega}_j)^2 .
\end{aligned} \tag{2.95}$$

Subsequently, whenever in this chapter, $\ln(Q_\kappa/V)$ is encountered it is expressed implicitly or explicitly by the truncated series 2.95. After the saddle point approximation this is our second approximation involved.

For $\kappa = hA$ eq. 2.95 reads in detail as follows

$$\begin{aligned}
\ln \frac{Q_{hA}}{V} \cong\ & \frac{(-\tau_{hA})^2}{2!V} \int \frac{d\boldsymbol{k}_i}{(2\pi)^3} \frac{d\boldsymbol{k}_j}{(2\pi)^3} (2\pi)^3 \delta(\boldsymbol{k}_i + \boldsymbol{k}_j) \times \\
& g^{(2)}_{hA}(\boldsymbol{k}_i, \boldsymbol{k}_j) \tilde{\omega}_{hA}(\boldsymbol{k}_i) \tilde{\omega}_{hA}(\boldsymbol{k}_j) + \\
& \frac{(-\tau_{hA})^3}{3!V} \int \frac{d\boldsymbol{k}_i}{(2\pi)^3} \frac{d\boldsymbol{k}_j}{(2\pi)^3} \frac{d\boldsymbol{k}_k}{(2\pi)^3} (2\pi)^3 \delta(\boldsymbol{k}_i + \boldsymbol{k}_j + \boldsymbol{k}_k) \times \\
& g^{(3)}_{hA}(\boldsymbol{k}_i, \boldsymbol{k}_j, \boldsymbol{k}_k) \tilde{\omega}_{hA}(\boldsymbol{k}_i) \tilde{\omega}_{hA}(\boldsymbol{k}_j) \tilde{\omega}_{hA}(\boldsymbol{k}_k) + \\
& \frac{(-\tau_{hA})^4}{4!V} \int \frac{d\boldsymbol{k}_i}{(2\pi)^3} \frac{d\boldsymbol{k}_j}{(2\pi)^3} \frac{d\boldsymbol{k}_k}{(2\pi)^3} \frac{d\boldsymbol{k}_l}{(2\pi)^3} (2\pi)^3 \delta(\boldsymbol{k}_i + \boldsymbol{k}_j + \boldsymbol{k}_k + \boldsymbol{k}_l) \times \\
& g^{(4)}_{hA}(\boldsymbol{k}_i, \boldsymbol{k}_j, \boldsymbol{k}_k, \boldsymbol{k}_l) \tilde{\omega}_{hA}(\boldsymbol{k}_i) \tilde{\omega}_{hA}(\boldsymbol{k}_j) \tilde{\omega}_{hA}(\boldsymbol{k}_k) \tilde{\omega}_{hA}(\boldsymbol{k}_l) - \\
& \frac{(-\tau_{hA})^4}{2(2!)^2 V^2} \int \frac{d\boldsymbol{k}_i}{(2\pi)^3} \frac{d\boldsymbol{k}_j}{(2\pi)^3} \frac{d\boldsymbol{k}_k}{(2\pi)^3} \frac{d\boldsymbol{k}_l}{(2\pi)^3} (2\pi)^6 \delta(\boldsymbol{k}_i + \boldsymbol{k}_j) \delta(\boldsymbol{k}_k + \boldsymbol{k}_l) \times \\
& g^{(2)}_{hA}(\boldsymbol{k}_i, \boldsymbol{k}_j) g^{(2)}_{hA}(\boldsymbol{k}_k, \boldsymbol{k}_l) \tilde{\omega}_{hA}(\boldsymbol{k}_i) \tilde{\omega}_{hA}(\boldsymbol{k}_j) \tilde{\omega}_{hA}(\boldsymbol{k}_k) \tilde{\omega}_{hA}(\boldsymbol{k}_l). \qquad (2.96)
\end{aligned}$$

Similar expressions hold for $\ln(Q_{hB}/V)$ and $\ln(Q_c/V)$.

Using eq. 2.95 in an expansion of the last term of eq 2.92, and further simplifying by using $\tilde{\omega}_\alpha$ and $\tilde{\omega}_\beta$ in place of $\tilde{\omega}_{hA}$, etc., Δf can be expressed

$$\begin{aligned}
\Delta f \cong\ & \frac{1}{V} \int' \frac{d\boldsymbol{k}}{(2\pi)^3} \chi \tilde{\phi}_\alpha(\boldsymbol{k}) \tilde{\phi}_\beta(\boldsymbol{k}) - \\
& \frac{1}{V} \int' \frac{d\boldsymbol{k}}{(2\pi)^3} [\tilde{\phi}_\alpha(\boldsymbol{k}) \tilde{\omega}_\alpha(-\boldsymbol{k}) + \tilde{\phi}_\beta(\boldsymbol{k}) \tilde{\omega}_\beta(-\boldsymbol{k})] - \\
& \frac{1}{2V} \mathcal{G}_{ij} \tilde{\omega}_i \tilde{\omega}_j + \\
& \frac{1}{6V} \mathcal{G}_{ijk} \tilde{\omega}_i \tilde{\omega}_j \tilde{\omega}_k - \\
& \frac{1}{24V} \mathcal{G}_{ijkl} \tilde{\omega}_i \tilde{\omega}_j \tilde{\omega}_k \tilde{\omega}_l, \qquad (2.97)
\end{aligned}$$

with the coefficients given in Appendix A; i, j, k and $l = \alpha$ or β. This expression for Δf is our new result, which together with the subsequent calculations constitute our modification of the Hong and Noolandi theory.

We need to relate the density distributions to the potentials. Since eq 2.95 is valid for *any* potential, it can be differentiated as indicated in eq. 2.82, and then the derivatives

can be evaluated at the saddle point. This results in saddle point expressions for each of the four densities, $\langle\hat{\rho}_p\rangle$, or equivalently the $\tilde{\phi}_p$, given in terms of only two potentials, $\tilde{\omega}_\alpha$ and $\tilde{\omega}_\beta$. For homopolymer p, where $p = hA$ or hB, we obtain

$$\begin{aligned}\tilde{\phi}_p(\boldsymbol{k}) \;\cong\; & -r_p\overline{\phi}_p g^p_{pj}\tilde{\omega}_j + \frac{1}{2}r_p^2\overline{\phi}_p g^p_{pjk}\tilde{\omega}_j\tilde{\omega}_k - \\ & \frac{1}{6}r_p^3\overline{\phi}_p(g^p_{pjkl} - \frac{3}{V}g^p_{pj}g^p_{kl})\tilde{\omega}_j\tilde{\omega}_k\tilde{\omega}_l,\end{aligned} \tag{2.98}$$

and similarly for copolymer cA and cB,

$$\begin{aligned}\tilde{\phi}_{cA}(\boldsymbol{k}) \;\cong\; & -r_c\overline{\phi}_c g^c_{Aj}\tilde{\omega}_j + \frac{1}{2}r_c^2\overline{\phi}_c g^c_{Ajk}\tilde{\omega}_j\tilde{\omega}_k - \\ & \frac{1}{6}r_c^3\overline{\phi}_c(g^c_{Ajkl} - \frac{3}{V}g^c_{Aj}g^c_{kl})\tilde{\omega}_j\tilde{\omega}_k\tilde{\omega}_l,\end{aligned} \tag{2.99}$$

and

$$\begin{aligned}\tilde{\phi}_{cB}(\boldsymbol{k}) \;\cong\; & -r_c\overline{\phi}_c g^c_{Aj}\tilde{\omega}_j + \frac{1}{2}r_c^2\overline{\phi}_c g^c_{Bjk}\tilde{\omega}_j\tilde{\omega}_k - \\ & \frac{1}{6}r_c^3\overline{\phi}_c(g^c_{Bjkl} - \frac{3}{V}g^c_{Bj}g^c_{kl})\tilde{\omega}_j\tilde{\omega}_k\tilde{\omega}_l,\end{aligned} \tag{2.100}$$

where $j, k, l = \alpha$ or β. Adding pairs of these expressions as indicated in eq. 2.89 and 2.90, yields, for $\boldsymbol{k} \neq 0$,

$$\tilde{\phi}_\alpha(\boldsymbol{k}) \cong -\mathcal{G}_{\alpha j}\tilde{\omega}_j + \frac{1}{2}\mathcal{G}_{\alpha jk}\tilde{\omega}_j\tilde{\omega}_k - \frac{1}{6}\mathcal{G}_{\alpha jkl}\tilde{\omega}_j\tilde{\omega}_k\tilde{\omega}_l, \tag{2.101}$$

and

$$\tilde{\phi}_\beta(\boldsymbol{k}) \cong -\mathcal{G}_{\beta j}\tilde{\omega}_j + \frac{1}{2}\mathcal{G}_{\beta jk}\tilde{\omega}_j\tilde{\omega}_k - \frac{1}{6}\mathcal{G}_{\beta jkl}\tilde{\omega}_j\tilde{\omega}_k\tilde{\omega}_l, \tag{2.102}$$

where $i, j, k = \alpha$ or β, and $\mathcal{G}$'s are the same as in eq. 2.97.

Finally, inverting these series eq. 2.101 and 2.102, yields $\tilde{\omega}_\alpha$ and $\tilde{\omega}_\beta$ in terms of $\tilde{\phi}_\alpha$ and $\tilde{\phi}_\beta$, which up to the third order is

$$\tilde{\omega}_\alpha(\boldsymbol{k}) \cong \Gamma^2_{\alpha i}\tilde{\phi}_i + \Gamma^3_{\alpha ij}\tilde{\phi}_i\tilde{\phi}_j + \Gamma^4_{\alpha ijk}\tilde{\phi}_i\tilde{\phi}_j\tilde{\phi}_k, \tag{2.103}$$

$$\tilde{\omega}_\beta(\boldsymbol{k}) \cong \Gamma^2_{\beta i}\tilde{\phi}_i + \Gamma^3_{\beta ij}\tilde{\phi}_i\tilde{\phi}_j + \Gamma^4_{\beta ijk}\tilde{\phi}_i\tilde{\phi}_j\tilde{\phi}_k, \tag{2.104}$$

where $i, j, k = \alpha$ or β, and Γ's are given in Appendix A. Substituting eq. 2.103 and 2.104 into eq. 2.97, we have

$$\begin{aligned}\Delta f \;\cong\; & {\sum_{\boldsymbol{k}_1}}' f^{(2)}(\boldsymbol{k}_1,-\boldsymbol{k}_1)\tilde{\phi}_\alpha(\boldsymbol{k}_1)\tilde{\phi}_\alpha(-\boldsymbol{k}_1)+ \\ & {\sum_{\boldsymbol{k}_1,\boldsymbol{k}_2}}' f^{(3)}(\boldsymbol{k}_1,\boldsymbol{k}_2,-\boldsymbol{k}_1-\boldsymbol{k}_2)\tilde{\phi}_\alpha(\boldsymbol{k}_1)\tilde{\phi}_\alpha(\boldsymbol{k}_2)\tilde{\phi}_\alpha(-\boldsymbol{k}_1-\boldsymbol{k}_2)+ \\ & {\sum_{\boldsymbol{k}_1,\boldsymbol{k}_2,\boldsymbol{k}_3}}' f^{(4)}(\boldsymbol{k}_1,\boldsymbol{k}_2,\boldsymbol{k}_3,-\boldsymbol{k}_1-\boldsymbol{k}_2-\boldsymbol{k}_3)\times \\ & \tilde{\phi}_\alpha(\boldsymbol{k}_1)\tilde{\phi}_\alpha(\boldsymbol{k}_2)\tilde{\phi}_\alpha(\boldsymbol{k}_3)\tilde{\phi}_\alpha(-\boldsymbol{k}_1-\boldsymbol{k}_2-\boldsymbol{k}_3), \end{aligned} \tag{2.105}$$

where the "prime" on the sums means to exclude $\boldsymbol{k}_i = 0$. The coefficients $f^{(2)}$, $f^{(3)}$ and $f^{(4)}$ are listed in Appendix A. This is the many wavenumber fourth order expansion of the free energy which can be approximately minimized as described in chapter 4. If we restrict to only one wavenumber in this expansion then the minimization procedure is significantly simplified as presented in chapter 5. Let us summarize, at this point, the differences between our approach and the Hong and Noolandi theory. First, due to special choice of blends, i.e., *A-b-B/A/B*, and χ parameters, we have reduced the number of saddle point potentials from 4 to 2, eq. 2.69 and 2.70. We have combined the densities of monomers of the same type, eq. 2.89 and 2.90, and expressed Δf, eq. 2.92, only in terms of two monomer densities. Next, using the incompressibility condition and expressing ω's in terms of ϕ's, eq. 2.103 and 2.104, we have obtained an expression for Δf, eq. 2.105, which allows us to calculate the free energy as a function of *A*-monomer density profile. This compares with the Hong and Noolandi expression for Δf which includes summation over all four components, i.e., hA, cA, hB and cB, with possible reduction to three components if the incompressibility condition is used.

Formally equations 2.103, and 2.104 could have also been derived by differentiating

equation 2.97 and equating them to zero

$$\frac{\delta \Delta f}{\delta \tilde{\omega}_\alpha(-\boldsymbol{k})} = 0, \tag{2.106}$$

$$\frac{\delta \Delta f}{\delta \tilde{\omega}_\beta(-\boldsymbol{k})} = 0. \tag{2.107}$$

2.4 Small Angle X-Ray Scattering from Copolymer/Homopolymer Blends

We start this section by sketching the derivation of an expression for the density-density correlation function, $\tilde{S}(\boldsymbol{k},-\boldsymbol{k})$, for an incompressible copolymer/homopolymer blend, *A-b-B/A/B*, in the disordered state, i.e., above the MST. This function is known [10] to be proportional to the elastic scattering intensity, $I(\boldsymbol{k})$, which can be measured experimentally by Small Angle X-Ray Scattering (SAXS), Small Angle Neutron Scattering (SANS) or light scattering.

The free energy, Δf, can be written, to the lowest order, using equation 2.105 as

$$\Delta f \cong \frac{1}{2}\sum_{\boldsymbol{k}}{}' \; 2\; f^{(2)}(\boldsymbol{k},-\boldsymbol{k})\langle\frac{\hat{\rho}_\alpha(\boldsymbol{k})}{\rho_{oA}}\rangle\langle\frac{\hat{\rho}_\alpha(-\boldsymbol{k})}{\rho_{oA}}\rangle, \tag{2.108}$$

where $\langle\hat{\rho}_\alpha(\boldsymbol{k})\rangle/\rho_{oA}$ is $\tilde{\phi}_\alpha(\boldsymbol{k})$, i.e., the Fourier transform of the monomer A density profile, $\phi_\alpha(\boldsymbol{r})$, given by eq. 2.89. The density-density correlation function, $\tilde{S}(\boldsymbol{k},-\boldsymbol{k})$, for an incompressible, *A-b-B/A/B*, copolymer/homopolymer blend is defined as

$$\tilde{S}(\boldsymbol{k},-\boldsymbol{k}) \equiv \langle\frac{\hat{\rho}_\alpha(\boldsymbol{k})}{\rho_{oA}}\frac{\hat{\rho}_\alpha(-\boldsymbol{k})}{\rho_{oA}}\rangle, \tag{2.109}$$

or equivalently

$$\tilde{S}(\boldsymbol{k},-\boldsymbol{k}) \equiv \langle\frac{\hat{\rho}_\beta(\boldsymbol{k})}{\rho_{oB}}\frac{\hat{\rho}_\beta(-\boldsymbol{k})}{\rho_{oB}}\rangle = -\langle\frac{\hat{\rho}_\alpha(\boldsymbol{k})}{\rho_{oA}}\frac{\hat{\rho}_\beta(-\boldsymbol{k})}{\rho_{oB}}\rangle. \tag{2.110}$$

Next we use a well known relation, from the general thermodynamic theory [60], between density-density correlation function and the quadratic coefficient in the free energy expansion, eq. 2.108,

$$\tilde{S}(\boldsymbol{k},-\boldsymbol{k}) \equiv \langle\frac{\hat{\rho}_\alpha(\boldsymbol{k})}{\rho_{oA}}\frac{\hat{\rho}_\alpha(-\boldsymbol{k})}{\rho_{oA}}\rangle = \frac{1}{2\; f^{(2)}(\boldsymbol{k},-\boldsymbol{k})}\;. \tag{2.111}$$

Using the expressions for $f^{(2)}(\boldsymbol{k},-\boldsymbol{k})$ from Appendix A, this can be expressed in Leibler's notation, [11, 71], as

$$\tilde{S}(\boldsymbol{k},-\boldsymbol{k}) = \frac{W(\boldsymbol{k})}{S(\boldsymbol{k}) - 2W(\boldsymbol{k})\chi}\;, \tag{2.112}$$

with

$$S(\boldsymbol{k}) = \mathcal{G}_{\alpha\alpha}(\boldsymbol{k}) + 2\mathcal{G}_{\alpha\beta}(\boldsymbol{k}) + \mathcal{G}_{\beta\beta}(\boldsymbol{k}) \tag{2.113}$$

$$W(\boldsymbol{k}) = \mathcal{G}_{\alpha\alpha}(\boldsymbol{k}) + \mathcal{G}_{\beta\beta}(\boldsymbol{k}) - \mathcal{G}_{\alpha\beta}(\boldsymbol{k})\mathcal{G}_{\alpha\beta}(\boldsymbol{k}), \tag{2.114}$$

where functions the $\mathcal{G}_{ij}(\boldsymbol{k})$ are given by eq. A.19.

Thus the scattering intensity can be presented as

$$I(k) \propto [\frac{S(k)}{W(k)} - 2\chi]^{-1}, \tag{2.115}$$

where k is the magnitude of the scattering vector $\boldsymbol{k}$, $k = 4\pi\lambda^{-1}\sin(\theta/2)$, λ is the wavelength of radiation, and θ the scattering angle. For pure copolymer ($\overline{\phi}_c = 1$) the calculated scattering intensity, $I(k)$, has a simple asymptotic form in both short and long wavelength limits:

$$I(k) \propto k^2 \quad \text{for small } k, \tag{2.116}$$

$$I(k) \propto k^{-2} \quad \text{for large } k. \tag{2.117}$$

Since $I(k)$ goes to zero in both limits, there is a maximum in $I(k)$, at k^*, which corresponds to a characteristic length, which is on the order of the radius of gyration. For copolymer/homopolymer blends the shortwave length limit is not necessarily zero but the maximum of $I(k)$ may still appear at some nonzero k^*, [10], indicating microphase separation. Otherwise, the maximum is at $k = 0$ which indicates the onset of macrophase separation of the blend. As the MST is approached the inverse of the maximum value of the scattering intensity, $[I(k^*)]^{-1}$, becomes very small, while $I(k^*)$ grows very large. Experimentally, the MST can be recognised by investigating the temperature dependence of $I(k^*)$. For every temperature, T, above the MST, one can measure the elastic scattering intensity, $I(k)$, by changing the scattering angle, θ. Then one can fit, by statistical methods, a value of χ which corresponds to the curve $I(k)$. In order to determine χ of high

molecular weight copolymers one can add neutral solvent, e.g., DOP (dioctlylphthalate) for *PS-b-PI/PI* [10], as elucidated in section 4.4. If, however, the molecular weights are sufficiently low then this is not necessary. It occurs that χ, determined experimentally by this method, is in most cases a linear function of T^{-1}, i.e.,

$$\chi = A + \frac{B}{T}, \tag{2.118}$$

with positive B. Hashimoto and coworkers [10] fitted the elastic scattering intensity to analytical form of $I(k)$ given by eq. 2.115, for different temperatures for a series of styrene/isoprene copolymer blends described in more detail in section 4.4. They found that χ depends linearly on T^{-1} for given volume fractions and degrees of polymerization. However, as they changed concentrations and molecular weights they also found dependencies on volume fractions and degrees of polymerization. The general functional form of this dependence is discussed in section 4.4. The polydispersity of individual components of copolymer/homopolymer blends also has its influence on the χ parameter, fitted, for a given temperature, to equation 2.115. Due to the fluctuation effects, mentioned in the Introduction in the context of Fredrickson and Helfand work [61], further complications arise when the MST is approached. If χ was always inversely proportional to temperature and the mean field theory always correct then, since functions $W(k)$ and $S(k)$ are independent of temperature, one would always have the following scaling relation

$$[I(k^*)]^{-1} \sim T^{-1} + \text{const.} \tag{2.119}$$

As, however, Bates et al. [72] have found in one set of experiments, this is not necessarily the case when the MST is approached. The inverse of the scattering intensity, $[I(k^*)]^{-1}$, is essentially nonlinear in T^{-1}. They managed to explain the discrepancy with mean field predictions by using Fredrickson and Helfand theory [61] discussed in the Introduction. Since we cannot calculate either χ or its dependencies, mentioned above, from the mean

field theory, χ should be taken from experiments as described in section 4.4. In this thesis we assume that for a given system χ is independent of concentration and do not attempt to relate it to the other quantities.

This preceding discussion shows one advantage of using the energy expansion, even only to the second order, compared with the numerical self-consistent approach which does not provide so much insight into the scattering properties of the copolymer blends.

Chapter 3

Lamellar Structure of Copolymer/Solvent Blends

3.1 Introduction

In this chapter we discuss some of the properties of diblock copolymer/selective solvent, *A-b-B/S*, blends using the full self-consistent theory developed by Hong and Noolandi [33, 52], and presented with slight modifications in section 2.2. We assume that layers are the equilibrium structure, even if, in the case of model calculations of subsection 3.2.1 this assumption may not always be justified. Using this approach, we explore the behaviour of these blends in both the strong and weak segregation regimes. We limit ourselves to overall volume fraction ratios of monomers of type A and B, A:B, close to 50:50, since we restrict attention to lamellar morphology.

The work of this chapter is complementary to that of Whitmore and Noolandi which is described in reference [30] where they investigated the properties of copolymer/nonselective solvent blends, and also in reference [73] which dealt, primarily, with properties of crystallizable block copolymers. By a perfectly nonselective (or neutral) solvent, s, we mean a solvent which is equally compatible with both species of monomers (A and B). In terms of Flory interaction parameters it can be expressed as

$$\chi_{AS} = \chi_{BS}. \tag{3.1}$$

Whitmore and Noolandi performed a series of calculations with values of χ_{AS} ranging from 0 to 0.3, but with $\chi_{AS} = \chi_{BS}$. They found that the results did not depend on χ_{AS}. Then they did series of model calculations with $\chi_{AS} = \chi_{BS} = 0$, varying the interaction

parameter, χ_{AB}, copolymer volume fractions and degrees of polymerization:

$$0.05 \leq \quad \chi_{AB} \quad \leq 0.3, \tag{3.2}$$

$$100 \leq \quad Z_c \quad \leq 2000, \tag{3.3}$$

$$0.1 \leq \quad \overline{\phi}_c \quad \leq 0.9, \tag{3.4}$$

$$12 \lesssim \quad \chi_{AB} Z_c \overline{\phi}_c \quad \leq 480. \tag{3.5}$$

They presented two series of calculated density profiles, and investigated the behaviour of the domain thickness in the strong and weak segregation regimes. Whitmore and Noolandi found that solvent is distributed almost uniformly, with a tiny maximum at the interface between lamellar subdomains. This uniformity is the basis of the *dilution approximation* which assumes that the interaction χ_{AB} parameter becomes weakened by the presence of nonselective solvent from χ_{AB} for pure copolymer to $\chi_{AB}\overline{\phi}_c$ for the blend. Thus in the mean field approximation (for model systems) the product $Z_c\chi_{AB}\overline{\phi}_c$ plays the role which is nearly equivalent to that of the $\chi_{AB}Z_c$ for pure copolymer. In particular, the calculated MST (for symmetric copolymers) was reported at $\chi_{AB}\overline{\phi}_c Z_c = 10.5$, in agreement with Leibler's result, eq. 1.2, for pure copolymer melt. Furthermore, they presented two examples of real system calculations for polystyrene-polyisoprene block copolymer/toluene (nonselective solvent), *PS-b-PI*/Toluene, blends with realistic χ parameters, densities, Kuhn lengths and degrees of polymerization. In this case, toluene is almost perfectly nonselective, with $\chi_{PS-TOL} = 0.44$ and $\chi_{PI-TOL} = 0.40$. They showed the density profiles for this system in the strong ($Z_c\chi\overline{\phi}_c \simeq 80$ and $\overline{\phi}_c = 0.4$) and relatively weak ($Z_c\chi\overline{\phi}_c \simeq 20$ and $\overline{\phi}_c = 0.1$) segregation regimes. Closer to the MST the solvent density distribution was almost uniform, without local maximum at the interface, while in some cases in the strong segregation regime the solvent density profile had a small but definite maximum.

In this chapter we report two sets of calculations. First, we compare our work with

one of the systematic series of model calculation of Whitmore and Noolandi. We assume $\chi_{BS} = \chi_{AB}$ and $\chi_{AS} = 0$ to contrast with nonselective solvent case, $\chi_{AS} = \chi_{BS} = 0$. Second, we perform systematic studies of a real system, *PS-b-PBD*/Styrene, the blend studied by Hong and Noolandi in the context of interfacial tension [74]. In the model calculations the selective solvent, s, is assumed to be identical with monomers constituting block cA with $\chi_{AS} = 0$. In real systems, however, this is not always the case, e.g. the polystyrene-styrene interaction is close to 0.5 [76]. (Fully self-consistent calculations for copolymer/selective solvent are also carried out in subsection 4.3.1 to compare the many wavenumber fourth order expansion approach with this method.)

The problem to be solved is the following. For a given copolymer/solvent blend, we wish to calculate the equilibrium domain thickness, d, the density profiles and the free energy. We specify all bulk densities, ρ_{op}, Kuhn lengths, b_p, degrees of polymerization, Z_p, interaction parameters, $\chi_{pp'}$, and volume fractions $\overline{\phi}_p$. Next, we assume some value of d and solve the self-consistent problem, eq. 2.58, and 2.60 with analogous equations for $\phi_{cB}(\mathbf{r})$ and $\omega_{cB}(\mathbf{r})$, along with the diffusion equation, eq. 2.16, for both cA and cB. From the converged solutions we calculate ΔF. Then, varying d, we repeat the procedure until we find the minimum of ΔF with respect to d. This gives us the equilibrium d, the density profiles, and ΔF for this system. We investigate here the variation of the equilibrium structure with $\overline{\phi}_c$, Z_c, and χ_{AB} for different systems. For a given blend we repeat the above procedure changing either $\overline{\phi}_c$, Z_c or χ_{AB}.

In the layered structure, the problem is one-dimensional with period d; hence we need to solve the diffusion equation for the functions $\overline{Q}_p(x,\tau|x')$ and $q_p(x,\tau)$ in the spatial interval $[0,d]$ and for $\tau\epsilon[0,1]$. To do so, these intervals are discretized into $N = 202$ and $M = 410$ equal subintervals respectively. We use an iterative procedure to find the self-consistent solution. At each iteration we have potentials $\omega_p^{(n)}(x)$ for which we solve the diffusion equation for $\overline{Q}_p^{(n)}$ and $q_p^{(n)}$, and calculate the volume fractions $\phi_{cA}^{(n)}(x)$ and

$\phi_{cB}^{(n)}(x)$, eq. 2.58, in one dimension. From these and the incompressibility condition, eq 2.51, we calculate $\phi_s^{(n)}(x)$, and then predict new potentials $\omega_p^{(n+1)}(x)$ from eq. 2.60. We iterate until the maximum error at any point is less than a prescribed value,

$$\max_{(x,p)} |\omega_p^{(n+1)}(x) - \omega_p^{(n)}(x)| < \delta \tag{3.6}$$

with $\delta = 10^{-7}$. The free energy is calculated from eq 2.48 using the converged solution.

The numerical scheme for solving the diffusion-type partial differential equations is based on the method of Crank and Nicholson described in reference [75]. We verified that the accuracy in the solutions to the modified diffusion equation and resulting density profiles is on the order of 6 significant figures.

3.2 Results

3.2.1 Model Calculations

In this subsection we discuss the variations of the domain thickness for copolymer/selective solvent blends. These are the model calculations so that all densities, ρ_{op}, are equal, and the Kuhn lengths for cA and cB are the same $b_A = b_B = b$. Moreover the diblock copolymer is symmetric, i.e. $Z_{cA} = Z_{cB} = Z_c/2$.

Figures 3.1, 3.2 and 3.3 show the dependence of the equilibrium layer thickness on copolymer volume fraction, $\overline{\phi}_c$ degree of polymerization Z_c, and interaction parameter, χ_{AB}, on "log-log" plots. The fact that all curves are nearly straight lines suggests that d/b scales approximately as powers Z_c, $\overline{\phi}_c$ and χ_{AB}, but with slightly varying exponents.

Figures 3.1 and 3.2 show the dependence of domain thickness, d, on the copolymer volume fraction, $\overline{\phi}_c$, ranging from 0.2 to 0.8 or 0.9, and on the degree of polymerization, Z_c, ranging from 200 to 2000. The interaction parameter, χ_{AB} is set to be equal to 0.1. The dependence of d on χ_{AB} for various Z_c and $\overline{\phi}_c$ is shown in figure 3.3. These results can be summarized approximately by

$$d/b \propto [\chi_{AB}]^p [Z_c]^q [\overline{\phi}_c]^r, \tag{3.7}$$

but with exponents which vary. In the strong segregation regime we find

$$p \simeq 0.2 \quad q \simeq 0.7 \quad r \simeq 0.2. \tag{3.8}$$

These exponents are virtually the same as the ones for copolymer/neutral solvent blends [30]. For all three cases, we find that the strongest dependence occurs in the weak segregation limit, with

$$p \simeq 0.5 \quad q \simeq 0.9 \quad r \simeq 0.5. \tag{3.9}$$

These differ from the values reported by Whitmore and Noolandi for this regime who obtained $p \simeq 1/3$, $q \simeq 0.8$ and $r \simeq 0.4$, compared to our values of p, q and r given

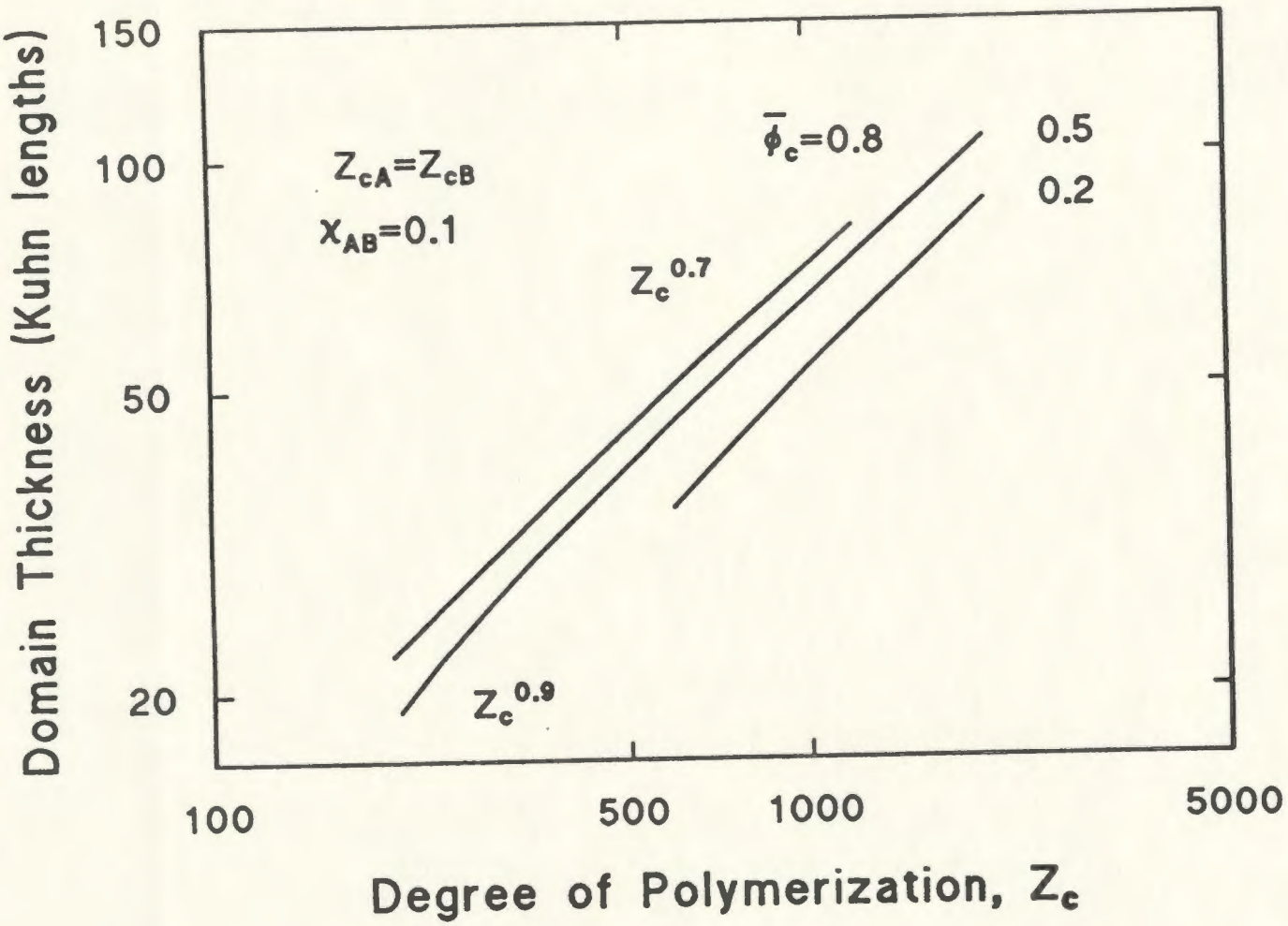

Figure 3.1: Equilibrium domain thickness, in units of Kuhn statistical lengths, as a function of copolymer degree of polymerization for three values of copolymer volume fraction $\bar{\phi}_c$, and for $\chi_{AB} = 0.1$. In the weak segregation regime, d varies approximately as $d \propto [Z_c]^{0.9}$, but the dependence weakens slightly in the strong segregation regime, approaching $d \propto [Z_c]^{0.7}$.

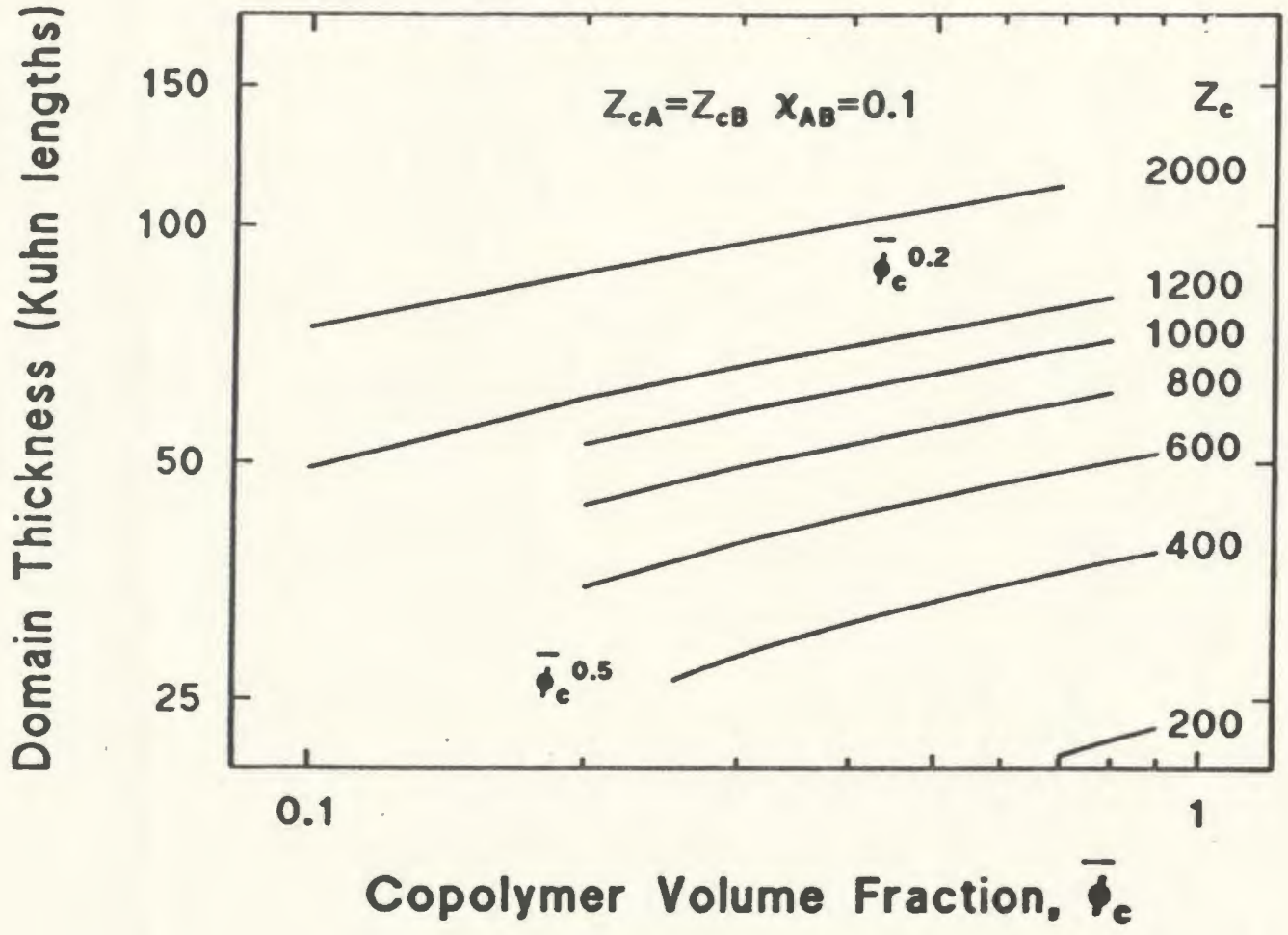

Figure 3.2: Equilibrium domain thickness d as a function of overall copolymer volume fraction $\bar{\phi}_c$ for $\chi_{AB} = 0.1$ and different degrees of polymerization Z_c. The lower left hand corner of the diagram, which is for small product of Z_c and $\bar{\phi}_c$, corresponds to the weak segregation regime. Here the curve for $Z_c = 400$ terminates at the value of $\bar{\phi}_c$ which corresponds to the MST. In this region the domain thickness, d, scales approximately as $d \propto [\bar{\phi}_c]^r$, with r approaching 0.5. Moving to higher copolymer content or higher Z_c corresponds to the strong segregation regime, where the dependence of d on $\bar{\phi}_c$ weakens to $d \propto [\bar{\phi}_c]^{0.2}$.

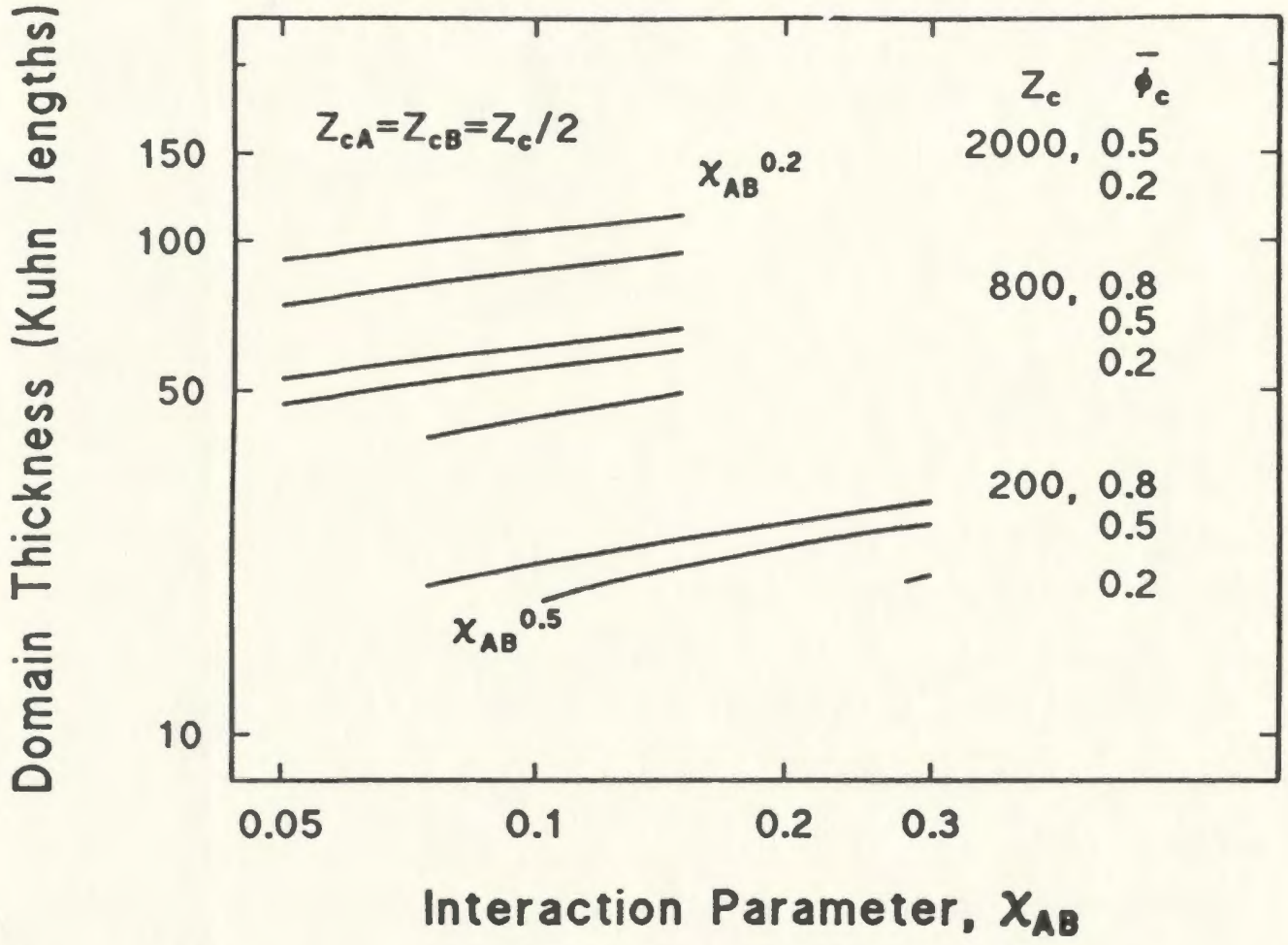

Figure 3.3: Equilibrium domain thickness, d, as a function of χ_{AB} for three copolymer volume fraction, $\bar{\phi}_c$, and three degrees of polymerization Z_c. Towards the weak segregation limit, d varies approximately as $d \propto [\chi_{AB}]^{0.5}$, but the dependence weakens in the strong segregation regime, to $d \propto [\chi_{AB}]^{0.2}$.

in eq. 3.9. However these differences do not reflect differences between selective and nonselective case. For the current work we have developed an improved version of the programme for self-consistent calculations which has allowed us to perform calculations closer to the MST. Thus the difference between the exponents may be attributed to the fact that we have explored the scaling behaviour in a very close proximity of the MST, whereas Whitmore and Noolandi [30] averaged over a broader range near the MST in their calculations. In particular, in figure 3.2, we have extended the curve for $Z_c = 400$ up to the MST, which is at $\overline{\phi}_c = 0.253$ while they varied $\overline{\phi}_c$ from 0.3 to 0.9. Similarly, for the $\overline{\phi}_c = 0.5$ curve on figure 3.1, they varied Z_c from 300 to 2000 while the MST determined by the improved version of the programme is at $Z_c = 205$. Finally the $Z_c = 200$, $\overline{\phi}_c$ curve of figure 3.3 has been extended to the MST at $\chi_{AB} = 0.102$ from the previous value of $\chi_{AB} = 0.15$ used by Whitmore and Noolandi in their calculations. If, however, we use the same minimum values of $\overline{\phi}_c$, Z_c and χ_{AB}, used by them instead of the MST values, for the model calculations summarized in figures, 3.1, 3.2 and 3.3, then the exponents are identical with those of Whitmore and Noolandi also in the weak segregation regime. As already mentioned in the previous section, we assumed the lamellar structure throughout, although very near the MST this assumption is probably not always satisfied. The exponent q has been determined experimentally (Small Angle Neutron Scattering) by Almdal et al. [37] in the vicinity of the MST as 0.8. This is the same as the value determined by Whitmore and Noolandi and close to our value in weak segregation.

3.2.2 Real System Calculations

In the previous subsection, solvent-polymer interactions were unrealistically small. In this subsection we investigate the properties of *PS-b-PBD/S* blend, where *PS* stands for polystyrene, *PBD* for polybutadiene, and *S* for styrene solvent (styrene monomers). The numerical values of densities, χ parameters, and Kuhn lengths are taken from references [74] and [76]:

$$\chi_{PS-S} = 0.49 \qquad \chi_{PBD-S} = 0.29 \qquad \chi_{PS-PBD} = 0.024 \tag{3.10}$$

$$\rho_{PBD} = 10.6 \text{ nm}^{-3} \qquad \rho_{PS} = 6.07 \text{ nm}^{-3} \qquad \rho_{S} = 5.25 \text{ nm}^{-3} \tag{3.11}$$

$$b_{PBD} = 0.68 \text{ nm} \qquad b_{PS} = 0.68 \text{ nm} \quad . \tag{3.12}$$

From numerical values of χ parameters we can conclude that styrene solvent, S, is more compatible with PBD than it is with PS. Therefore styrene, S, can be considered as a selective solvent. It is interesting, however, that χ_{PS-S} is greater than χ_{PBD-S} so that the styrene solvent tends to be preferentially localized in PBD subdomains for microphase separated blends.

One of our objectives is the calculation of d vs Z_c and $\overline{\phi}_c$ for the lamellar structure. In order to do so we needed an estimate of the values of Z_{cPS} and Z_{cPBD} for which layers are stable over a range of $\overline{\phi}_c$ for this blend. This was provided by Mr. J. Vavasour who did self-consistent calculations for lamellar and cylindrical structures, locating the the phase boundaries between the lamellae and cylinders. He found, varying $\overline{\phi}_c$, that blends with copolymers having blocks of equal volume fractions, $f_{PS} = f_{PBD} = 0.5$, yields consistently the lamellar equilibrium structure below the MST, although he did not investigate very close to the MST. This corresponds to $Z_{PS} = 0.364 Z_c$ and $Z_{PBD} = 0.636 Z_c$ which we use throughout this subsection. Next, in order to demonstrate that the blends we consider do not macrophase separate, we have also calculated the total free

energy density

$$f(\overline{\phi}_c) = f_{hom} + \Delta f, \tag{3.13}$$

where $\Delta f = \Delta F/(V\rho_o)$ and f_{hom} is the free energy density of a uniform, homogeneous blend relative to a fully demixed, homogenous system (the free energy of mixing), as in equation 2.86. We have verified that the curvature of $f(\overline{\phi}_c)$ was positive for all $\overline{\phi}_c$, i.e. the blend was stable with respect to macrophase separation as elucidated in reference [29] and also in chapter 5. Subsequently we present our calculations for the *PS-b-PBD/S* blend varying $\overline{\phi}_c$ and Z_c.

Figures 3.4 and 3.5 show the equilibrium domain thickness as a function of copolymer degree of polymerization for three different copolymer volume fractions, and as a function of $\overline{\phi}_c$ for four different copolymer degrees of polymerization, respectively, keeping fixed Z_{cPS}/Z_c and Z_{cPBD}/Z_c. For pure copolymers with $f_A = f_B = 0.5$, but with different bulk densities, Whitmore and Noolandi [29] showed that the microphase separation occurs if

$$r_c\chi_{AB} \geq 10.5, \tag{3.14}$$

where r_c is given by eq. 2.77. For copolymer, *PS-b-PBD*, considered in this subsection, we have $r_c = 0.63Z_c$. We estimated the order-disorder transition for this blend with $\overline{\phi}_c = 0.8$ and 0.2, finding $r_c\chi = 11.6$ for $\overline{\phi}_c = 0.8$, and 20 for $\overline{\phi}_c = 0.2$. This shows that added S tends to dissolve the microphase. On the other hand, the product $r_c\chi\overline{\phi}_c$ at the MST decreases from about 10.5 to 9.3 (for $\overline{\phi}_c = 0.8$), and to 4 (for $\overline{\phi}_c = 0.2$). This compares with the copolymer/neutral solvent case, in which, at the MST, $r_c\chi$ would need to increase to 13 and 52.5, and $r_c\chi\overline{\phi}_c$ would remain constant at 10.5. This demonstrates a difference between selective and nonselective cases.

Turning now to the scaling in the weak segregation regime, with the product $r_c\chi\overline{\phi}_c = 4.2$, for the first point, we calculate $q \simeq 0.9$, which is close to the model calculation result, and the dependence weakens in the strong segregation where $q \simeq 0.7$, which,

again, is the same as for the model calculations both in our work as well as in reference [30]. On the other hand, $p \simeq 0.2$ in the weak segregation regime, while the dependence weakens in the strong segregation with $p \simeq 0.03$. This represents a significant departure from the model calculation exponents. The reason for the small values of exponents may be the relatively small value of χ_{PS-PBD} compared with χ_{PS-S} and χ_{PBD-S}. This might result in weakened dependence of the "effective" χ_{PS-PBD} parameter on copolymer volume fraction, compared with the dilution approximation, and consequently the smaller exponents. To explore this point we show a panel of density profiles for $Z_c = 1600$ with seven copolymer volume fractions, figure 3.6. The first panel of figure 3.6 shows the copolymer and solvent density profiles for $\overline{\phi}_c = 0.2$ in weak segregation. The solvent is preferentially localized in the *PBD* subdomain, but the variation of the solvent density is small. If the dilution approximation [27] were valid for this blend then it would be a homogenous one, with $r_c\chi\overline{\phi}_c = 4.9 < 10.5$, where $\overline{\phi}_c = 0.2$ and, again, $\chi \equiv \chi_{PS-PBD}$. Next $\overline{\phi}_c$ is increased gradually from 0.2 to 0.8. The solvent remains preferentially localized in the PBD subdomain with small variations of density profiles, with the maximum variation for $\overline{\phi}_c = 0.5$ of about ± 0.04. The density profiles of the corresponding blocks, i.e. *PS* and *PBD*, show increasing localization in the respective subdomains, but degree of segregation and the layer thickness increase more slowly than in the case of the density profiles shown by Whitmore and Noolandi [29]. This is reflected in the small value of p in the strong segregation regime. Unlike the nonselective case, no local maxima are visible at the interface between subdomains.

To summarize briefly, in this chapter we have found that, for the model systems studied, the scaling behaviour of the layer thickness is the same for the selective and non-selective solvent cases. For *PS-b-PBD/S* blend, the selective solvent was preferentially localized in the favorable subdomain, without the local maxima at the interfaces which were found in model calculations for the nonselective solvent case [30]. The behaviour

differs significantly from that for neutral solvent as represented by the dilution approximation. However, the solvent density variations were small in both cases. The scaling of d with Z_c, as expressed by the exponent q for the *PS-b-PSB* blend was the same as for the model calculations, while the scaling with $\overline{\phi}_c$ differed; p was significantly smaller, particularly in the strong segregation. For the *PS-PBD/S* blend, the product $r_c\overline{\phi}_c\chi$ at the MST was found to be smaller from that for the neutral solvent case, especially for low copolymer volume fraction.

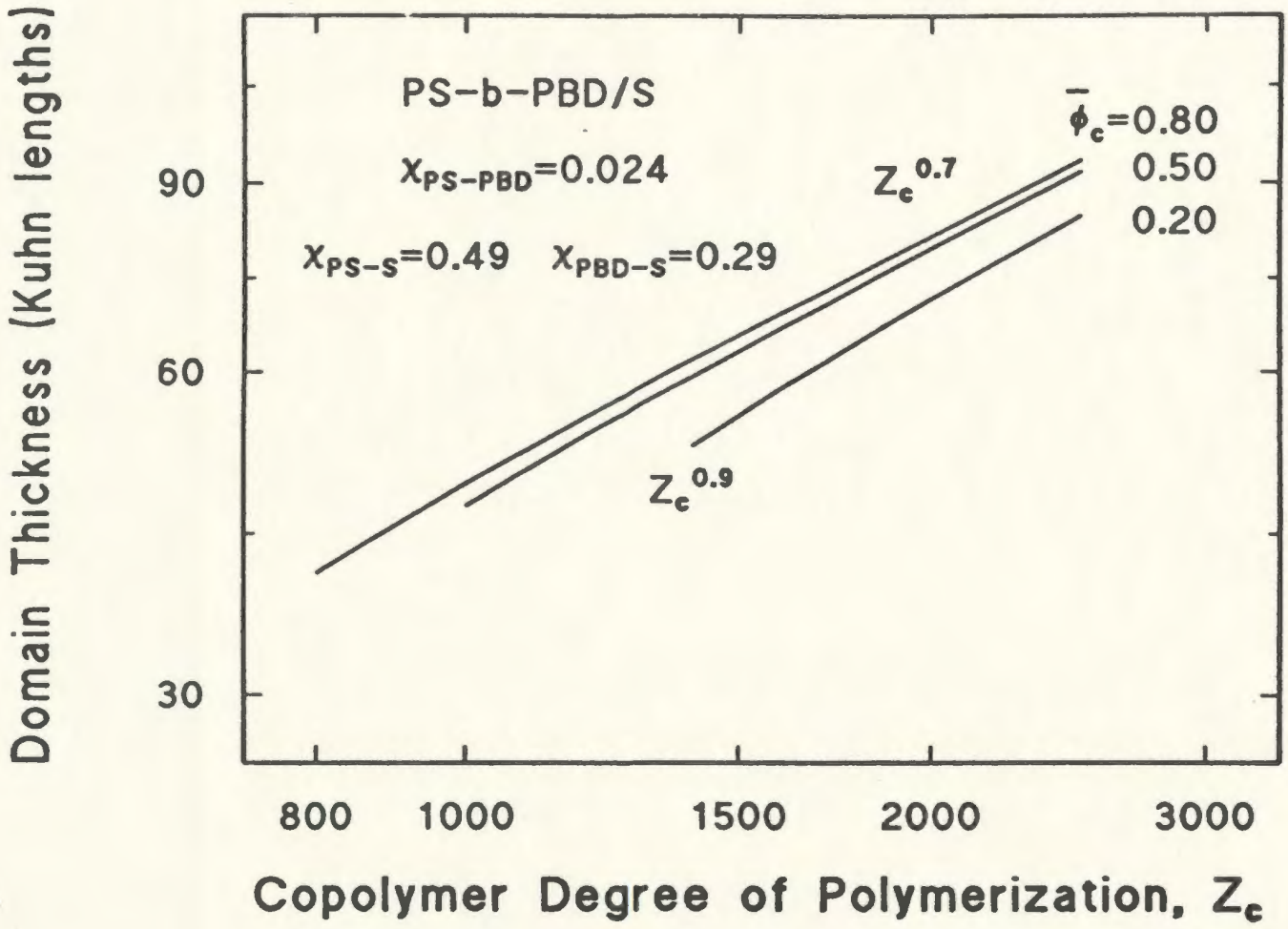

Figure 3.4: Equilibrium domain thickness as function of copolymer degree of polymerization for three different copolymer volume fractions. This is *PS-b-PBD/S* blend. In weak segregation regime $q \simeq 0.9$, but the dependance weakens in strong segregation $q \simeq 0.7$

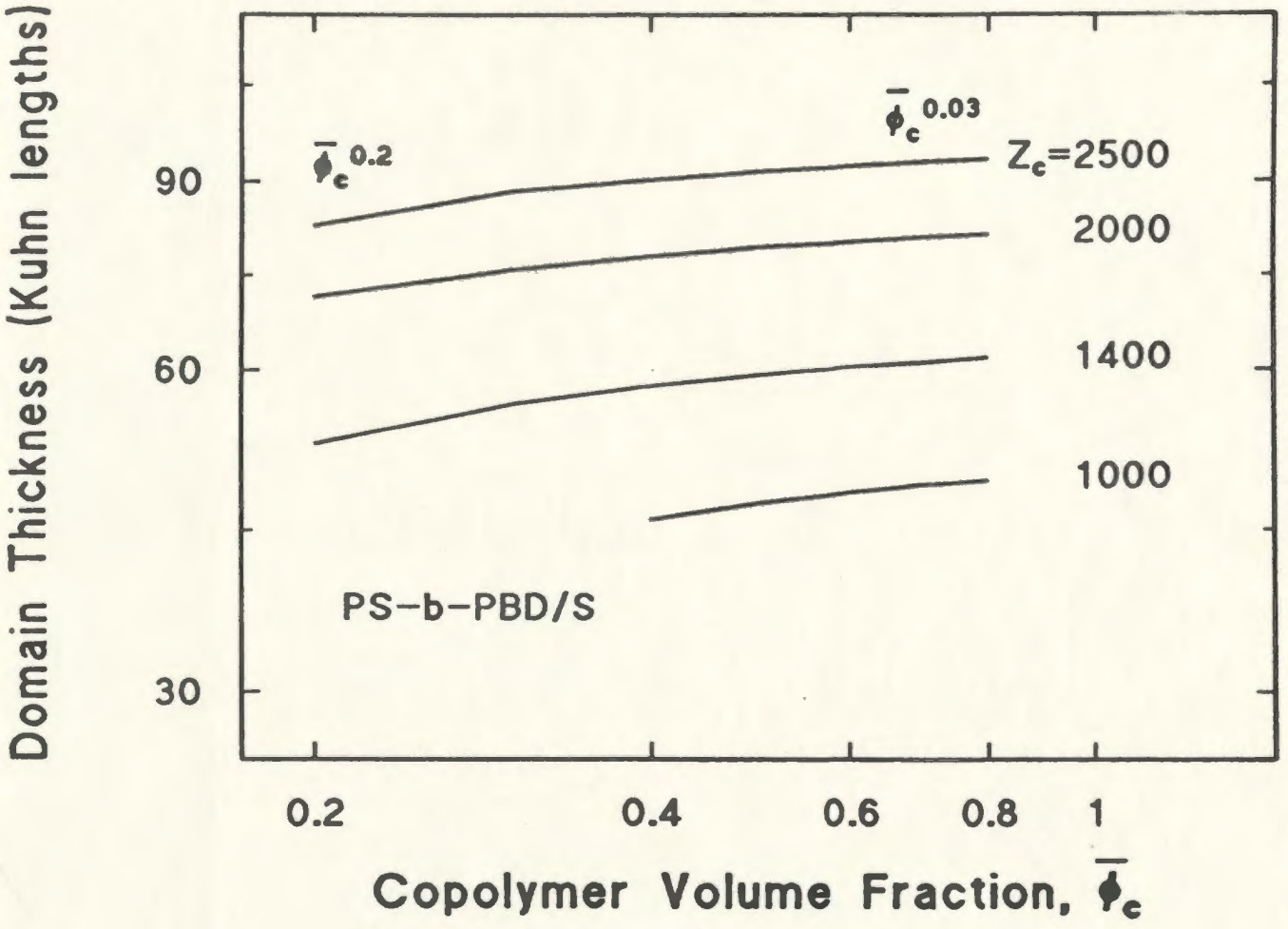

Figure 3.5: Equilibrium domain thickness as function of copolymer volume fraction for four different copolymer degrees of polymerization. This is *PS-b-PBD/S* blend. In weak segregation regime $p \simeq 0.2$, but the dependance weakens in strong segregation $p \simeq 0.03$

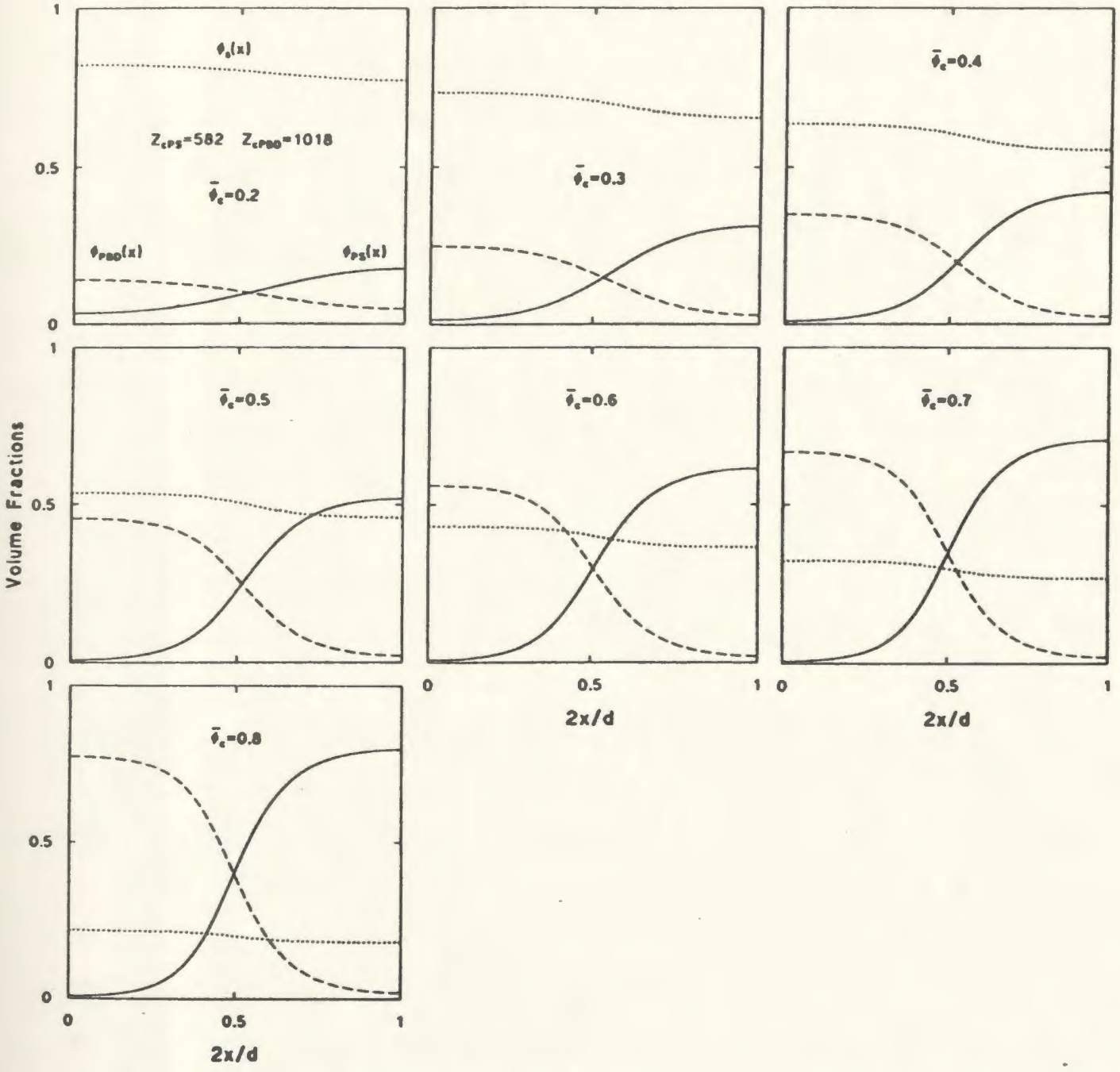

Figure 3.6: Density profiles for different overall copolymer volume fractions for $Z_c = 1600$. The first panel corresponds to 20% copolymer volume fraction, and is in the weak segregation regime. Successive panels correspond to progressively more copolymer, up to 80% with $Z_c\chi\bar{\phi}_c = 30.8$. In all cases the solvent is preferentially localized in the PBD subdomain, but the density variation is relatively small.

Chapter 4

Lamellar Structure of Block Copolymer/Homopolymer Blends

4.1 Introduction

As already discussed in the Introduction block copolymers and block copolymer/homopolymer and block copolymer/solvent blends can exhibit a variety of structures and phase behaviour, undergoing both microphase and macrophase separation. The goal of this chapter is to provide some additional understanding of the lamellar structure of such blends near the microphase separation transition (MST), i.e., in the weak segregation regime.

The questions of interest for this chapter have been studied experimentally by Quan et al. [18], Hashimoto et al. [13, 14, 15], and Winey [16]. They measured the domain and subdomain thicknesses for series of copolymer/homopolymer blends, and extracted the dependence of these quantities on the degrees of polymerization of the homopolymers and the copolymer blocks, blend composition, and temperature. Hashimoto et al., and Winey related their results to the distribution of the added homopolymers within the compatible subdomains, and the degree of lateral swelling of the copolymers.

In this chapter we study *A-b-B/A* and *A-b-B/A/B* copolymer/homopolymer blends, using the approximate approach based on the perturbative solutions to the diffusion equation presented in section 2.3. We assume a lamellar structure, limiting ourselves to systems with overall *A:B* volume ratios near 50:50, and, using theory of the phase behaviour of these systems which is presented in chapter 5 and reference [66], restrict

our attention to blends which do not macrophase separate. We focus on the variation of the lamellar thickness with the copolymer and homopolymer degrees of polymerization and overall volume fractions, and on the distribution of copolymers and homopolymers within each subdomain. We also investigate the temperature (χ parameter) dependence of the A-B interphase region.

In the early work of Hong, Noolandi and Whitmore [27, 29], as well as in our work presented in the next chapter, the fourth order expansion is combined with the assumption that near the MST, the density profiles can be modeled by simple cosine-like variations about their mean values, i.e., only the dominant wavenumber is included. Comparison with numerical self-consistent calculations suggests that this "one wavenumber approximation" provides a reasonable result for the free energy of the system, but it fails to account for changes in the lamellar thickness with overall concentrations and temperature [27, 30]. We have, therefore, incorporated into our approach a model for the density distributions which goes beyond this assumption.

Section 4.2 of this chapter along with Appendix B describe the formalism, including the model for the density distributions. Section 4.3 begins with a comparison of this approach with numerical self-consistent calculations, and goes on to present results for model binary and ternary blends. Section 4.4 summarizes the experiments mentioned above, which are made on systems in the strong segregation regime, and compares the predictions of the theory with them. It ends with calculations for these specific blends in the weak segregation regime.

4.2 Model Density Profiles

The essential step, underlying all the calculations in this and the next chapter, is the minimization of approximate expansion for Δf, eq. 2.105, and subsequent calculation of all four density profiles (in the weak segregation regime) in this chapter. The first step is to calculate the Fourier components $\tilde{\phi}_\alpha(\boldsymbol{k})$ by minimizing Δf, i.e., eq. 2.105. Then using $\tilde{\phi}_\beta(\boldsymbol{k}) = -\tilde{\phi}_\alpha(\boldsymbol{k})$, the two fields $\tilde{\omega}_\alpha$ and $\tilde{\omega}_\beta$ are calculated from eq. 2.103 and 2.104. From these the four individual density profiles are calculated from eq. 2.99, 2.100 and 2.98. Because of the inversion of eq. 2.101, and 2.102 and minimization of a truncated series for Δf, in order to maintain a consistent level of approximation, at this last step we truncate eq. 2.99, 2.100 and 2.98 to second order. For example, eq. 2.98 for $p = hA$, is evaluated as

$$\tilde{\phi}_{hA}(\boldsymbol{k}) \cong -r_{hA}\overline{\phi}_{hA}g^{hA}_{hAj}\tilde{\omega}_j + \frac{1}{2}r^2_{hA}\overline{\phi}_{hA}g^{hA}_{hAjk}\tilde{\omega}_j\tilde{\omega}_k. \tag{4.1}$$

Detailed expressions are given in Appendix C, eq. C.11–C.14.

In principle, we need to minimize Δf with respect to all the Fourier components $\tilde{\phi}_\alpha(\boldsymbol{k})$. In practice we consider a restricted family of possible $\tilde{\phi}_\alpha(\boldsymbol{k})$, in order to carry out the minimization in a numerically efficient way. This family is chosen on the basis of two assumptions. The first is that it must include the simple cosine form for $\phi_\alpha(x)$ expected for the limiting case of the system approaching the MST, i.e., the $\tilde{\phi}_\alpha(\boldsymbol{k})$ and $\tilde{\phi}_\beta(\boldsymbol{k})$ must include the possibilities

$$\phi_\alpha(x) \to \overline{\phi}_\alpha + \Psi_\alpha \cos(k^* x), \tag{4.2}$$

$$\phi_\beta(x) \to \overline{\phi}_\beta + \Psi_\beta \cos(k^* x), \tag{4.3}$$

with $\Psi_\beta = -\Psi_\alpha$. Here $k^* = 2\pi/d$, d being the lamellar thickness in this limit, and Ψ_α and Ψ_β are the amplitudes of the variation in $\phi_\alpha(x)$ and $\phi_\beta(x)$, respectively. As the system parameters evolve away from the MST, then the amplitudes Ψ_α and Ψ_β increase,

the density profiles $\phi_\alpha(x)$ and $\phi_\beta(x)$ become flatter within each subdomain, and the interphase regions become narrower evolving towards a hyperbolic tangent shape [40, 78]. For pure block copolymers this has been shown theoretically by Ohta and Kawasaki [40]. They divided the expression for the free energy into two parts:

- a fourth order expansion analogous to that of Cahn and Hilliard [77] (and also to Landau-Ginzburg [60] expansion),
- long range interactions.

Next they argued that close to the interface the long range interactions can be ignored, so that the Cahn-Hilliard theory can be directly applied. This theory, presented in reference [77], shows, by direct analytical minimization of the free energy, that the interfacial composition profile has, indeed, the hyperbolic tangent shape. In practice, this limit is never reached in our calculations.

In our procedure, we represent $\phi_\alpha(x)$ and $\phi_\beta(x)$ by

$$\phi_\alpha(x) = \overline{\phi}_\alpha + \Psi_\alpha u(x; d, p, q), \tag{4.4}$$

$$\phi_\beta(x) = \overline{\phi}_\beta + \Psi_\beta u(x; d, p, q), \tag{4.5}$$

where d is the domain thickness, and p and q control the shape of $\phi_\alpha(x)$, including the width of the interface and the subdomain thicknesses, as discussed in Appendix B. For some values of p and q, the function $u(x)$ reduces to the single cosine function, whereas for other values it can give a $\phi_\alpha(x)$ appropriate to the strong segregation regime, with values of 0 and 1 in each subdomain, connected by interfaces whose shapes are hyperbolic tangents. The functional form chosen for $u(x)$ is discussed in Appendix B.

Substituting eq. 4.4 into eq. 2.105 provides an expression for Δf which is a function of four variables Ψ_α, d, p and q. For any values of these, we evaluate the multiple sums appearing in eq. 2.105. Minimizing this function with respect to these variables gives us

the calculated equilibrium layer thickness d and density profile $\tilde{\phi}_\alpha$. From this we calculate $\tilde{\phi}_\beta = -\tilde{\phi}_\alpha$, the two potentials $\tilde{\omega}_\alpha$ and $\tilde{\omega}_\beta$ from eq. 2.103 and 2.104, and then the four $\tilde{\phi}_p$ from eq. 2.98, 2.99 and 2.100, but truncated to second order as eq. 4.1.

Having completed such a calculation, we convert the results to real space, and finish by verifying that the solution which has been obtained is physically acceptable, i.e., that all four local volume fractions $\phi_p(x)$ remain between 0 and 1 everywhere. It turns out that this restriction limits the calculations to near the MST, and the profiles do not reach the hyperbolic tangent shape. We generally needed to keep on the order 10 wavenumbers in the expansions. We verified that dropping the third order term from eq. 2.98, 2.99, and 2.100 caused an error which was small near the MST.

Finally, we identify the point of inflection in $\phi_\alpha(x)$ as the point which divides d into the two subdomains, of thicknesses d_A and d_B [78]. The interfacial width, a_I, is defined in Appendix B.

4.3 Model Calculations

4.3.1 Comparison with Self-consistent Calculations

In this section, we examine a model system in which all reference densities and Kuhn lengths are equal and, for purposes of illustration, usually choose the copolymer degree of polymerization to be $Z_c = 400$. Perfectly symmetric copolymers with this value of Z_c microphase separate at $\chi Z_c = 10.5$, or $\chi \simeq 0.0263$ (in this level of approximation), and this sets the overall scale of the values of χ used here. This value is also close to that for the copolymers in the work of Hashimoto et al. [13, 14, 15]. In most of the cases we exhibit, all homopolymers are assumed to have the same degree of polymerization, in which case we simplify the notation by relabeling them $Z_{hA} = Z_{hB} \equiv Z_h$. When applicable, we also use label h for hA or solvent case.

We begin by comparing results using the approximate approach used throughout this chapter with results obtained from the full mean field self-consistent theory, for binary copolymer/solvent blends, as outlined in section 2.2 and fully described in chapter 3. For this comparison we use symmetric copolymers, i.e., $Z_{cA} = Z_{cB} = Z_c/2$, and choose the interaction parameters to be $\chi_{SB} = \chi_{AB} = \chi$ and $\chi_{SA} = 0$. Within the approximate approach, the solvent is represented as an hA homopolymer with $Z_h = 1$. This comparison is meant to test the combination of the fourth order free energy expansion with the model density, near the MST. It does not test mean field theory itself, nor does it necessarily represent a realistic model of a real system. For example, the polystyrene-styrene interaction parameter has been determined to be close to 0.5, rather than zero [76], as discussed in subsection 3.2.2.

The self-consistent calculations are carried out as described in references [30, 33], and also in chapter 3, but with the parameter describing the range of the potential, labeled σ in those references, set to zero. Near the MST where the free energy Δf approaches

zero, the required accuracy in the self-consistent solutions to the diffusion equation and resulting density profiles is on the order of 6 significant figures.

Three series of calculations are shown. In two of them, $Z_c = 400$, and $\overline{\phi}_c = 0.4$ (series 1) or 0.8 (series 2). For the third, $\overline{\phi}_c = 0.4$ as in the first series, but Z_c was increased to 800. The first and second columns of figure 4.1 show, respectively, the free energy Δf and the domain thickness d as a function of χ for the three systems calculated both ways. At least to within the numerical accuracy, in both methods the free energy vanishes with zero derivative at values of χ which agree to 3 figures, and Δf and d agree as the MST is approached. As χ increases, the self-consistent calculations give a slightly higher value of Δf, a difference attributable to the truncation of the expansion. As seen in the second column, both calculations predict an increase in d with χ, with the approximate calculation predicting a slightly faster increase. The difference virtually vanishes near, but not solely at, the MST. Expressing the dependence of d on χ as $d \propto \chi^p$, then for all 3 systems shown, very close to the MST, the self-consistent calculations give $p = 0.50 \pm 0.01$ and the approximate method gives $p = 0.51 \pm 0.01$. This contrasts with the one wavenumber approximation in which d is independent of χ.

Figure 4.2 shows calculated density profiles for each blend of figure 4.1. For each case, we have chosen the largest value of χ used in the corresponding panel of figure 4.1, where the difference between the two sets of calculations is the largest. The left hand column of figure 4.2 shows the three density profiles for each system, $\phi_{cA}(x)$, $\phi_{cB}(x)$ for copolymer constituents, and $\phi_h(x)$ for the solvent; the right hand side reproduces $\phi_h(x)$ on a greatly expanded scale. Qualitatively, the two approaches give the same results. Quantitatively, the fourth order expansion overestimates the amplitude of the variations of $\phi_{cA}(x)$ and $\phi_{cB}(x)$ by about 10 to 25%. In all cases the density variation of the solvent, $\psi_h(x)$, is very small, and the two approaches predict almost identical density profiles.

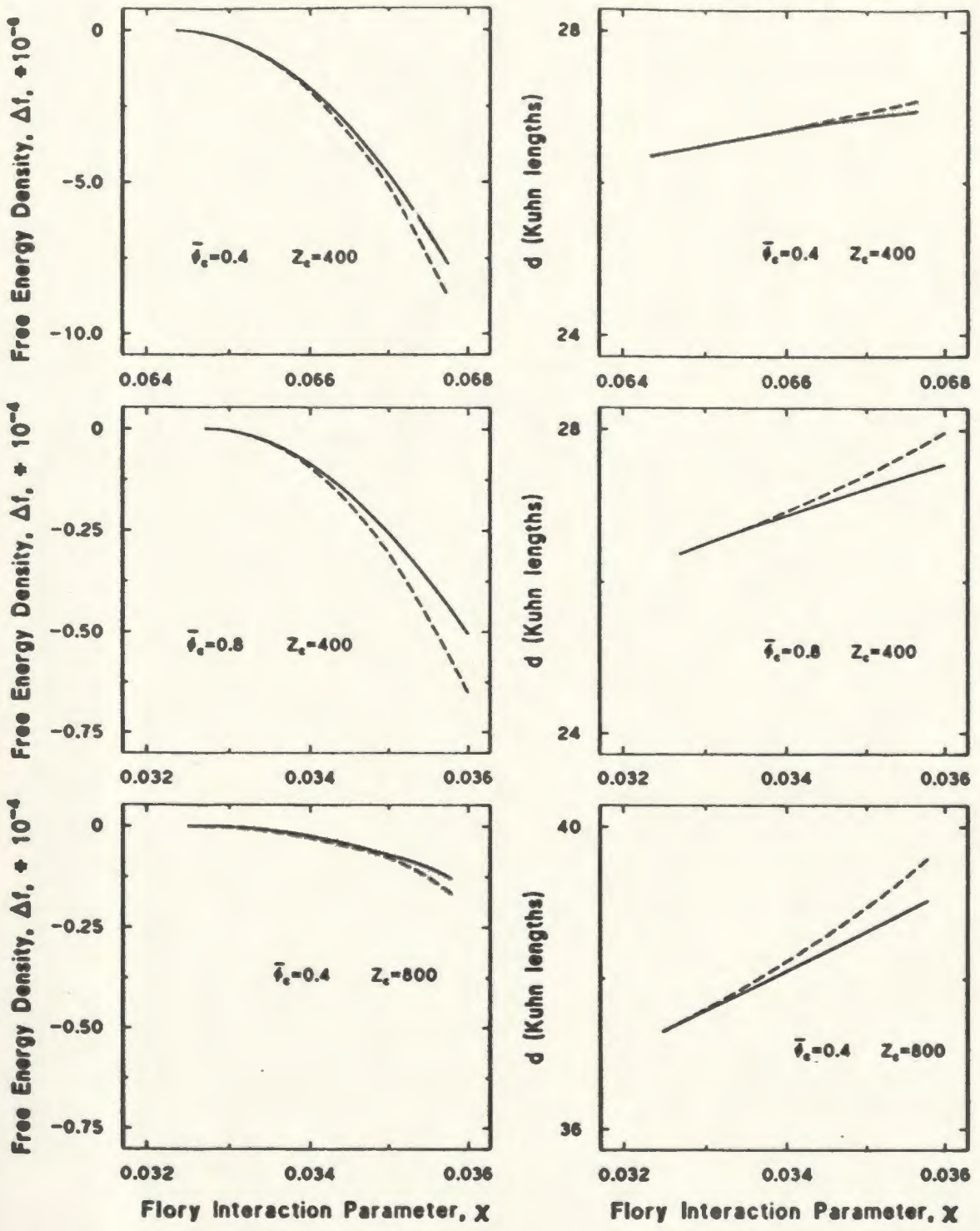

Figure 4.1: Comparison of self-consistent calculations and approximate method: equilibrium free energy (left hand column) and domain thickness (right hand column) for three cases, as indicated. The solid lines are the results of numerical solutions to the full self-consistent equations, and the dashed lines were calculated using the method based on the fourth order expansion, with $Z_h = 1$.

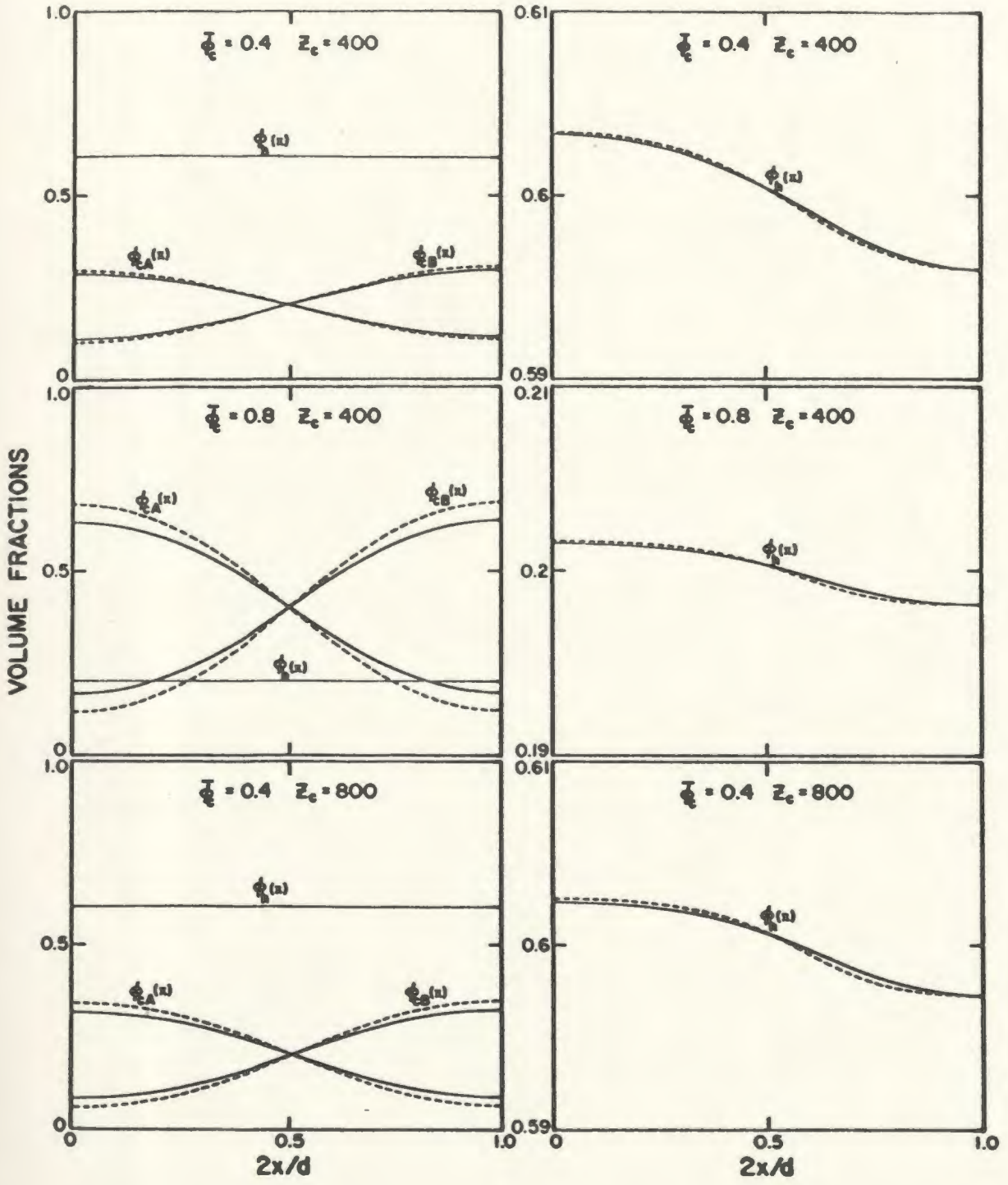

Figure 4.2: Comparison of self-consistent calculations and approximate method: local volume fractions $\phi_{cA}(x)$, $\phi_{cB}(x)$ and $\phi_h(x)$, for the three cases of figure 4.1. The solid lines are the results of numerical solutions to the full self-consistent equations, and the dashed lines were calculated using the method based on the fourth order expansion, with $Z_h = 1$. The panels in the right hand column show the solvent density profiles on an expanded scale. For purposes of illustration, the horizontal axis is normalized to $d/2$.

4.3.2 Domain and Subdomain Thicknesses

Figure 4.3 shows the first series of calculations for model binary copolymer/homopolymer blends with $Z_c = 400$, and different homopolymer degrees of polymerization with Z_h varying from 1 to 120. As in most of the experiments discussed in section 4.4 and in references [13]–[15], [16, 18], we consider homopolymer volume fractions up to $\overline{\phi}_h = 0.2$, which for the case of symmetric copolymers corresponds to an overall *A:B* composition ratio of 60:40. Over at least most of this range, we expect the lamellar structure to be the equilibrium structure [79]. As well, we choose $\chi = 0.03$, so that for the pure copolymer $\chi Z_c = 12$, which places the system near but not at the MST.

Figure 4.3 shows the calculated changes in d, and subdomain thicknesses d_A and d_B resulting from the addition of the homopolymers. Beginning with the lamellar thickness d, the top panel shows that for "small" Z_h, d decreases, but for larger Z_h, it increases. The curve for $Z_h = 1$ terminates at $\overline{\phi}_c = 0.87$, because this is the MST for this system. There is a threshold value of Z_h, say Z_h^{th}, such that if $Z_h = Z_h^{th}$ then small amounts of hA induce no change in d. The precise value Z_h^{th} depends on what is meant by "small', but it is clear that it is about

$$Z_h^{th} \simeq Z_c/5. \tag{4.6}$$

We verified that this threshold holds for different Z_c. For very small amounts of hA, the changes in d and can be expressed

$$\frac{d}{d_o} \simeq 1 + a\overline{\phi}_h, \tag{4.7}$$

where $\overline{\phi}_h$ is the overall homopolymer volume fraction, which for these binary blends is $\overline{\phi}_h = \overline{\phi}_{hA}$, and d_o is the layer thickness for the pure copolymer. The values of a range from about -1.0 for small Z_h to about 0.4 for $Z_h = 0.3Z_c$. These values, as well as related ones for other model systems, are summarized in table 4.1.

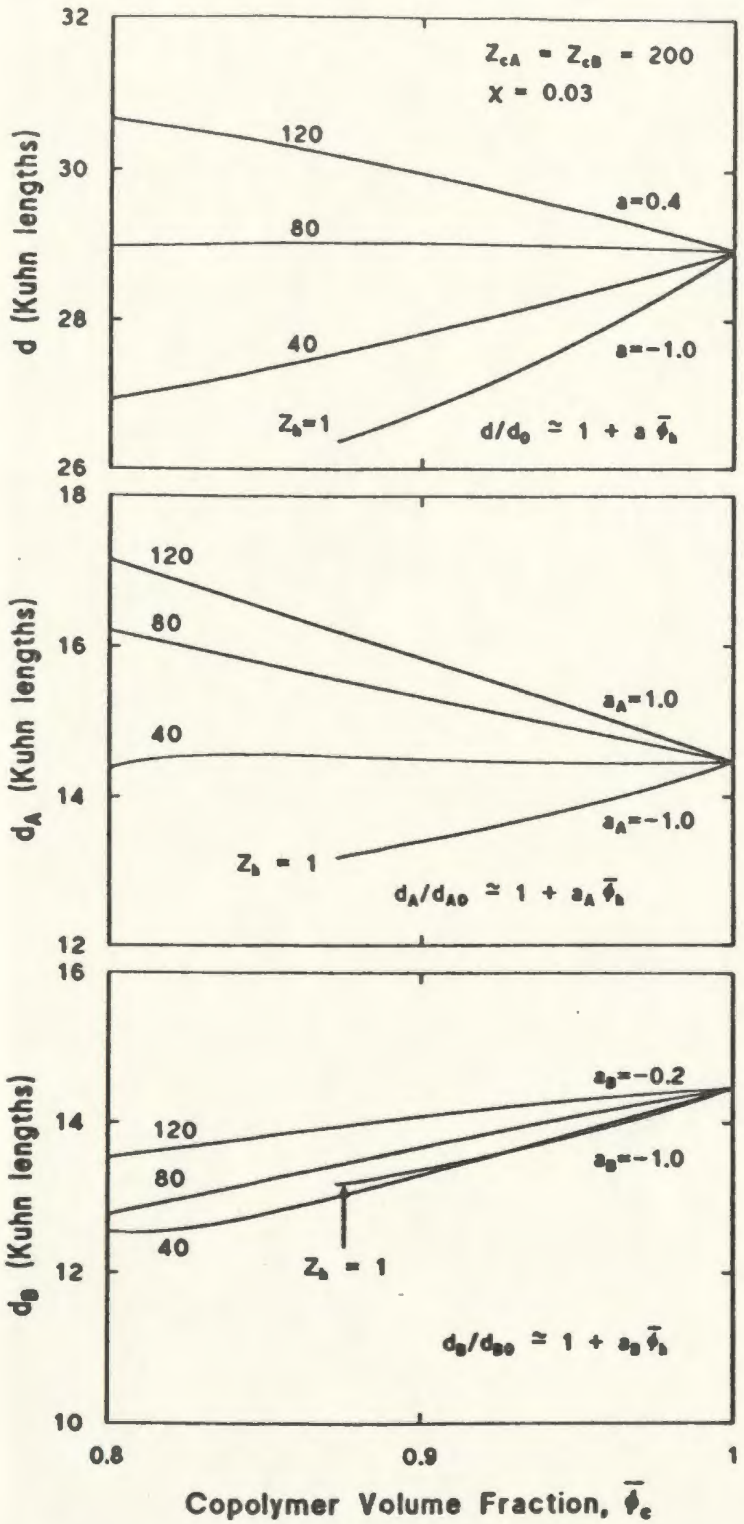

Figure 4.3: Equilibrium domain thickness d, (upper panel), and subdomain thicknesses d_A and d_B, (middle and lower panels), as functions of copolymer content $\bar{\phi}_c$ for the model binary blend with $Z_{cA} = Z_{cB} = 200$, for different degrees of polymerization of the added homopolymer, Z_h, as indicated. The curves for $Z_h = 1$ terminate at $\bar{\phi}_c = 0.87$, corresponding to the MST.

Table 4.1: Initial dependence of the domain thickness d and subdomain thicknesses d_A and d_B on small amounts of homopolymer, for binary *A-b-B/A* and ternary *A-b-B/A/B* blends. For all cases, $\chi = 0.03$. For the ternary blends, the homopolymers have equal degrees of polymerization, $Z_{hA} = Z_{hB} \equiv Z_h$, and they are added in a proportion to maintain the blends on the isopleth. The coefficients a, a_A and a_B are defined by eq. 4.7, 4.11 and 4.12.

			Binary Blends			Ternary Blends		
Z_c	Z_{cA}/Z_c	Z_h	a	a_A	a_B	a	a_A	a_B
400	0.5	1	-1.0	-1.0	-1.0	-1.0	-1.0	-1.0
		120	0.4	1.0	-0.2	0.4	0.4	0.4
	0.4	1	-0.6	-0.3	-0.8	-0.6	-0.4	-0.8
		120	0.9	1.5	0.5	0.4	0.3	0.5

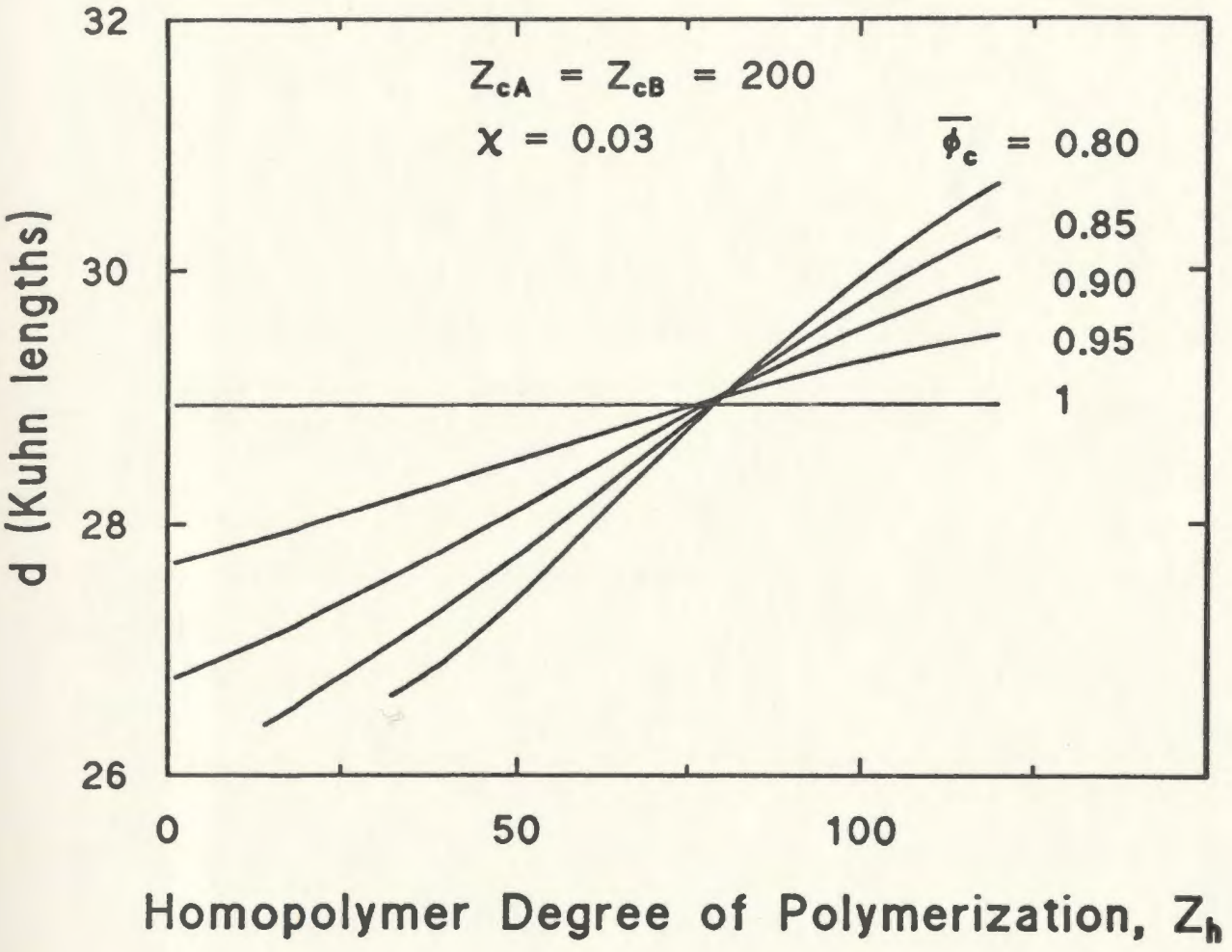

Figure 4.4: Equilibrium domain thickness, d, as a function of Z_h for different copolymer volume fractions $\overline{\phi}_c$, for the model blend of figure 4.3. The curves for $\overline{\phi}_c = 0.8$ and 0.85 terminate at $Z_h = 32$ and 14 respectively, corresponding to the MST in each case.

Figure 4.4 reproduces the information of this panel in a different way, explicitly showing the dependence of d on Z_h for different copolymer volume fractions. If the curves on figure 4.3 were straight lines, then the five curves of figure 4.4 would intersect at a single point; this is nearly the case. As a result, for all volume fractions shown, for $Z_h \lesssim Z_h^{th} \simeq Z_c/5$ the added homopolymer induces a decrease in d, for $Z_h \gtrsim Z_h^{th}$ it induces an increase in d, and for $Z_h \simeq Z_h^{th}$, d is unchanged.

This behaviour, including the existence of the threshold, differs qualitatively from what is predicted by the one wavenumber approximation, shown for this system in figure 4.5. In that approach, d is determined by minimizing the second order term in the free energy. Two points are apparent from the figure. First this approach always underestimates d, giving the value appropriate for the MST. Second, it predicts that added homopolymers always induce an increase in d, irrespective of Z_h or Z_c, although for small values of Z_h/Z_c, in particular for solvent, d becomes virtually independent of $\overline{\phi}_h$.

This prediction can be easily understood. For small $\overline{\phi}_h$, it is straightforward to show that the predicted change in d is

$$\frac{d}{d_o} \simeq 1 + 2\overline{\phi}_h \left(\frac{Z_h}{Z_c}\right)^2 \frac{g_h'(2Z_h x_o^*/Z_c)}{x_o^* g_c''(x_o^*)}, \tag{4.8}$$

where

$$g_h(x) = g_h^{(2)}(x), \tag{4.9}$$

$$g_c(x) = g_{cA}^{(2)}(x) - [g_{cA}^{(1)}(x)]^2, \tag{4.10}$$

and $g_h^{(2)}$, $g_{cA}^{(2)}$ and $g_{cA}^{(1)}$, which are directly related to the $g_{i...}^{\kappa}$, are defined in Appendix A. The primes denote derivatives, and x_o^*, which denotes the location of the maximum of g_c, has the value $x_o^* = 22.7/12$. It is related to d_o by $x_o^* = Z_c b^2 [k^*]^2/12$, with $d_o = 2\pi/k^*$. Since x_o^* corresponds to the maximum in g_c, and since g_h is monotonically decreasing, therefore the combination g_h'/g_c'' is always positive. On the other hand, for very small

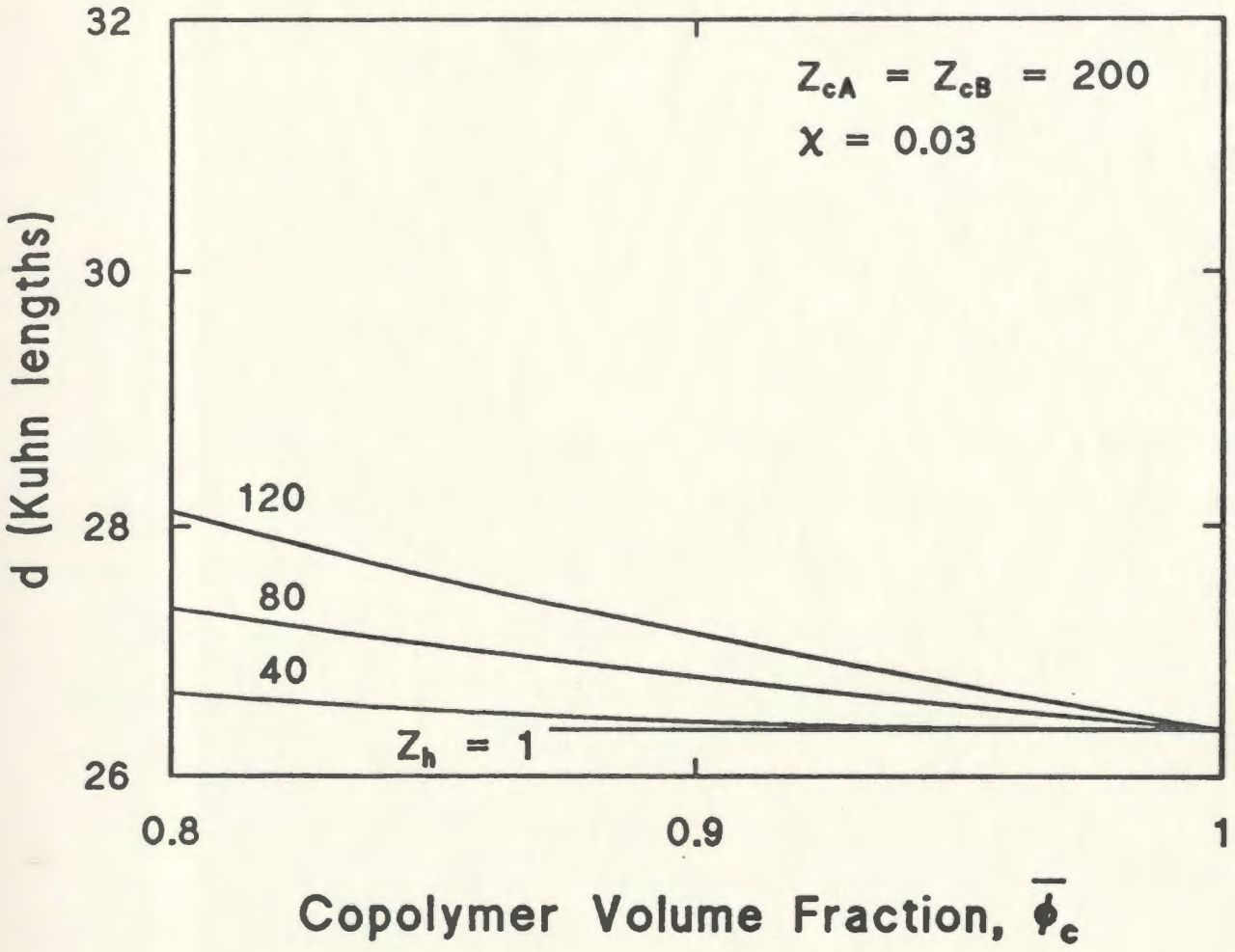

Figure 4.5: Equilibrium domain thickness, d, as a function of $\bar{\phi}_c$ for the model binary blend of figure 4.3 and 4.4, for different degrees of polymerization of the added homopolymer, Z_h, as indicated, but calculated using the one wavenumber approximation. The curve for $Z_h = 1$, terminates at $\bar{\phi}_c = 0.87$, corresponding to the MST.

homopolymer degree of polymerization, $Z_h/Z_c \rightarrow 0$, and so the dependence on $\overline{\phi}_h$ vanishes.

The prediction of the one wavenumber approximation that added solvent induces virtually no change in the layer thickness is similar to an earlier comment by Hong and Noolandi made for neutral solvent. They predicted no dependence of d on solvent concentration [27], and pointed out that the higher order effects, i.e., those originating from inclusion of many wavenumbers or application of numerical self-consistent approach, lead to a reduction in d with added solvent [30].

We can understand the behaviour of d, and in particular the relationship between the one wavenumber results and the current results, in the following way. The first point to note is that for these copolymers, at the MST the domain thickness would be $d_o/b \simeq 26.4$, i.e, the one wavenumber value. However, for the chosen value of χ, $\chi Z_c = 12$, and hence d_o is larger, $d_o/b \simeq 29$. Second, it is known from reference [29] and further discussed in chapter 5 that induced microphase formation is predicted to occur for this blend if $Z_h \gtrsim Z_c/4$. This implies that addition of lower molecular weight homopolymers drives the system towards the weak segregation regime, the density profiles tend towards simple cosine functions, and d relaxes downwards towards its MST value. For the case shown in figure 4.3 which reaches the order-disorder transition, $Z_h = 1$, the value of d at the transition is just that predicted by the one wavenumber approximation, shown in figure 4.5. Conversely, adding higher molecular weight homopolymers at least initially drives the system towards the strong segregation regime, which of itself would induce a further increase in d. Thus the tendency to stabilize or destabilize the microphase is correlated with the tendency to cause d to increase or decrease. This picture, as well as other results such as the values of the threshold Z_h^{th} and the coefficient a, (and a_A and a_B defined below), very likely depend on where the system is in terms of the weak or strong segregation regimes.

Returning now to figure 4.3, the subdomain thicknesses d_A and d_B for this system are illustrated in the lower two panels. The initial behaviour of d_A resembles that of d, except that for a given Z_h, the increase in d_A is greater than the increase in d, and d_A increases for all $Z_h \gtrsim 40$. This compares with the threshold value for d for this system of $Z_h^{th} \simeq 80$. By contrast, in all cases, d_B initially decreases as A homopolymers are added. Expressing these initial changes in d_A and d_B as in eq. 4.7:

$$\frac{d_A}{d_{Ao}} \simeq 1 + a_A \overline{\phi}_h \tag{4.11}$$

and

$$\frac{d_B}{d_{Bo}} \simeq 1 + a_B \overline{\phi}_h \tag{4.12}$$

we find the initial slopes range from $a_A = a_B \simeq -1.0$ for $Z_h = 1$ to $a_A \simeq 1.0$ and $a_B \simeq -0.2$ for $Z_h = 120$.

For larger homopolymer concentrations, the changes in d_A and d_B are more complex, reflecting three effects. First, the overall increase in $\overline{\phi}_\alpha$ tends to induce an increase in d_A. Second, in general the added homopolymers tend to drive the system towards either the weak or the strong segregation regimes, tending to induce a decrease or an increase in d, respectively. Finally, as a system approaches the MST, both d_A and d_B tend towards $d/2$. The case $Z_h = 40$ illustrates these. For d_A, there is initially a balance of the first two effects, and it is nearly constant for homopolymer content up to $\overline{\phi}_h \simeq 0.17$, at which point it begins to decrease towards $d/2$ as the system approaches the MST. On the other hand, d_B initially decreases, reaching a minimum near $\overline{\phi}_h \simeq 0.17$, after which it increases slightly. For $Z_h = 1$, the system reaches the MST at $\overline{\phi}_c = 0.87$, where $d_A = d_B = d/2$.

We next consider one example with asymmetric copolymers, chosen to have $Z_c = 400$ as above, but $Z_{cA} = 160$ and $Z_{cB} = 240$, so the overall composition ratio is $\overline{\phi}_\alpha$:$\overline{\phi}_\beta = 40{:}60$. The addition of 20% hA changes this ratio to 52:48, and so once again the structure probably remains lamellar throughout this range. Figure 4.6, which is analogous to

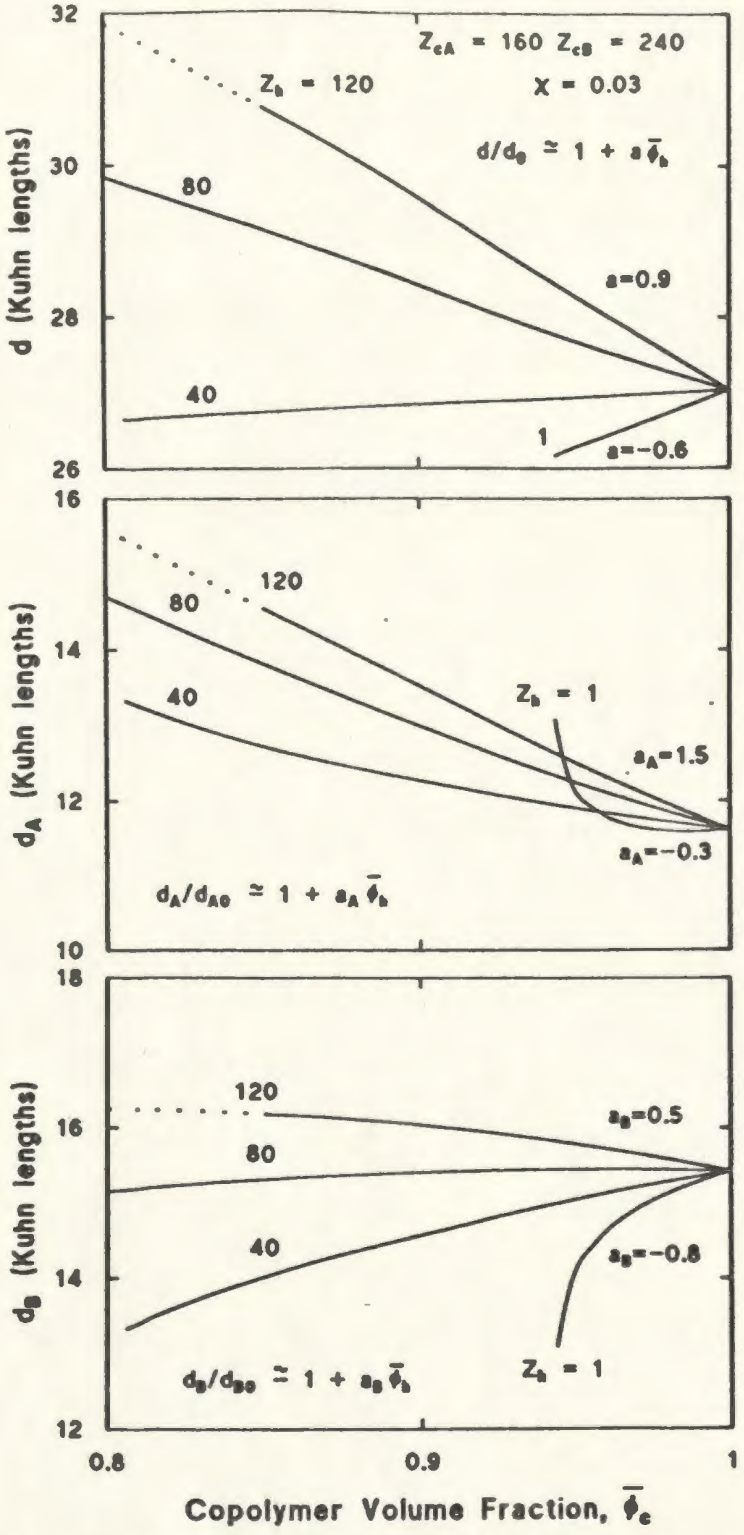

Figure 4.6: Equilibrium domain thickness, d, and subdomain thicknesses d_A and d_B, as a function of $\bar{\phi}_c$ for the model binary blend with asymmetric copolymers, $Z_{cA} = 160$, $Z_{cB} = 240$, for different degrees of polymerization of the added homopolymer, Z_h, as indicated. The curves for $Z_h = 1$ and 40 terminate at $\bar{\phi}_c = 0.94$ and 0.81 respectively, corresponding to the MST in each case. For $Z_h = 120$, the dotted lines are extrapolations of the calculations to $\bar{\phi}_c < 0.85$, where the method gives unphysical densities.

figure 4.3, shows d, d_A and d_B as functions of $\overline{\phi}_c$ for this case. For this system, the curves for $Z_h = 1$ and $Z_h = 40$ both terminate where the blends reach the MST. For the case $Z_h = 120$, we terminated the calculations at $\overline{\phi}_c = 0.85$, because beyond this the calculated density distributions became unphysical, as described in section 4.2. We indicate this by extrapolating with a dotted line.

Considering d first, in all cases its increase is greater than for the corresponding case with the symmetric copolymers. Consistent with this, there is again a threshold value of Z_h such that for larger (smaller) Z_h, the overall domain thickness d increases (decreases), but in this case it is at $Z_h^{th} \simeq 45 \simeq Z_c/9 \simeq Z_{cA}/3.5$, which compares with $Z_h^{th} \simeq Z_c/5 \simeq Z_{cA}/2.5$ found above for the symmetric copolymer case.

The variations of d_A and d_B are particularly interesting. For neat copolymer, $d_A \simeq 11.5 < d/2$ and $d_B \simeq 13.5 > d/2$. As very low molecular weight homopolymers are added, the system moves towards the MST, d decreases, and both d_A and d_B initially follow, e.g. for $Z_h = 1$, $a \simeq -0.6$, $a_A \simeq -0.3$ and $a_B \simeq -0.8$. However, with the addition of only small amounts of these homopolymers, the tendency for d_A and d_B to change towards $d/2$ dominates, causing d_A to increase and d_B to decrease rapidly. For the higher molecular weight homopolymers, e.g. $Z_h = 120$, both d_A and d_B increase, in contrast with corresponding behaviour for the symmetric copolymer/homopolymer blends, in which d_B decreased.

Turning to ternary blends, we begin with model systems with symmetric copolymers blended with equal amounts of A and B homopolymers with equal degrees of polymerization, i.e., $\overline{\phi}_{hA} = \overline{\phi}_{hB} = \overline{\phi}_h/2$ and $Z_{hA} = Z_{hB} \equiv Z_h$. This simplifies the results, because $d_A = d_B = d/2$. Figure 4.7, which is analogous to the upper panel of figure 4.3, shows calculated values of d for such blends with $Z_c = 400$, and Z_h varying from 1 to 120. For small Z_h, the behaviour of d is virtually identical to that for the binary blends. For larger Z_h, it is almost the same for very low $\overline{\phi}_h$, reflected in the fact that the values of

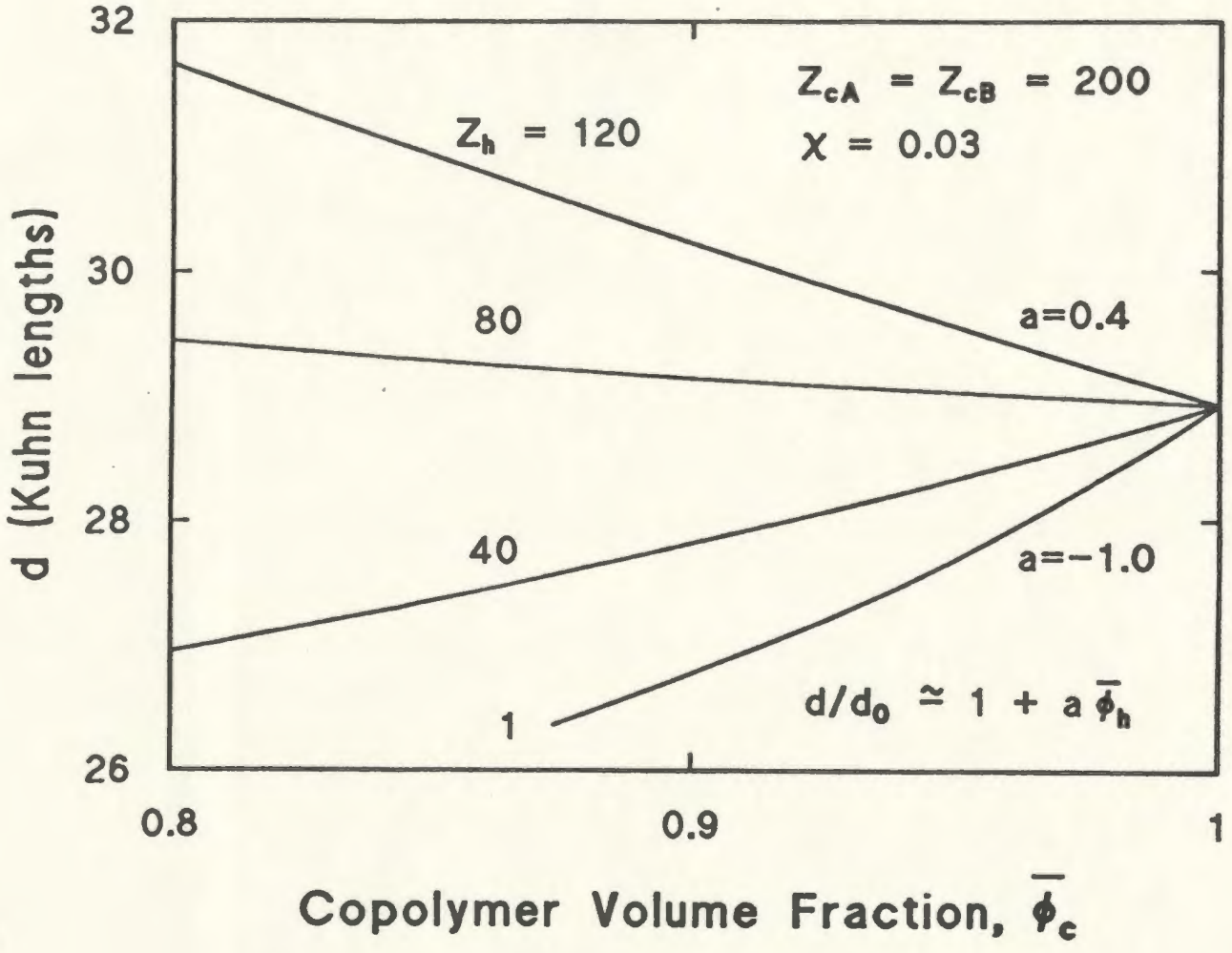

Figure 4.7: Equilibrium domain thickness, d, as a function of $\bar{\phi}_c$ for the model ternary blend with $Z_{cA} = Z_{cB} = 200$, for different degrees of polymerization of the added homopolymer, Z_h, as indicated. The systems are on the isopleth, so $d_A = d_B = d/2$. The curve for $Z_h = 1$ terminates at $\bar{\phi}_c = 0.873$, corresponding to the MST.

the coefficient a are the same in corresponding cases, and furthermore in this limit the threshold value of Z_h remains the same, $Z_h^{th} \simeq Z_c/5$. However, as $\overline{\phi}_h$ is increased, there are quantitative differences. Finite concentrations of homopolymer, e.g. 10-20%, tend to induce a larger increase in d than in the binary case; for example for $Z_h = 120$, the increase in d at $\overline{\phi}_c = 0.8$ is about 50% larger. Another (obvious) difference from the binary blends in this case is that $d_A = d_B = d/2$.

For the final model system, we consider ternary blends with the same asymmetric copolymers as in figure 4.6, blended with A and B homopolymers with equal degrees of polymerization, but added in a proportion to maintain the system on the isopleth, i.e., the overall volume fractions remain $\overline{\phi}_\alpha$:$\overline{\phi}_\beta$ = 40:60. Figure 4.8 shows d, d_A and d_B as a function of $\overline{\phi}_c$ for this case. As for the cases using symmetric copolymers, the results for binary and these ternary blends are almost identical for $Z_h = 1$. However, the differences for larger Z_h are more pronounced, reflecting in part the fact that the overall A:B concentration remains 40:60, and the MST is reached at higher $\overline{\phi}_c$. In general, the decrease in d is faster, or its increase is slower, and the threshold (for the limit $\overline{\phi}_h \to 0$) is increased by about 50% to $Z_h^{th} \simeq 70 \simeq Z_c/6$. For $Z_h = 40$, because the MST is reached sooner in the ternary blends, the rapid changes in d_A and d_B (towards $d/2$) occur at larger $\overline{\phi}_c$. For larger Z_h and the volume fractions shown, the increases in d_A are smaller but the tendency for d_B to increase is larger, in the ternary blends compared with the binary blends.

Figures 4.9 and 4.10 show the calculated variation of d with the interaction parameter χ for the systems modeled above with the symmetric copolymers. In all cases we restrict attention to the region very near the MST, with each line terminating at the value of χ corresponding to the MST. Referring back to the results shown in figure 4.1, it is probable that the variation in d is well represented by our model over this range of χ, (to the extent that mean field theory is adequate). It was observed that $d \propto \chi^p$ over a

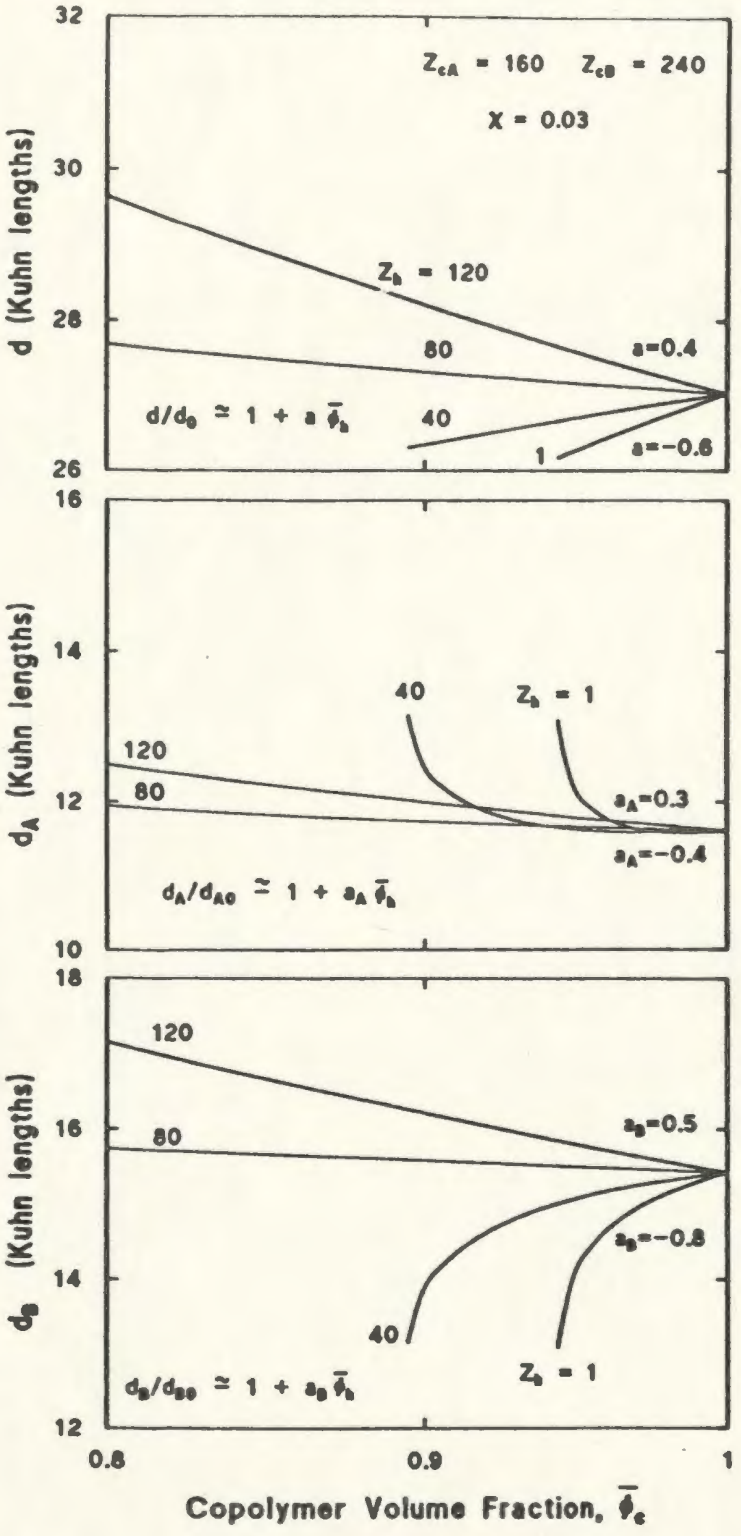

Figure 4.8: Equilibrium domain thickness, d, and subdomain thicknesses d_A and d_B, as a function of $\bar{\phi}_c$ for the model ternary blend with asymmetric copolymers, $Z_{cA} = 160$, $Z_{cB} = 240$. In each case, $Z_{hA} = Z_{hB} \equiv Z_h$ as indicated. The systems are on the isopleth, maintaining a constant overall ratio $\bar{\phi}_\alpha$:$\bar{\phi}_\beta$ = 2:3. The curves for $Z_h = 1$ and 40 terminate at $\bar{\phi}_c = 0.944$ and 0.895 respectively, corresponding to the MST in each case.

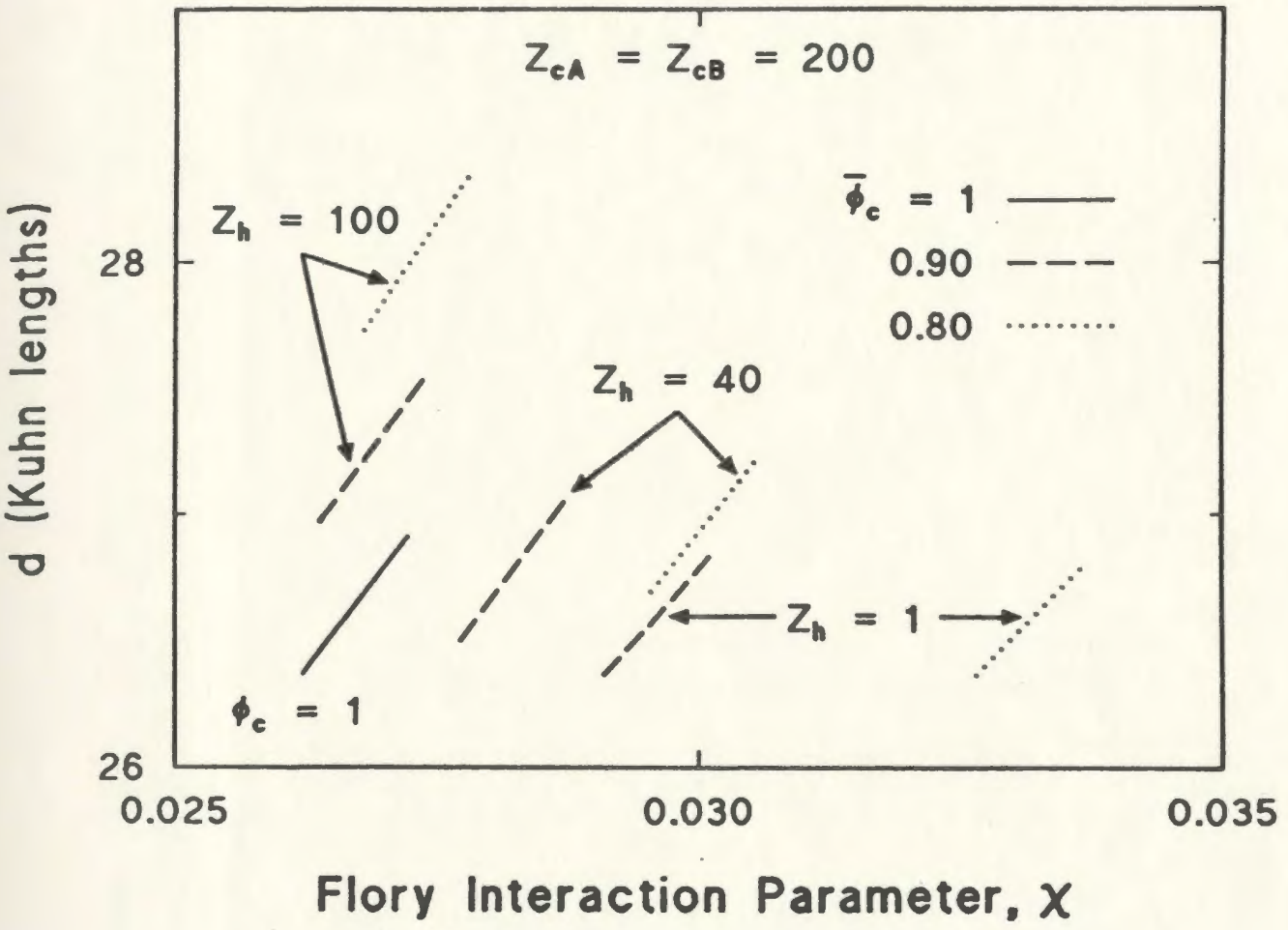

Figure 4.9: Equilibrium domain thickness, d, as a function of interaction parameter χ for binary blends with symmetric copolymers, $Z_{cA} = Z_{cB}$. The solid line represents pure copolymer, dashed lines represent blends with $\bar{\phi}_c = 0.9$, and the dotted lines blends with $\bar{\phi}_c = 0.8$. Results are shown for three different homopolymer degrees of polymerization, Z_h, as indicated.

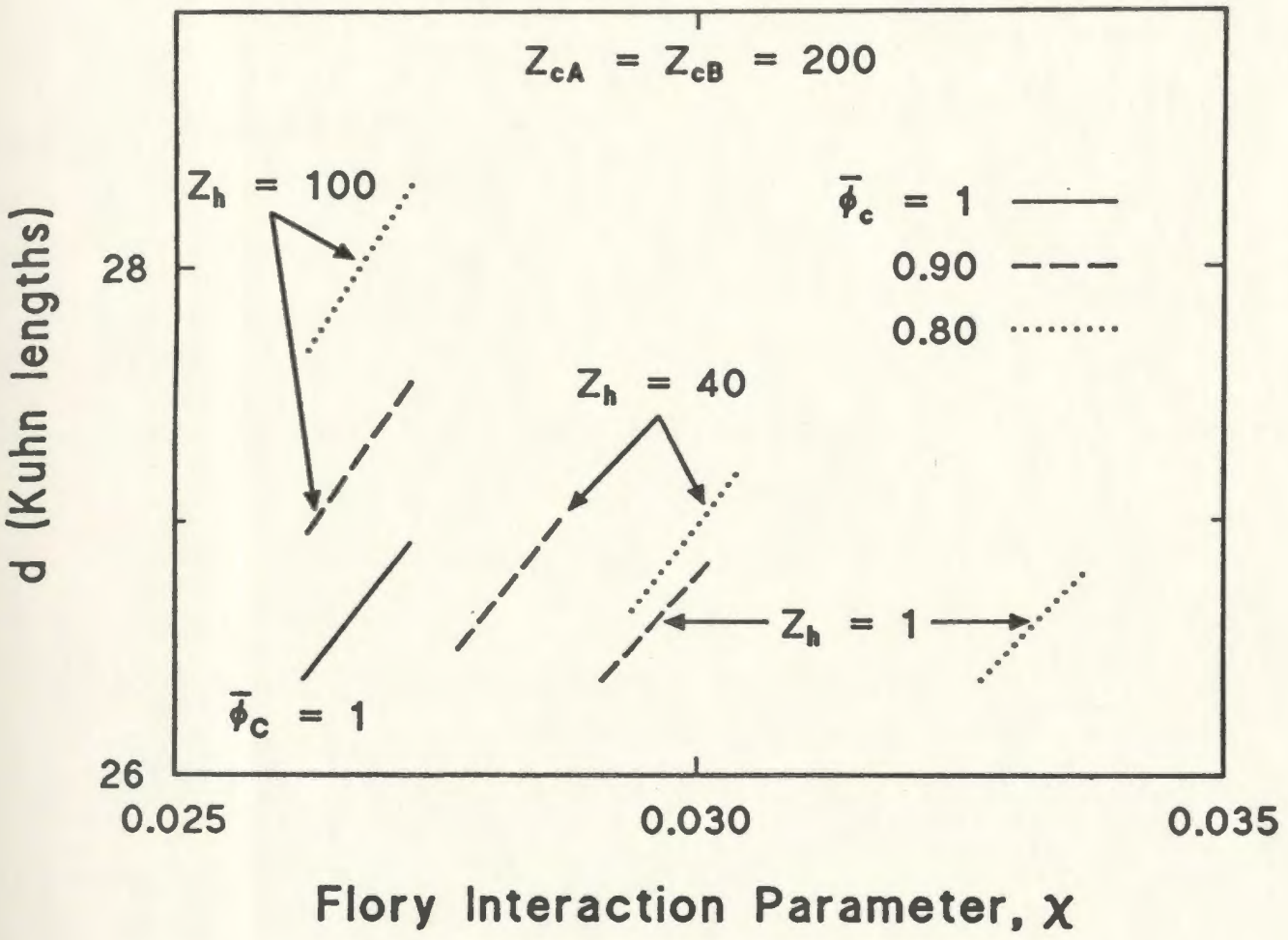

Figure 4.10: Equilibrium domain thickness, d, as a function of χ for ternary blends with symmetric copolymers, $Z_{cA} = Z_{cB}$. The solid line represents pure copolymer, dashed lines represent blends with $\bar{\phi}_c = 0.9$, and the dotted lines blends with $\bar{\phi}_c = 0.8$. Results are shown for three different homopolymer degrees of polymerization, Z_h, as shown. The systems are on the isopleth, so $\bar{\phi}_{hA} = \bar{\phi}_{hB} = \bar{\phi}_h/2$.

range of χ [10] and for that reason we express it in this way over the limited region of χ.

The calculations show a number of effects, at least qualitatively. First, expressing the results again as $d \propto \chi^p$, for the pure copolymer $p \simeq 0.5$, as above. Second, there is very little difference between the binary and ternary blends. Third, in both binary and ternary blends, as solvent is added, the transition is shifted to higher values of χ, for a given χ the value of d decreases, and the value of p remains very near 0.5. For $Z_h = 40$, the transition remains shifted to higher values of χ and for a given χ the value of d is again decreased. However, the dependence of d on χ strengthens slightly as homopolymers are added; p increases to almost 0.6 at $\overline{\phi}_c = 0.8$. For $Z_h = Z_c/4$, the transition is nearly unshifted, for a given χ the value of d is increased, and the dependence of d on χ further increases slightly, with $p = 0.6$ at $\overline{\phi}_c = 0.8$ in the binary blend, and p slightly greater than 0.6 in ternary blend.

Figure 4.11 shows the calculated variation of interfacial width, a_I, with the interaction parameter χ for the systems discussed above with the symmetric copolymer. In all cases we restrict attention to the region very near the MST, with each line terminating at the value of χ shifted away from the MST by 0.01. Since the differences between binary and ternary blends were very small, only binary case is presented here.

We, again, express our results in the form $a \sim \chi^s$. For pure copolymer $s \simeq -0.45$, while for $\overline{\phi}_c = 0.8$ and $Z_h = 100$ the s changes down to -0.6. Quantitatively, in this series of calculations, s decreases with increasing Z_c and decreasing $\overline{\phi}_c$. In strong segregation, Helfand et al. [45, 78] found theoretically that $s = -0.5$ for pure copolymers, which is close to our values of this exponent. It has to borne in mind, however, that our calculations have been performed in the weak segregation regime.

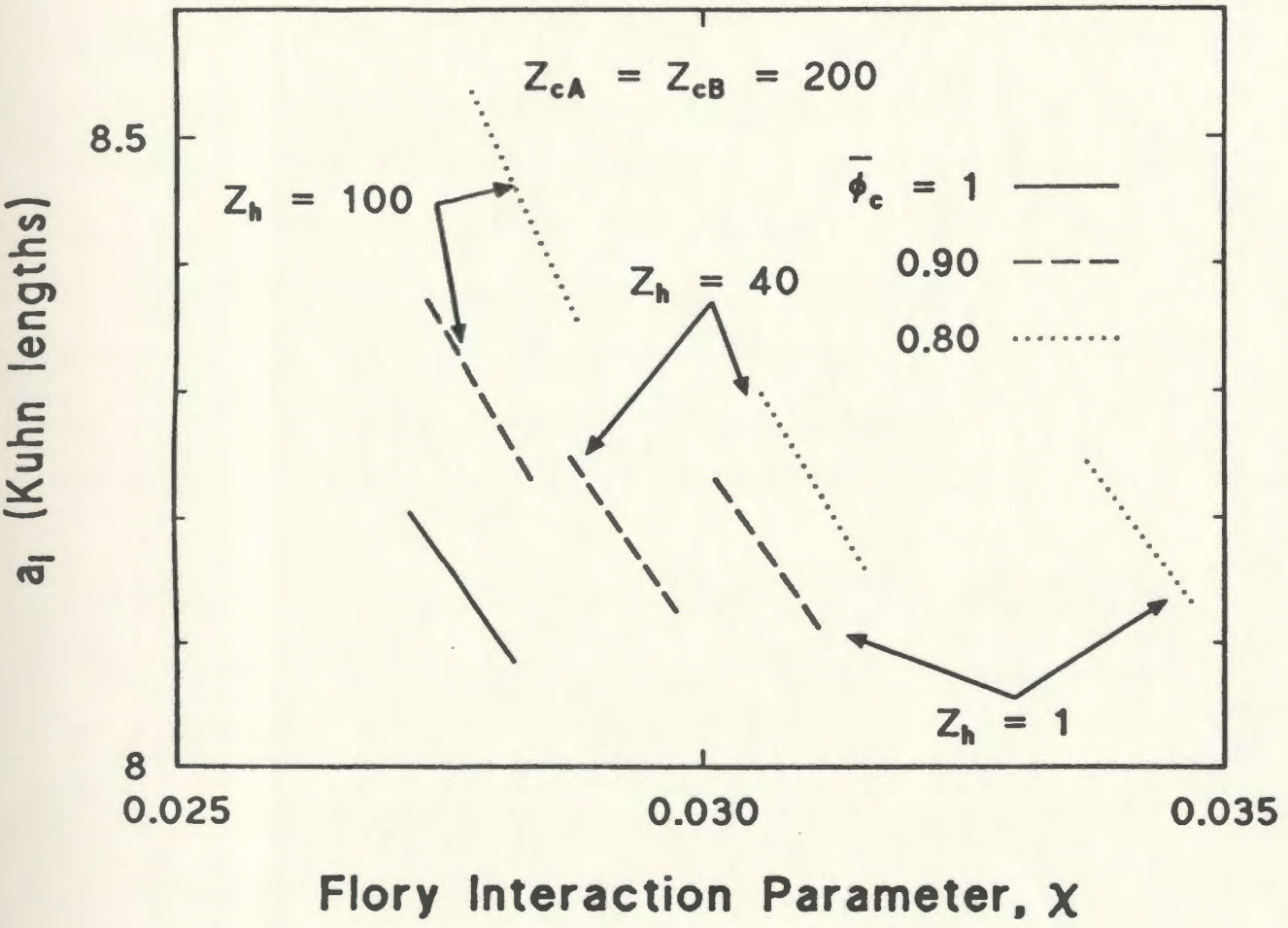

Figure 4.11: Equilibrium interfacial width, a_I, as a function of χ for binary blends with symmetric copolymers, $Z_{cA} = Z_{cB}$. The solid line represents pure copolymer, dashed lines represent blends with $\bar{\phi}_c = 0.9$, and the dotted lines blends with $\bar{\phi}_c = 0.8$. Results are shown for three different homopolymer degrees of polymerization, Z_h, as indicated.

4.3.3 Homopolymer Localization and Density Profiles

We next turn to relating the above results to the distribution of each component within the domains and subdomains. Following Tanaka et al. [14], we begin by considering the square root of the average cross sectional area per copolymer molecule in each domain, a_J. (In the strong segregation regime, a_J is proportional to the average nearest-neighbor distance between joints.) The degree to which a_J increases as solvent or homopolymers are added indicates the degree to which the added molecules penetrate within the copolymers and swell the system laterally. If added solvent penetrates both subdomains, then both d_A and d_B decrease. On the other hand, if hA is preferentially solubilized in the A domain, e.g. in binary blends, then d_A increases but the induced lateral swelling of the copolymers causes d_B to decrease. If added homopolymers are solubilized in both domains, e.g. in ternary blends, then d_A and d_B can either increase or decrease.

Changes in a_J are quantitatively related to changes in $\overline{\phi}_c$ and d by

$$\frac{a_J}{a_{Jo}} = [\frac{d_o}{d\overline{\phi}_c}]^{1/2}, \tag{4.13}$$

where a_{Jo} is a_J for pure copolymer, and for low homopolymer concentrations, the variation in a_J is simply related to the variation in d. Substituting eq. 4.7 into eq 4.13 and expanding yields

$$\frac{a_J}{a_{Jo}} \simeq 1 + (\frac{1-a}{2})\overline{\phi}_h, \tag{4.14}$$

where a is the coefficient appearing in eq. 4.7. If there is no penetration by the added homopolymer, then $a_J = a_{Jo}$, $a = 1$, and $d/d_o \simeq 1 + \overline{\phi}_h$. The greater the penetration is, the faster the increase in a_J/a_{Jo} is, the smaller the value of the coefficient a is, and the slower the increase in d is.

Figures 4.12 and 4.13 show this function for the model systems discussed above. Figure 4.12 is for binary and ternary blends with symmetric copolymers with $Z_{cA} = Z_{cB} =$

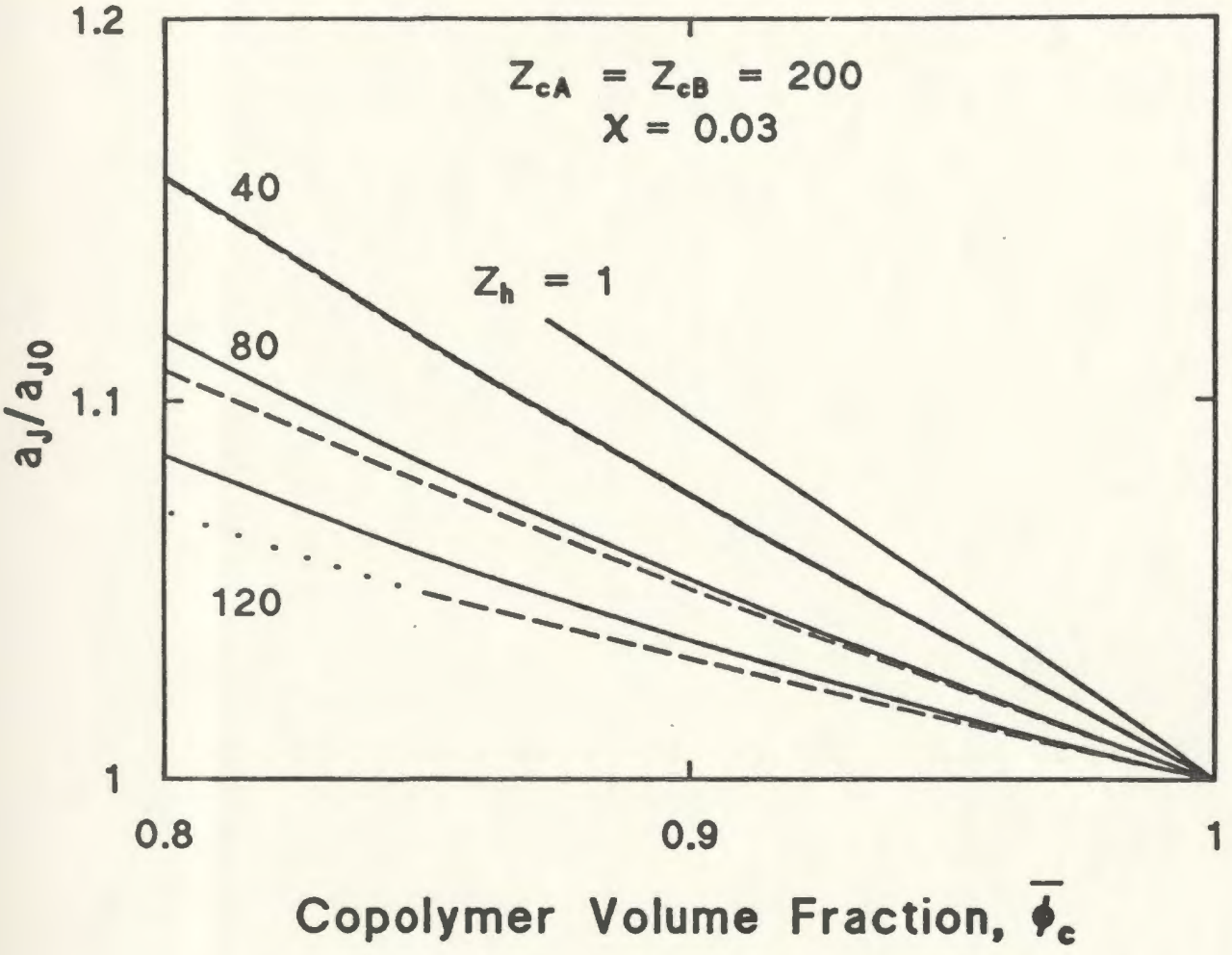

Figure 4.12: Square root of the average cross sectional area per copolymer molecule in each interface, a_J, relative to its value for the neat copolymer system, a_{Jo}, as a function of $\bar{\phi}_c$, for the systems with symmetric copolymers. The solid curves correspond to binary blends, as in figure 4.3, and the dashed curves correspond to ternary blends on the isopleth as in figure 4.7.

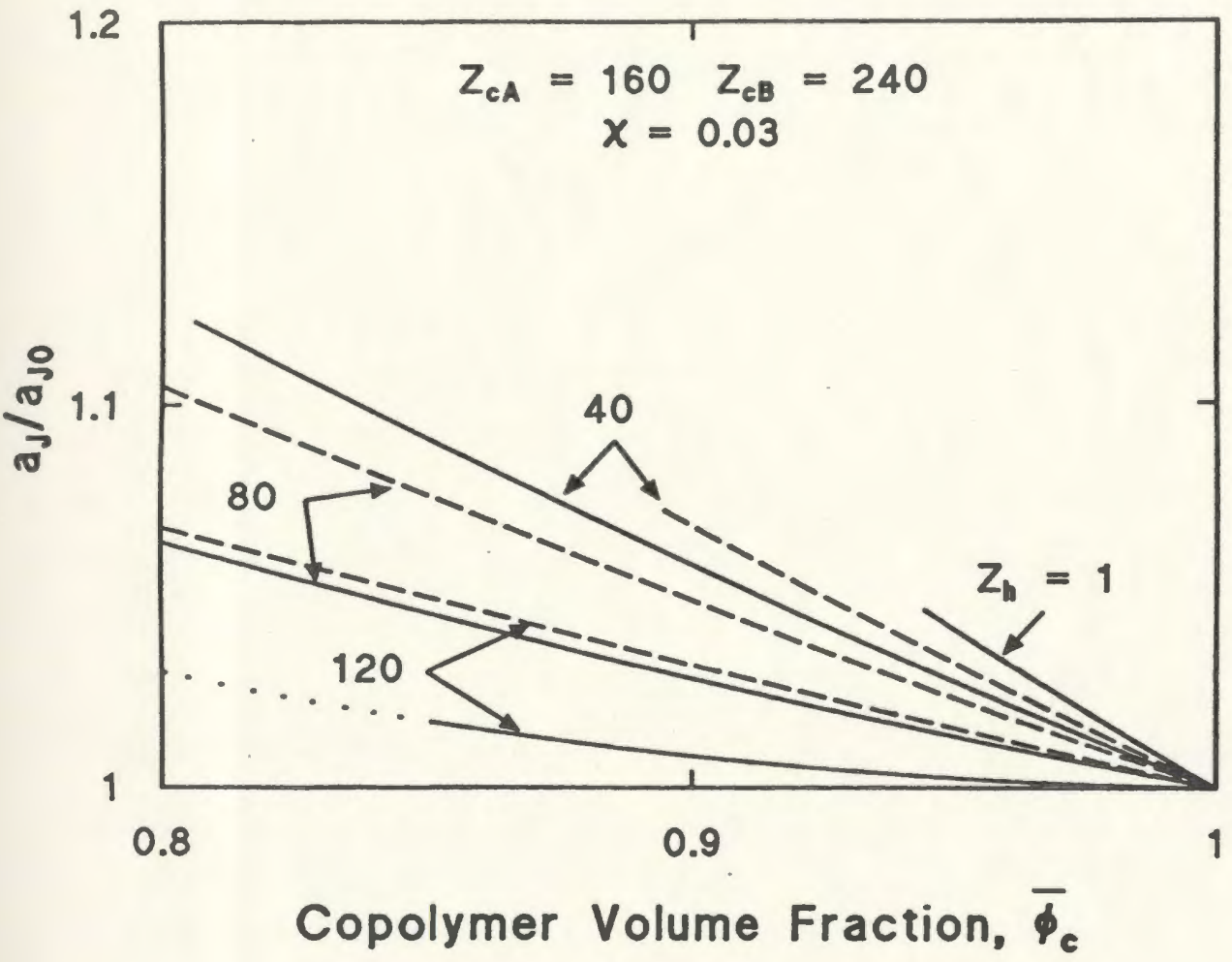

Figure 4.13: Square root of the average cross sectional area per copolymer molecule in each interface, a_J, relative to its value for the neat copolymer system, a_{Jo}, as a function of $\bar{\phi}_c$, for the systems with asymmetric copolymers. The solid curves correspond to binary blends, as in figure 4.6, and the dashed curves correspond to ternary blends on the isopleth as in figure 4.8.

200, and figure 4.13 is for the binary and ternary blends with asymmetric copolymers with $Z_{cA} = 160$ and $Z_{cB} = 240$. (The ternary blends are on the isopleths.) In all cases a_J/a_{J_o} increases with added homopolymers, with the largest increase occurring for smallest Z_h. This implies that the smaller the homopolymer is, the greater is its tendency to penetrate within the copolymers. It is also apparent that for a given copolymer, added solvent has virtually the same effect in binary blends as it does in ternary blends. For blends with symmetric copolymers, figure 4.12, a_J/a_{J_o} is almost the same for binary and ternary blends, being slightly larger in the binary blends. For blends with asymmetric copolymers, figure 4.13, the differences are enhanced and reversed: a_J/a_{J_o} is somewhat larger in the ternary blends. For the binary blends, solid line on each figure, a_J/a_{J_o} is smaller for the asymmetric copolymers than for the symmetric ones. This is largely also the case for ternary blends, (dashed lines on each figure) except for the larger values of Z_h; at $Z_h = 120$ they are almost the same.

Figures 4.14 to 4.16 show calculated density profiles which complement the above calculations. Figure 4.14 is for the binary blends with the symmetric copolymers. The upper panel is for the pure copolymer, and illustrates the two profiles $\phi_{cA}(x)$ and $\phi_{cB}(x)$. The second panel in the first column shows the profiles for a blend with 20% of hA with $Z_h = 40$, and beside this are the profiles for a blend with 20% of hA but with $Z_h = 120$. The final panel is for 40% of hA with $Z_h = 120$. A direct comparison of the panels corresponding to $\overline{\phi}_h = 0.8$ shows that homopolymers with the larger degree of polymerization are the more localized, both between subdomains and within the favorable A-subdomain. This localization is even more apparent in the final panel. In this case the maximum of $\phi_{cA}(x)$ has shifted from the centre of the A-rich subdomain towards the A-B interface. The degree of this localization depends on both the relative degrees of polymerization and the strength of χ, presumably being enhanced in the strong segregation regime.

Figure 4.15 is similar to figure 4.14, except it is for the asymmetric copolymers,

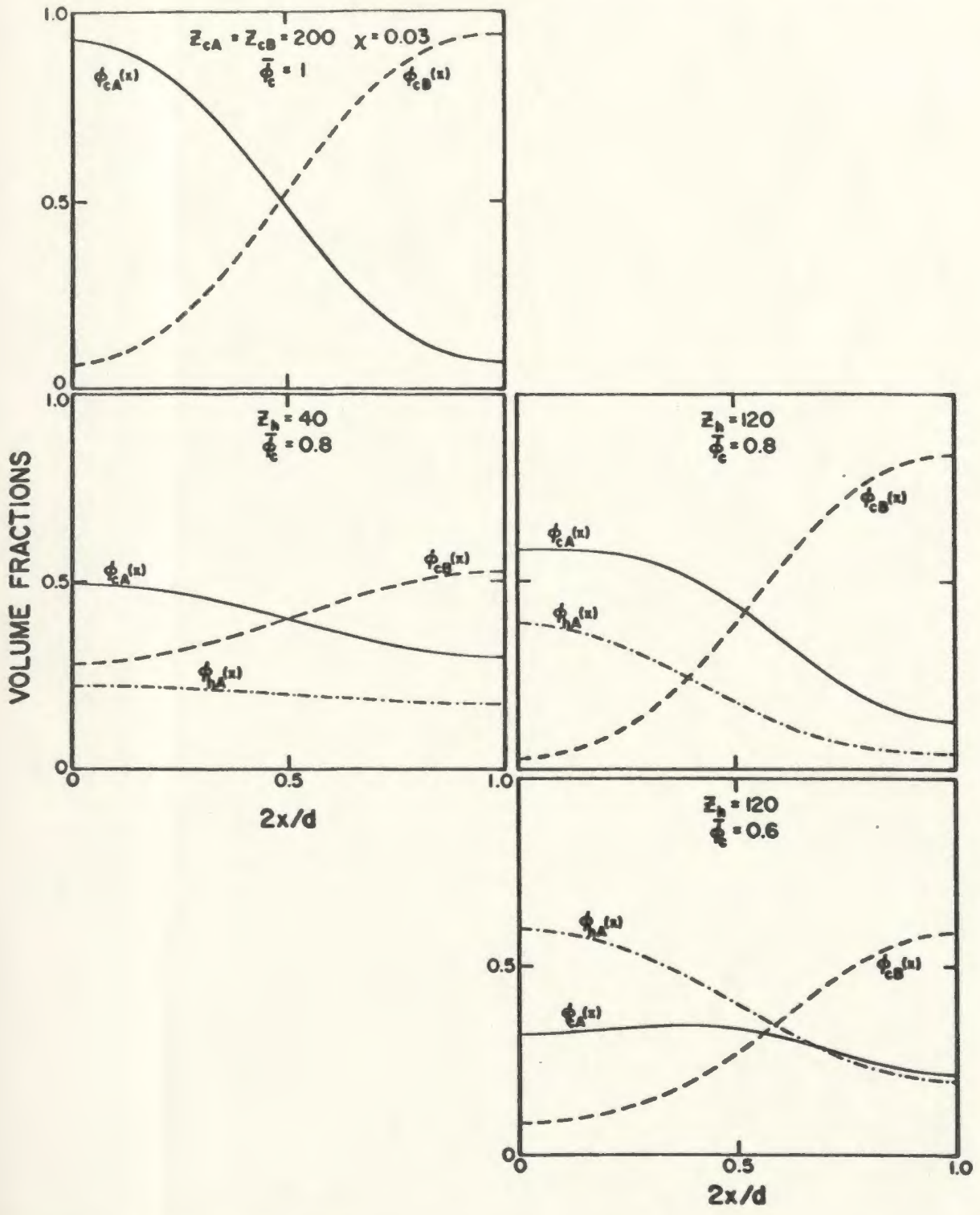

Figure 4.14: Local volume fractions for binary copolymer/homopolymer blends for different overall volume fractions, $\bar{\phi}_c$, as indicated. The top panel is for symmetric copolymers with $Z_{cA} = Z_{cB} = 200$. The others are for blends with added hA for which $Z_h = 40$, left hand column, and $Z_h = 120$, right hand column. The local volume fractions due to the A and B blocks of the copolymer are labeled $\phi_{cA}(x)$ and $\phi_{cB}(x)$, respectively, and that due to the homopolymers is $\phi_{hA}(x)$.

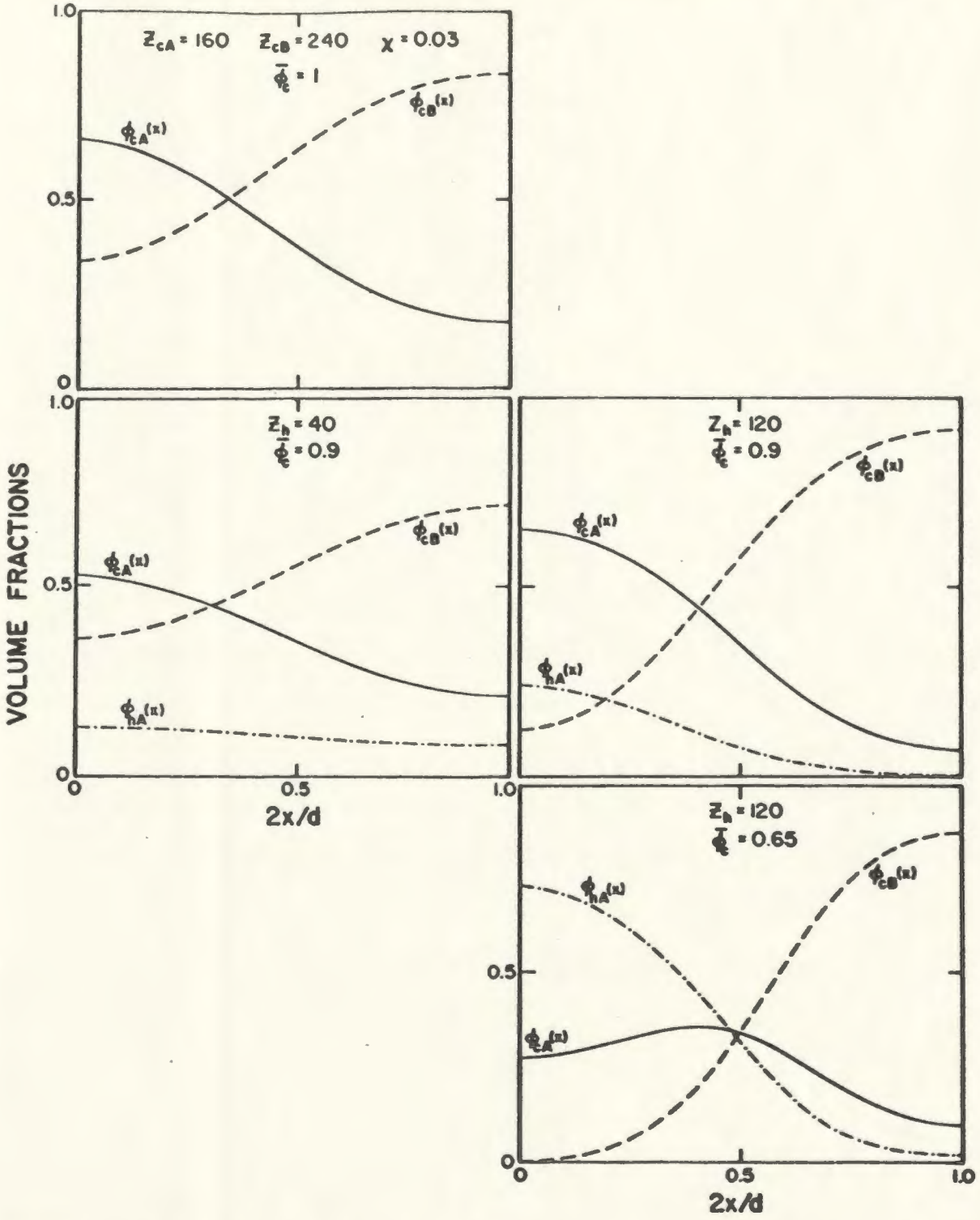

Figure 4.15: Local volume fractions for binary copolymer/homopolymer blends for different overall volume fractions, $\bar{\phi}_c$, as indicated. The top panel is for asymmetric copolymers with $Z_{cA} = 160$, $Z_{cB} = 240$. The others are for blends with added hA for which $Z_h = 40$, left hand column, and $Z_h = 120$, right hand column. The notation is as in figure 4.14.

$Z_{cA} = 160$ and $Z_{cB} = 240$. The calculations indicate that for this value of χ, an 80/20 blend of these copolymers with hA of $Z_h = 40$ is not microphase separated, and so we compare the two systems with $\overline{\phi}_c = 0.9$ instead of $\overline{\phi}_c = 0.8$ as in figure 4.13. Also, the theory predicts that a 60/40 blend with homopolymers with $Z_h = 120$ macrophase separates [66], and so $\overline{\phi}_c = 0.65$ was used for the final panel. The results are qualitatively the same as for the blends with symmetric copolymers but there is a quantitative change. In the case $Z_h = 120$, the localization of the hA within the subdomain is slightly greater and the local minimum in $\phi_{cA}(x)$ is more pronounced.

Finally, figure 4.16 shows density profiles for a ternary blend with the asymmetric copolymers used above and unequal homopolymer degrees of polymerization. For this case we chose $Z_{hA} = 120 = 0.75 Z_{cA}$, and $Z_{hB} = 40 = 0.17 Z_{cB}$, so that the degree of polymerization of the A homopolymers is relatively large compared with that of the corresponding copolymer block, whereas the degree of polymerization of the B homopolymers is relatively low. The resulting profiles reflect these choices. The B homopolymers are distributed much more uniformly throughout the full domain than the A homopolymers, which are almost fully expelled from the B subdomains and furthermore are quite localized within the A subdomains. Reflecting this, $\phi_{cB}(x)$ peaks at the centre of the B subdomains, but $\phi_{cA}(x)$ has a broad, shallow minimum at the centre of the A subdomain, as in the last panels of figure 4.14 and 4.15.

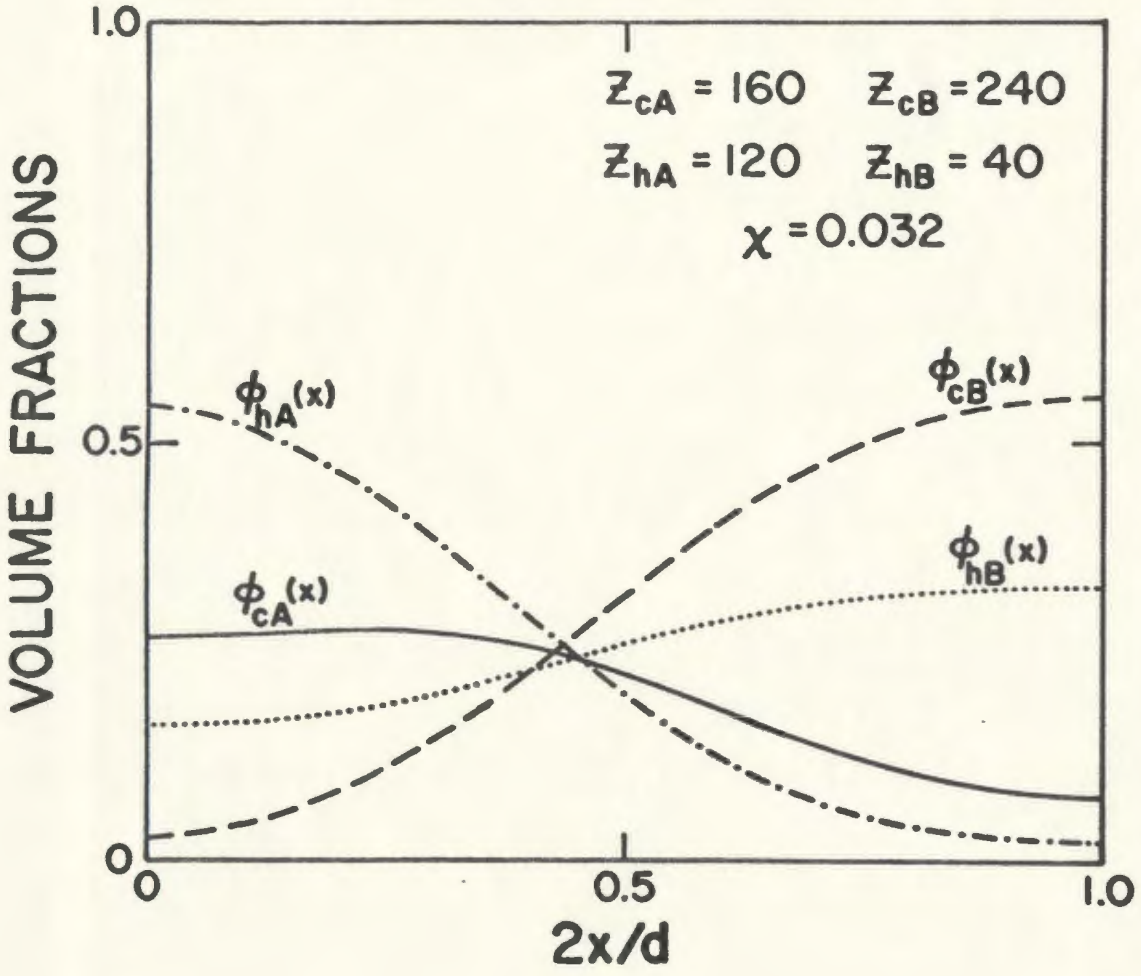

Figure 4.16: Local volume fractions for ternary copolymer/homopolymer blend. As indicated the copolymer is asymmetric with $Z_{cA} = 160$, $Z_{cB} = 240$. The homopolymers have different degrees of polymerization. The overall copolymer volume fraction is $\overline{\phi}_c = 0.45$, and the overall homopolymer volume fractions are chosen so that the system is on the isopleth, i.e., $\overline{\phi}_{hA} : \overline{\phi}_{hB} = 160 : 240$.

4.4 Experimental Comparison

We discuss three sets of experiments, beginning with those carried out by Hashimoto et al. [13, 14, 15]. They used Transmission Electron Microscopy to identify the morphologies (lamellae, cylinders or spheres) of copolymer blends in the strong segregation regime. However, their primary experimental technique was SAXS. They measured the elastic scattering intensity as a function of wavevector (angle θ) which exhibited regularly spaced maxima ("peaks") from which domain thickness could be calculated and type of morphology determined. In particular, the lamellar structure was confirmed by maxima at the peak positions, which were integer multiples of the wavenumber of the first-order peak, $1 : 2 : 3 : 4 : \cdots$. For cylinders and spheres the maxima were at $1 : \sqrt{3} : \sqrt{4} : \sqrt{7} : \cdots$, and $1 : \sqrt{2} : \sqrt{3} : \sqrt{4} : \cdots$, respectively, relative to that of the first order. Furthermore, by volumetric considerations [14, 80], subdomain thicknesses and a_J/a_{J_o} were calculated.

Hashimoto et al. used styrene-isoprene copolymers, which they labeled *HY8*, with a total degree of polymerization of $Z_c \simeq 385$, block degrees of polymerization $Z_{cPS} \simeq 145$ and $Z_{cPI} \simeq 240$ and volume fractions $\overline{\phi}_{cPS} \simeq 0.45$ and $\overline{\phi}_{cPI} \simeq 0.55$. They used homopolymer *PS* (*hPS*) with degrees of polymerization $Z_{hPS} \simeq 25$, 40, 100 and 160, and homopolymer *PI* (*hPI*) with $Z_{hPS} \simeq 25$. These were labeled *S02, S04, S10, S17* and *HI* respectively. Most of the measurements were for binary blends using the *hPS*, with up to 80% homopolymer. For blends with *S02, S04* or *S10*, the structure remained lamellar at $\overline{\phi}_h = 0.2$, changing to cylindrical for $\overline{\phi}_h = 0.5$. However, blends using *S17* remained lamellar up to $\overline{\phi}_h = 0.5$. They also studied ternary *HY8/S02/HI* blends, choosing the overall blend composition to maintain the system on the isopleth, i.e., $\overline{\phi}_{PS} \simeq 0.45 = 1 - \overline{\phi}_{PI}$. This system maintained a lamellar structure with long range order for copolymer volume fractions as low as 10%.

Many of their results focussed on the domain and subdomain thicknesses d, d_{PS} and d_{PI}, the average distance between joints in each interface, and the dependence of these quantities on composition, degrees of polymerization and temperature. They also interpreted their results in terms of the localization of the homopolymers within the subdomains. In all cases, their analysis indicated that the systems were in the strong segregation regime, and that the solubilized homopolymers were completely segregated into the favorable subdomains.

Some of their data are reproduced in figure 4.17 and 4.18. We summarize the results which relate to the current work as follows:

1. In ***binary*** systems:

   - at a given temperature T, adding hPS always caused an increase in d and d_{PS} and a decrease in d_{PI};
   - for a given $\overline{\phi}_{hPS}$, d always decreased with increasing temperature;
   - the temperature dependence of d increased with decreasing Z_{hPS}, and for $Z_{hPS} < Z_{cPS}$ it increased with increasing $\overline{\phi}_{hPS}$;
   - for a given $\overline{\phi}_{hPS}$ and T, d always increased with increasing Z_{hPS}.

2. In ***ternary*** blends, adding homopolymers always caused an increase in d, d_{PS} and d_{PI}.

3. In binary and ternary blends, a_J/a_{J_o} always increased upon addition of homopolymers, and the increase was faster for small Z_{hPS} than for large Z_{hPS}. This implied that the low molecular weight homopolymers were solubilized relatively uniformly

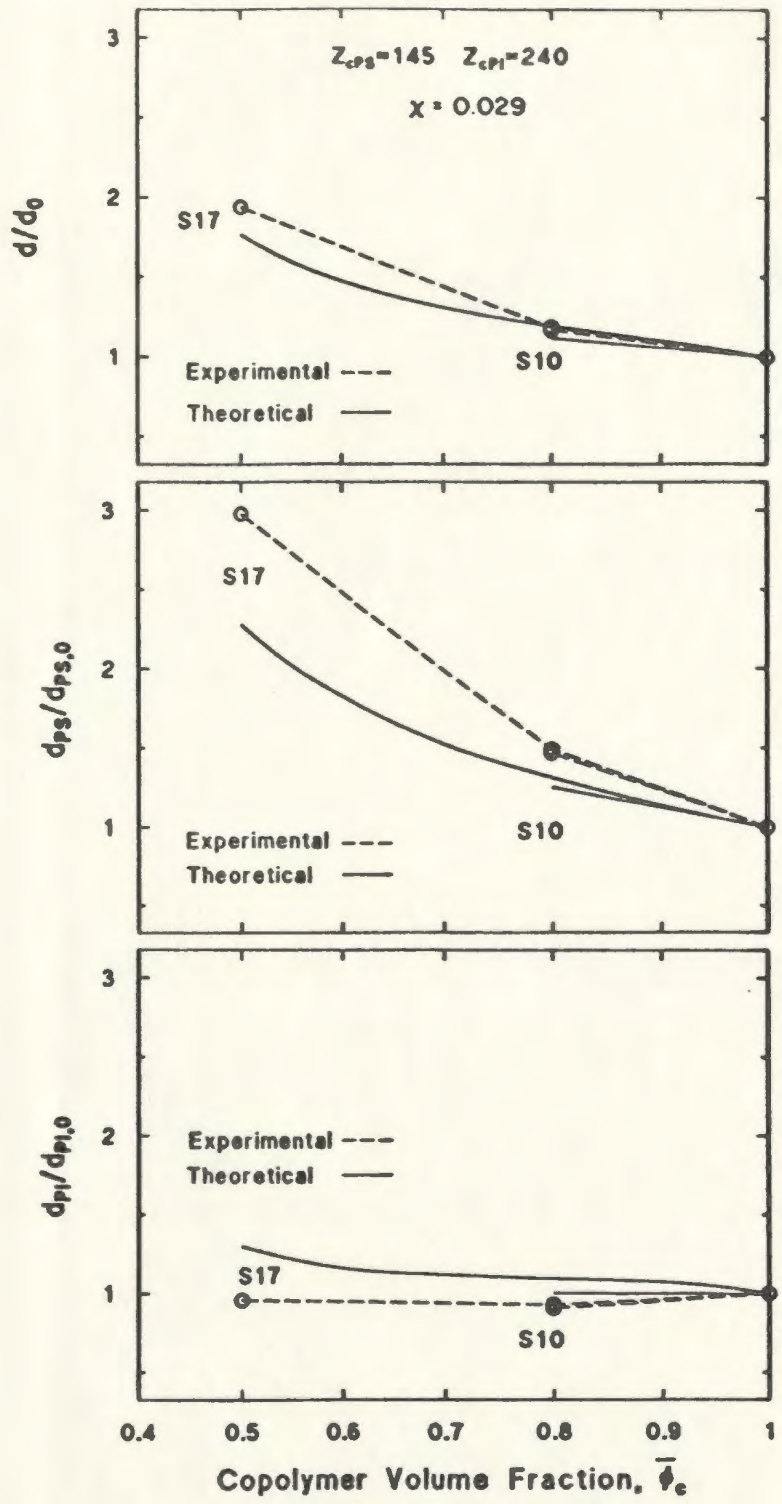

Figure 4.17: Calculated and measured values of d, d_{PS}, and d_{PI}, for *PS-b-PI/PS* blends for copolymers with block degrees of polymerization as shown, and for homopolymers with degrees of polymerization $Z_{hPS} = 100$ and 160. These correspond to the *HY8/S10* and *HY8/S17* blends studied by Hashimoto at al. The points are the experimental values, and the solid curves the calculations which were done with a constant value of χ, chosen to be 0.029.

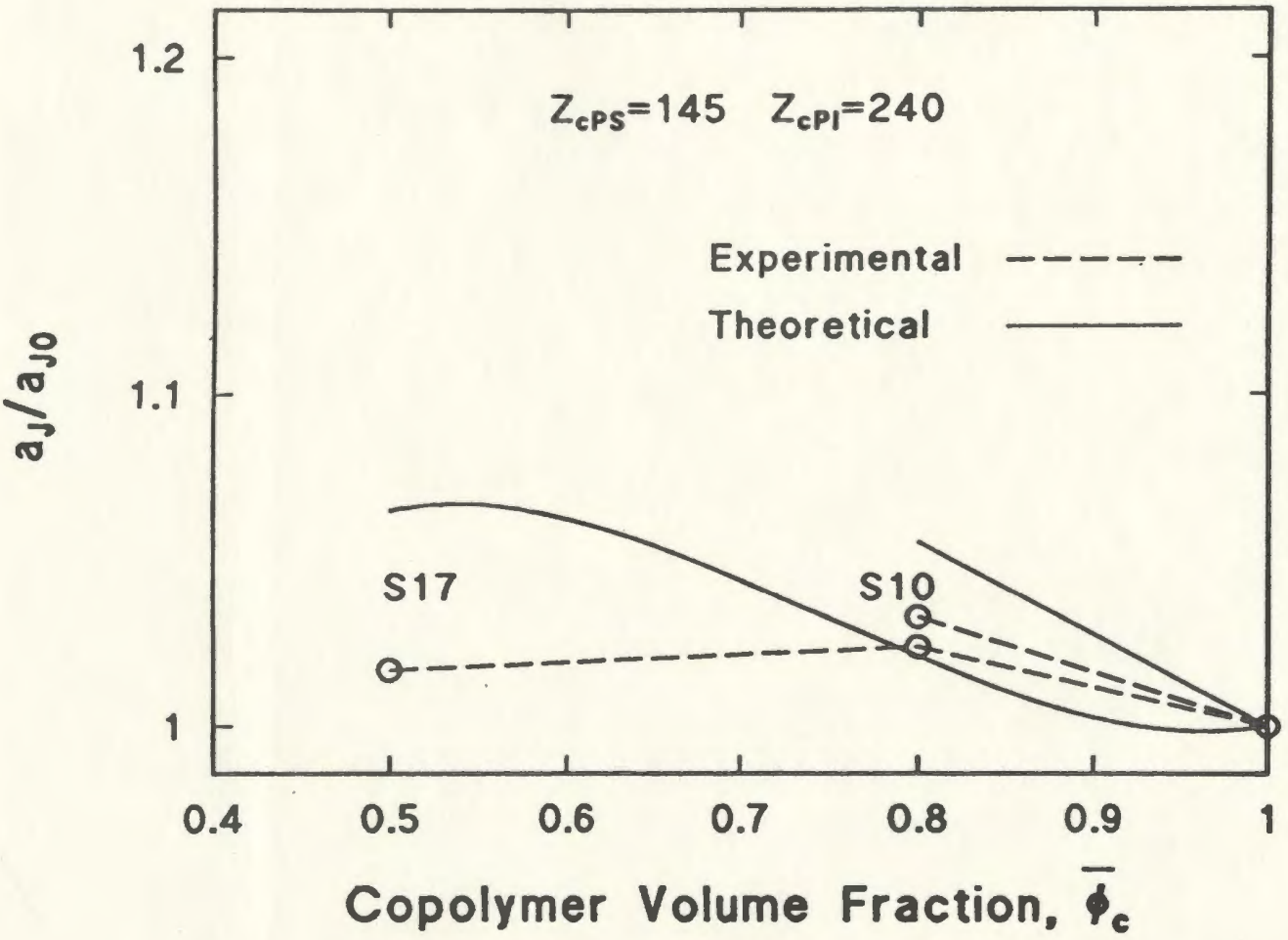

Figure 4.18: Calculated and measured values of a_J/a_{J_o} for the *PS-b-PI/PS* blends of figure 4.17. The points are the experimental values, and the solid curves the calculations which were done with a constant value of χ, chosen to be 0.029. The dashed lines joining the experimental points are intended as visual guides.

within the corresponding subdomains, while the higher molecular weight homopolymers were more localized within the centres of the subdomains. For these copolymers, the variation of a_J/a_{J_o} with $\overline{\phi}_c$ was virtually the same for binary and ternary blends.

The effective value of χ was determined in related experiments [10, 81] by SAXS measurements of the elastic scattering intensity in disordered single phase states, as discussed in section 2.4. In these experiments the temperature range, at which the systems were in a disordered state, was expanded by addition of neutral solvent DOP to the blends. In the context of dilution approximation, discussed in section 3.1, the "effective" χ parameter can be expressed as

$$\chi_{\text{eff}} = \chi\phi_p, \tag{4.15}$$

where ϕ_p is the total polymer volume fraction. For these *HY8* copolymers, they found $\chi \simeq 0.035$, with the precise value depending on temperature. Adding up to 50% of *S02*, *S04* or *S10* homopolymers caused χ to increase, by as much as 50%. For a given $\overline{\phi}_{hPS}$, χ increased with decreasing Z_{hPS}. Adding up to 50% of *S17* homopolymers caused a decrease in χ of about 10%. The temperature dependence of χ tended to be greater for smaller Z_{hPS}.

In the second set of experiments, Winey [16] applied the same experimental techniques as Hashimoto et al. [13, 14, 15], i.e., SAXS in ordered blends and Transmission Electron Microscopy. They also used styrene-isoprene copolymers, (labeled *SI* 27/22) with $Z_{cPS} \simeq 255$ and $Z_{cPI} \simeq 325$, and corresponding volume fractions $\overline{\phi}_{cPS} \simeq 0.51$ and $\overline{\phi}_{cPI} \simeq 0.49$. They studied blends with *hPS* with $Z_{hPS} \simeq 25$, 60, 135 and 355, which they labeled *2.6 hPS*, *6 hPS*, *14 hPS* and *37 hPS* respectively, using homopolymer weight fractions w_h up to 20% for all cases except *14 hPS*, where w_h was as high as 0.24. They estimated a

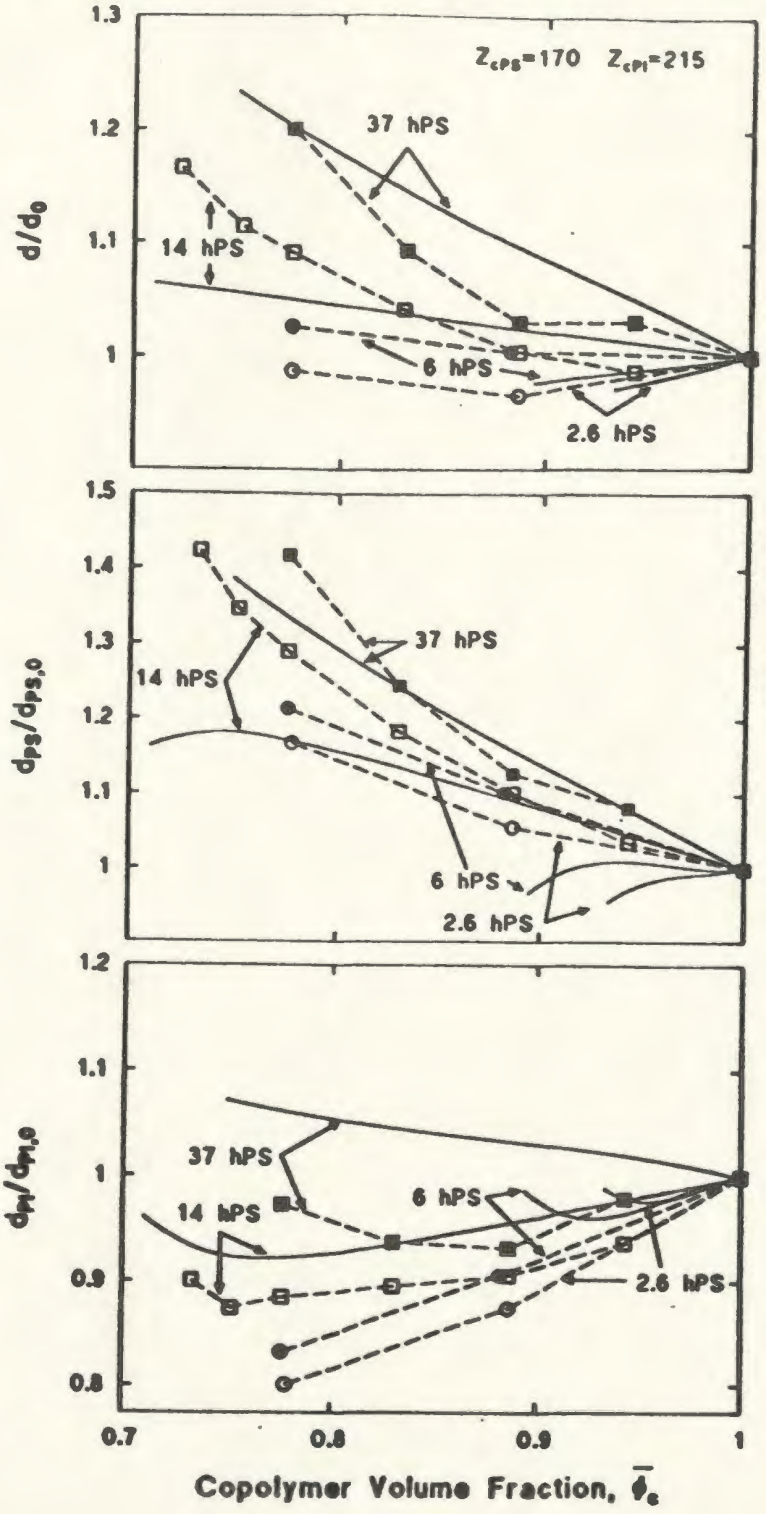

Figure 4.19: Calculated and measured values of d, d_{PS}, and d_{PI}, for *PS-b-PI/PS* blends for copolymers with block degrees of polymerization as shown, and for homopolymers with degrees of polymerization $Z_{hPS} = 15$, 40, 90, and 235. These correspond to the four blends studied by Winey [16], as indicated by the labeling on this diagram, except that all degrees of polymerization have been rescaled by a common factor, and χ has been set to 0.029. The points are the experimental values, and the curves the calculations which were done with $\chi = 0.029$. For different panels, we use different units on vertical axis.

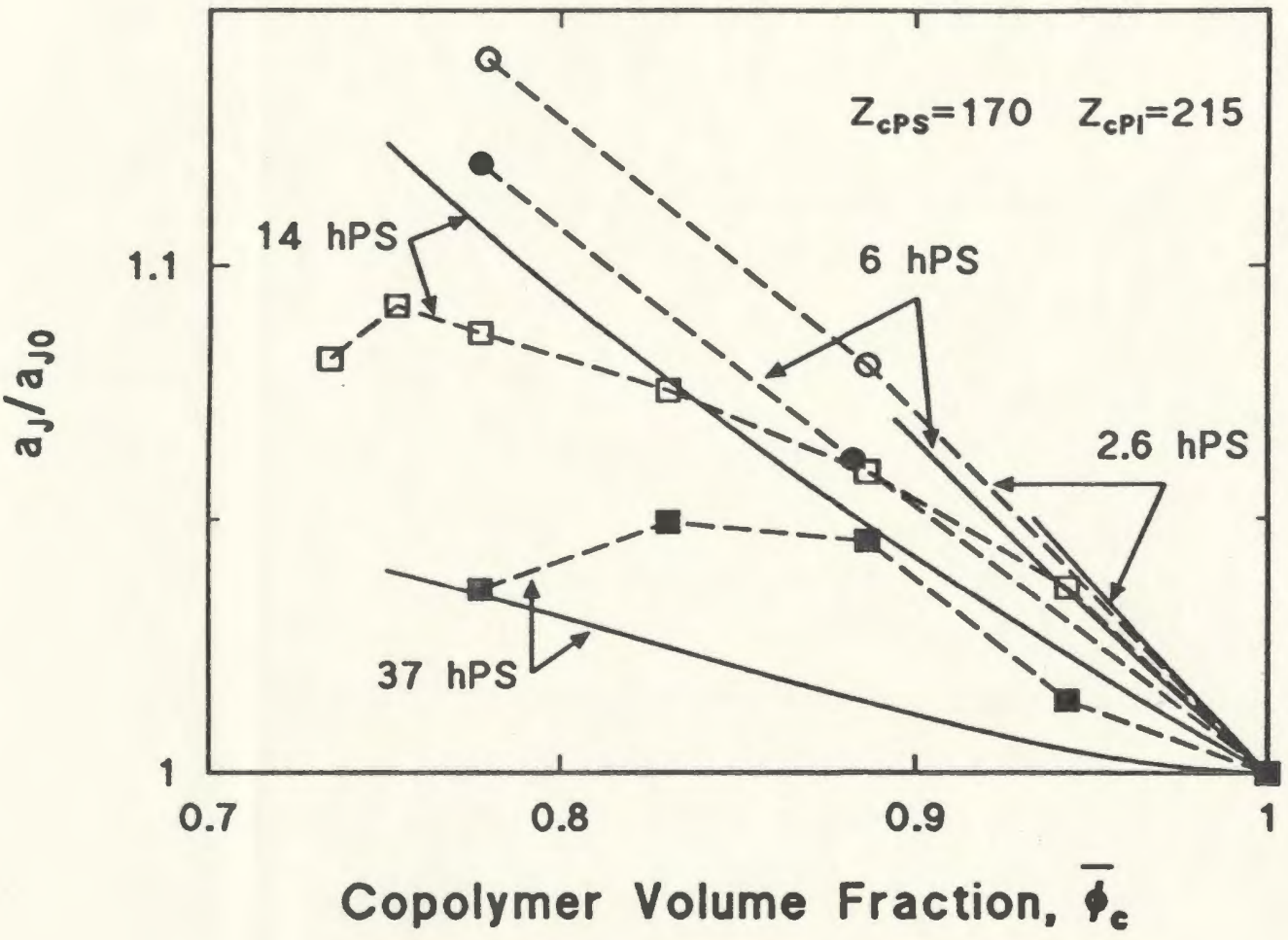

Figure 4.20: Calculated and measured values of a_J/a_{Jo} for the *PS-b-PI/PS* blends of figure 4.19. The points are the experimental values, and the solid curves the calculations which were done with a constant value of χ, chosen to be 0.029.

value of $\chi Z_c \simeq 32$, which corresponds to the strong segregation regime. All these blends exhibited the lamellar structure.

The observations in these experiments, reproduced in figure 4.19 and 4.20, were more complex than those found by Hashimoto et al. [13, 14, 15]. The addition of small amounts of either *2.6 hPS* or *14 hPS* induced small decreases in d, which were followed by increases as additional homopolymers were added. In 90:10 blends with either *6 hPS* or *14 hPS*, the value of d was virtually the same for as for the neat copolymers. The addition of *37 hPS* consistently induced an increase in d. These results are consistent with the existence of an approximate threshold Z_h^{th}, with a value in the vicinity of $Z_h^{th} \simeq 100 \simeq Z_{cPS}/2.5$. The existence of this apparent threshold contrasts with the results of Hashimoto et al., but this difference may be attributable to molecular weight and composition dependencies of χ.

Otherwise, the results agree with those of Hashimoto et al. For a given T and $\overline{\phi}_h$, the domain thickness is an increasing function of Z_{hPS}, and the associated lateral swelling is a decreasing function of Z_{hPS}. The *PS* subdomain thickness always increased as a function of both Z_{hPS} and $\overline{\phi}_h$. The *PI* subdomain thickness decreased as *hPS* was added, except for weight fractions $w_{hPS} \gtrsim 0.2$ for the *14 hPS* and *37 hPS* cases. The decrease in d_{PI} was smaller for large Z_{hPS}. The area per chain decreased or increased as d_{PI} increased or decreased, respectively.

Finally, Quan et al. [18] used Small Angle Neutron Scattering (SANS) to measure the SANS intensity as a function of scattering wavevector, and to determine the domain thicknesses for a series of hydrogenated butadiene homopolymers in a matrix of styrene-hydrogenated butadiene-styrene triblock copolymers, with weight fractions $w_{hPB} = 0.2$. The copolymers had weight fractions $w_{cPS} = 0.49$ and $w_{cPB} = 0.51$, and block degrees of polymerization $Z_{cPB} \simeq 1{,}000$ and $Z_{cPS} \simeq 270$, (each block). They found that the lamellar thickness d decreased for homopolymers with $Z_{hPB} \simeq 200$, and increased for

$Z_{hPB} \simeq 600$ and 1,100. Their data suggest a threshold value near $Z_{hPB} \simeq 250 \simeq Z_c/4$.

Because all these systems are in the strong segregation regime, and also because the last ones involve triblock copolymers, we should not expect quantitative agreement between the current theory and these experiments. Furthermore, the experiments indicate that a full understanding of these systems would require a detailed knowledge of the variation of χ with molecular weights and overall composition, information which is not currently available for these systems in the weak segregation regime. Nonetheless, we can make a qualitative comparison of the predictions for the weak segregation regime with the results of these experiments. We also have performed a series of calculations relevant to the experimental systems.

We consider the qualitative comparisons first.

- For binary systems the theory predicts that, for constant χ, the addition of homopolymers with relatively high degrees of polymerization causes an increase in the layer thickness, and the size of the increase is an increasing function of Z_h and $\overline{\phi}_h$. This is consistent with all three sets of experiments. The prediction of a threshold value Z_h^{th}, such that if $Z_h < Z_h^{th}$ then d decreases, contrasts with the first set of experiments but agrees with the other two. The predicted values of Z_h^{th} are similar, but not equal, to those found in the latter two sets of experiments.

- The theory predicts that d increases with χ. This is consistent with the finding that d always decreased with increasing T.

- The prediction that, for a given $\overline{\phi}_h$, d always increases with Z_h agrees with the experiments for the case $Z_{hPS} < Z_{cPS}$.

- The prediction that a_J/a_{J_o} always increases with added homopolymers and that the size of the increase is a decreasing function of Z_h agrees with the experiments.

Furthermore, for symmetric copolymers a_J/a_{J_o} is virtually the same for binary and ternary blends, as found experimentally.

- Expressing the dependence of d on χ as $d \propto \chi^p$, the theory predicts that p increases slightly as both $\overline{\phi}_h$ and Z_h increases. This compares with the finding that the temperature dependence of d strengthens with increasing $\overline{\phi}_h$ but decreasing Z_h. This is another case in which a conclusive comparison would require the full temperature, composition and molecular weight dependencies of χ, in the appropriate regime.

Turning now to related calculations, the first set is shown in figure 4.17 and 4.18. For the numerical work we choose the copolymer degrees of polymerization of each block to be those used in the experiments, $Z_{cPS} = 145$ and $Z_{cPI} = 240$, and use independently determined reference densities and Kuhn lengths: $\rho_{oS} = 6.07$ nm^{-3} and $b_S = 0.68$ nm for polystyrene and $\rho_{oI} = 8.07$ nm^{-3} and $b_I = 0.59$ nm for polyisoprene [82, 83]. In order to stay within the weak segregation regime, we choose $\chi = 0.029$ as in the model calculations of the previous section 4.3. This compares with the experimental value of about 0.035 for the copolymers, or an (approximate) effective value of less than 0.035 for the systems diluted with DOP [10]. In this context, we do not feel that it is appropriate to include any variation in χ with composition, although it would be straightforward to do so.

The upper panel of figure 4.17 shows the variation of d/d_o with composition for two sets of blends, $Z_{hPS} = 100$ and $Z_{hPS} = 160$, corresponding to the experimental blends as indicated on the figure. For these cases, the measurements indicate little dependence of χ on volume fractions [10, 84]. In both cases the layer thickness increases as homopolymers are added, with a faster increase for the $Z_{hPS} = 160$ blend. As indicated, these changes are very similar to those found experimentally in the strong segregation regime. On the other hand, the predictions for the blends using lower molecular weight homopolymers

for this regime would differ from the experiments; for constant χ, d/d_o would decrease as homopolymers are added, which compares with the small increase found experimentally. Furthermore, for the chosen value of χ the MST would soon be reached. However, as previously discussed the χ parameter not only is constant but it increases upon addition of low molecular weight homopolymer [10], which might prevent the system from reaching the MST, and further contribute to this difference.

The other panels of figure 4.17 compare the calculated values of the subdomain thicknesses with the experimental ones for these systems. The results for these blends are again in qualitative agreement; $d_{PS}/d_{PS,o}$ increases, with the largest increase occurring for the *S17* blend, and $d_{PI}/d_{PI,o}$ is nearly constant. However, there are quantitative differences; the increase in $d_{PS}/d_{PS,o}$ found in the experiments is larger than that in the calculations, and the small decrease in $d_{PI}/d_{PI,o}$ found in the experiments contrasts with the small increase in the calculations.

Figure 4.18 compares the experimental and theoretical values of a_J/a_{J_o} for these two systems. In all cases, its change is on the order of only 5% over the composition ranges studied, with the larger increases occurring for the lower Z_{hPS} blends. Both theory and experiment indicate that the variation of a_J/a_{J_o} is non-monotonic for the *S17* blends. More data would be needed to compare the locations of the indicated maximum.

The small increase in a_J/a_{J_o} implies a relatively high degree of localization of homopolymer. This is further illustrated in figure 4.21 which shows the density profiles for 3 copolymer volume fractions of *HY-8/S17* corresponding to figure 4.17 and 4.18. The first panel represents the calculated density profiles for the pure copolymer. The middle and lower panels, corresponding to $\overline{\phi}_c = 0.9$ and 0.6, illustrate that adding these homopolymers drives the system towards the strong segregation regime, with the amplitudes of the copolymer density variations increasing. Of particular interest is the localization of the homopolymer within the corresponding subdomain. It is larger here than in any of

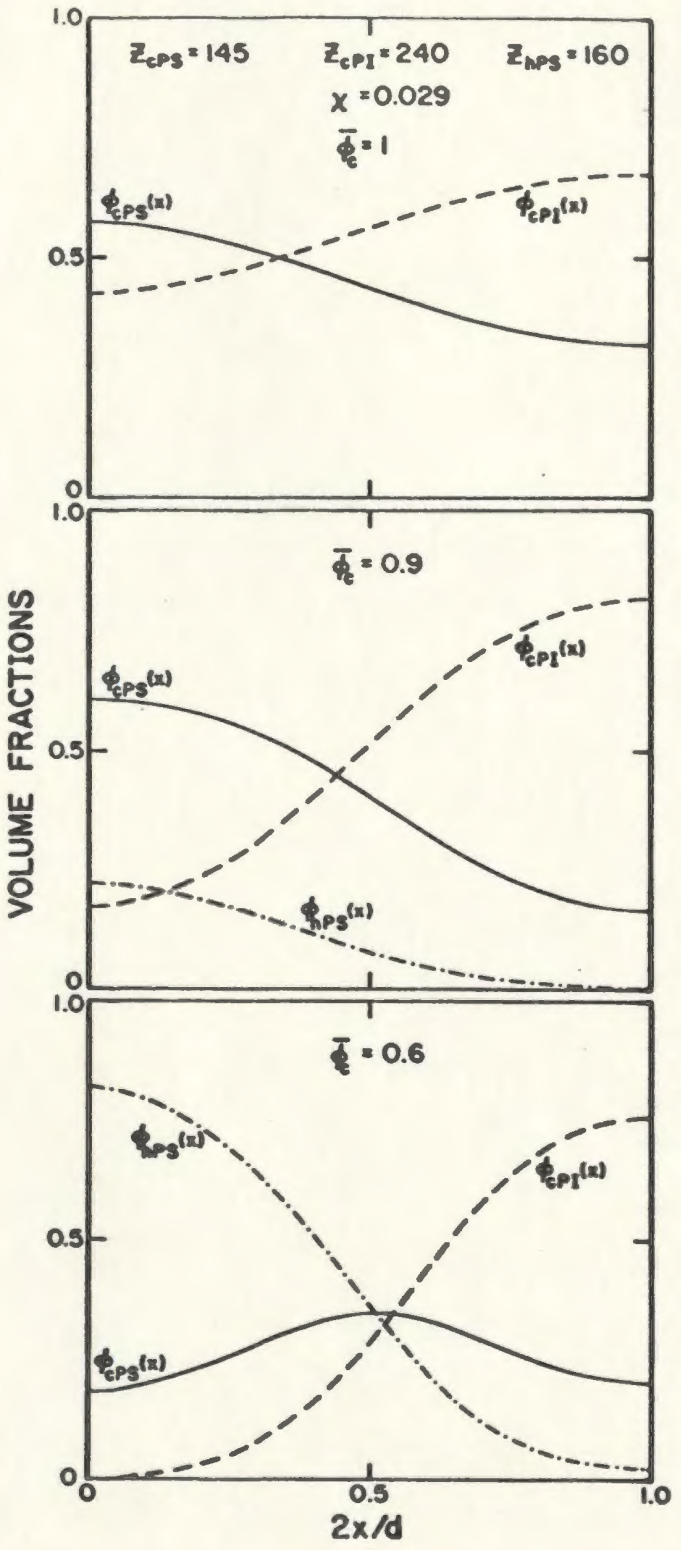

Figure 4.21: Calculated local volume fractions corresponding to the *HY8/S17* blend of figure 4.17 and 4.18, for three compositions as shown, and for $\chi = 0.029$.

the model calculations illustrated in Section 4.3 of this chapter, with the local minimum in $\phi_{cPS}(x)$ at the centre of the *PS* subdomain being particularly pronounced in this case.

Finally, figure 4.19 and 4.20 compare theoretical calculations with the experiments of Winey. Once again, in order to stay within the weak segregation regime we choose $\chi = 0.029$ as before, but we also rescale all degrees of polymerization by a factor of 385/580, so that $Z_c = 385$ as in the cases shown in figure 4.17, 4.18 and 4.21. The calculations should be thought of as an exploration of the effects of the relative degrees of polymerization, not the total. (We could equally have chosen the total degrees of polymerization to be those used by Winey but introduced a new value of χ to place the system in the weak segregation regime.)

The upper panel of figure 4.19 compares the values of d/d_o. The experimental data show more structure than the calculations, but otherwise there is qualitative agreement. The layer thickness generally increases in the two higher Z_{hPS} cases, and decreases for the lowest Z_{hPS} case. For the *6 hPS* blend the calculations show a decrease in d, but the experiments show virtually no change.

The lower panels of figure 4.19 compare the calculated values of the subdomain thickness with the experimental ones for these systems. For *37 hPS* the experiment shows an increase in d_{PS} upon addition of homopolymers, in agreement with the calculations. Also for *14 hPS* there is a qualitative agreement upon addition of homopolymers. However, when more *14hPS* is added, our calculations indicate that the system moves towards the MST, which reduces the d_{PS}, while the experimental data show consistent increase in d_{PS}. This discrepancy might be due to the smaller values of χ which we used in our calculations, as already discussed in the case of preceding experiments of Hashimoto et al. Similar discrepancies are observed in the behaviour of d_{PS} for *6 hPS* and *2.6 hPS*. The last panel of figure 4.19 shows a calculated increase in d_{PI} for *37 hPS*, upon addition of homopolymers, while the experiment shows an initial decrease followed by an increase.

For *14 hPS* the qualitative behaviour of d_{PI} is the same for both the experiments and the calculations, i.e., an initial decrease followed by an increase. The qualitative disagreement of the behaviour of d_{PI}, for both *6 hPS* and *2.6 hPS*, might have the same origin as the one for d_{PS} for these two homopolymers, i.e., small value of theoretical χ, and consequent dissolution of the ordered structure.

Finally, figure 4.20 compares the calculated and measured values of a_J/a_{J_o} for these systems. The overall scale and qualitative behaviour are the same, but there are the same quantitative differences as there are in figure 4.19. In particular, there is significant structure in the experimental results for the *37 hPS* blends which is not present in the calculations.

In conclusion to this chapter we recall the most interesting results. We compared the results of the fourth order expansion calculations with the numerical self-consistent ones for the related problem of *A-b-B*/selective solvent blends, finding that the results of the two calculations agreed very well for values of χ within about 10% of its value at the MST. Using the fourth order expansion, we performed both model and real system calculations, based on experimental work of Hashimoto et al., Winey and Quan et al. Subsequently we name the most important results of those calculations. We found that, for constant χ, the addition of homopolymers with relatively high degrees of polymerization, Z_h, caused an increase in the layer thickness, and the size of the increase was an increasing function of Z_h. Homopolymers with relatively small Z_h lead to a decrease in d, and so there was a threshold value $Z_h \cong Z_c/5$. Low molecular weight homopolymers were relatively uniformly solubilized in the subdomains, while homopolymers of high molecular weight were progressively more localized towards the subdomain centre. This was illustrated by calculated density profiles in the weak segregation regime. In the case of real system calculations, we mostly found a qualitative agreement with experiments.

Chapter 5

Phase Behaviour of Ternary Copolymer/Homopolymer Blends

5.1 Introduction

The goal of this chapter is to provide a contribution to the understanding of microphase and macrophase separation in ternary copolymer/homopolymer blends of the form *A-b-B/A/B*, e.g. *PS-b-PI/PS/PI*. We discuss here the phase behaviour of these blends on the basis of a mean field theory which employs the fourth order expansion of the free energy of the microphase, developed in chapter 2 and used in 4. In this chapter this expansion is simplified by the assumption that near the MST, the density profiles can be modeled by simple cosine-like variations about their mean values, i.e., only the dominant wavenumber is included in summations. Even for ternary systems which do not undergo an order-disorder transition, e.g. those described by a simple Flory-Huggins model for the free energy, there is a multitude of possible phase diagram topologies [85]. In this chapter we consider some of the interesting possibilities for systems which undergo both microphase and macrophase separation. Because we use one wavenumber approximation, we limit the discussion to the weak segregation regime, but reemphasize that even here the results should be considered primarily as guides to the behaviour which can occur. The approach does not include fluctuation effects, numerical solutions to the self-consistent field equations, or equation of state effects, i.e., the temperature and pressure dependence of polymer densities. Because of these limitations, we made no attempt to discriminate between different morphologies (lamellae, cylinders, spheres). Instead we

explicitly assumed the lamellar structure. This can be at least partly justified on the grounds that, except very near to the order-disorder transition, the difference between the free energies of any two microphases is generally much smaller than the difference between the free energy of any microphase and the homogeneous phase [86]. This approach can be thought of as the simplest treatment of these systems which incorporates both microphase and macrophase separation.

The calculations here complement the recent discussion of ternary phase diagrams of such blends by Broseta and Fredrickson, which was based on the Leibler RPA theory, using what corresponds to the second order term in the expansion of the free energy of the microphase [87]. Their discussion of different topologies of ternary phase diagrams was restricted to isotropic mixtures, i.e., either for block copolymer/homopolymer, *A-b-B/A/B*, blends above the MST for all concentrations, or for random copolymer/homopolymer blends, *A-co-B/A/B*. First they discussed the symmetric copolymer, i.e., copolymer containing the same number of A and B monomers, and homopolymers with the same degree of polymerization. Following Leibler [11], they also assumed that monomers had equal volumes, and Kuhn lengths for A and B are identical. They found that the topology of the phase diagram of such a blend depends only on two parameters: α and h, where $\alpha = Z_c/Z_h$ and $h = Z_c\chi$. In particular, they predicted the criteria for the existence of three-phase region. Next they showed the limits of their theory by considering the second order term (or equivalently the inverse of the calculated scattering intensity, $I(k)$) of the free energy polynomial expansion for block copolymer/homopolymer blends. If the initial slope of $I(k)$, as a function of k at $k = 0$, was positive then the maximum of $I(k)$ was reached at some k^* different from zero. This indicated the possibility of microphase separation and was excluded from Broseta and Fredrickson's work. If, on the other hand, this initial slope was negative that suggested a macrophase separation, i.e., $k^* = 0$ instability. The system could macrophase separate into either a two-phase or

three-phase region.

When modeling the blend we assume that each phase is either a homogeneous mixture or an ordered microphase, but these are not the only possibilities. In particular, copolymer micelles can form within each homopolymer rich phase, or the copolymers could migrate to interfaces between homopolymer domains. Using a model of micelle formation developed by Whitmore and Noolandi [31], we have tried to identify and thereby avoid systems in which micelles form. We also assume that at equilibrium only an insignificant fraction of the copolymers migrates to interfaces (for those cases where macrophase separation occurs).

Section 5.2 of this chapter describes the theory and detailed formulae appropriate for this chapter, and section 5.3 presents results. Given the limitations of the approach these results cannot be considered quantitatively reliable, but instead should be used as guides to understanding the systems and the phenomena that can occur.

5.2 Calculation of Phase Diagrams

In this section we show the method of calculating the phase diagrams of these systems in the weak segregation regime, assuming a lamellar structure for the microphase, and using the one wavenumber approximation. To do so, for each system we first calculate the free energy per unit volume for all concentrations, $\overline{\phi}_{hA}$, $\overline{\phi}_{hB}$ and $\overline{\phi}_c$, including Δf if so indicated. Because we are treating the weak segregation regime, for the purposes of calculating Δf and for speed of calculations we approximate $\phi_\alpha(x)$ by the simple circular function [11, 87]

$$\phi_\alpha(x) = \overline{\phi}_\alpha + \Psi_\alpha \cos(k\,x), \tag{5.1}$$

and of course $\phi_\beta(x) = 1 - \phi_\alpha(x)$. The second term in eq. 5.1 models the variation of $\phi_\alpha(x)$ about its mean value, with Ψ_α being the amplitude of this variation. Away from the order-disorder transition, other wavenumbers must be included to calculate the density profiles, domain thicknesses, etc. [30], as in chapter 4 of this thesis, but in this chapter we make no attempt to calculate these other quantities. This simplification of the assumed density variation, $u(x;d,p,q)$ of eq. 4.4, is meant to facilitate the time-consuming numerical calculations of this chapter.

A consequence of using eq. 5.1 and assuming the lamellar structure is that only wavevectors of magnitude k appear in the summations of eq. 2.105, and furthermore the third order term vanishes. The remaining sums for $f^{(2)}$ and $f^{(4)}$ are independent of Ψ_α, and result in an expression of the form

$$\Delta f = A(k){\Psi_\alpha}^2 + B(k){\Psi_\alpha}^4. \tag{5.2}$$

The next step is to locate the minimum of $A(k)$, say at k^*. If $A(k^*) > 0$ then it indicates that the homogeneous phase is stable relative to the microphase, and the free energy density for that blend is $f = f_{hom}$. If, however, $A(k^*) < 0$ then it indicates that the

microphase is stable relative to the homogeneous mixture. In this case we evaluate $B(k^*)$, and minimize eq. 5.2 by calculating $\Psi_\alpha = [-A(k^*)/2B(k^*)]^{1/2}$, giving

$$\Delta f = -\frac{A(k^*)^2}{4B(k^*)}. \tag{5.3}$$

The resulting (negative) value for Δf is then added to the Flory Huggins free energy f_{hom}, to give the free energy density of a single phase at that composition. The test calculations show that the differences between the numerical values of Δf, obtained in many wavenumber and and one wavenumber expansions, are small in the vicinity the MST. Furthermore, Whitmore and Noolandi [30] have demonstrated that, in case of copolymer/nonselective blend, the free energy obtained from the self-consistent calculations differs from the one wavenumber 4^{th} order expansion by about 10%, even in the strong segregation regime.

This produces a full free energy surface for the system. From this surface we next locate order-disorder transition lines, where $A(k^*) = 0$, and the spinodals for macrophase separation, where, e.g.,

$$\begin{vmatrix} \frac{\partial^2}{\partial \phi_{kA}^2} f & \frac{\partial^2}{\partial \phi_{kA} \partial \phi_{kB}} f \\ \frac{\partial^2}{\partial \phi_{kA} \partial \phi_{kB}} f & \frac{\partial^2}{\partial \phi_{kB}^2} f \end{vmatrix} = 0. \tag{5.4}$$

Having located the spinodals, the next step is finding the tie lines and binodals. Two phases coexist at points 1 and 2 of the phase diagram if there exists a plane which is tangent to the free energy surface at those two points, but which lies below it everywhere else [88]. Such a pair of points is connected by a tie-line, and the locus of these pairs of points constitutes binodal lines. If there is a plane which is tangent to the free energy surface at three different points but which lies below it elsewhere, then these three points enclose a three phase region. In this chapter we consider two and three phase regions.

The numerical procedure for finding the tangent planes, which we have developed, is

based on that of Hsu and Prausnitz [89], and consists of minimizing a convenient function of three (for a two phase region) or six (for a three phase region) variables. The free energy density $f(\overline{\phi}_{hA}, \overline{\phi}_{hB}, \overline{\phi}_c)$ formally depends on the three concentrations $\overline{\phi}_{hA}$, $\overline{\phi}_{hB}$ and $\overline{\phi}_c$. But since $\overline{\phi}_{hA} + \overline{\phi}_{hB} + \overline{\phi}_c = 1$, any two concentrations (or any two linearly independent combinations of all of them) can serve as independent variables. Here we list some of the possible choices: $\{\overline{\phi}_{hA}, \overline{\phi}_{hB}\}, \{\overline{\phi}_c, \overline{\phi}_{hA}\}, \{\psi = \overline{\phi}_{hA} + \overline{\phi}_{hB}, \eta = \overline{\phi}_{hA} - \overline{\phi}_{hB}\}$. Finding a plane tangent to the free energy surface at two points, 1 and 2 with coordinates (x_1, y_1) and (x_2, y_2) respectively , amounts to solving of a system of the subsequent equations

$$\nabla_x f|_1 = \nabla_x f|_2, \tag{5.5}$$

$$\nabla_y f|_1 = \nabla_y f|_2, \tag{5.6}$$

$$f(2) - f(1) = \nabla_x f|_1 (x_2 - x_1) + \nabla_y f|_1 (y_2 - y_1). \tag{5.7}$$

where x and y are one of the possible choices of independent variables. This system is solved numerically by minimizing the function

$$\begin{aligned} g(x_1, x_2, y_1, y_2) = \tfrac{1}{C}\{ & [\nabla_x f|_1 - \nabla_x f|_2]^2 + \\ & [\nabla_y f|_1 - \nabla_y f|_2]^2 + \\ & [f(1) - f(2) + \\ & \nabla_x f|_1 (x_2 - x_1) + \nabla_y f|_1 (y_2 - y_1)]^2\}, \end{aligned} \tag{5.8}$$

where

$$C = (x_1 - x_2)^2 + (y_1 - y_2)^2, \tag{5.9}$$

and is meant to exclude the possibility of finding trivial solution, i.e., $x_1 = x_2$ and $y_1 = y_2$.

One additional "independent" variable can be eliminated by the following reasoning. When a ternary system is placed into an unstable region at composition described by coordinates (x^*, y^*) then it macrophase separates into, at least, two equilibrium phases

characterized by concentrations (x_1, y_1) and (x_2, y_2) such that they satisfy equations 5.5, 5.6 and 5.7. Two of those equation, eq. 5.5 and 5.6, express the equality of chemical potentials of the corresponding phases, 1 and 2. The additional condition which x_1, x_2, y_1, and y_2 have to fulfill is that points (x_1, y_1), (x^*, y^*) and (x_2, y_2) are collinear. This requirement further reduces the number of independent variables to 3. The third equation, eq. 5.7, along with the above condition ensures the conservation of mass.

It was straightforward to generalize the preceding considerations for the case where the system macrophase separates into three equilibrium phases denoted by 1, 2 and 3. The system of equations for a plane tangent to the free energy surface at three points 1, 2 and 3 can be readily generalized. The minimized function g becomes dependent on six variables in this case.

5.3 Results

5.3.1 Symmetric Model Systems

We begin with model system calculations for which all reference densities and Kuhn lengths are taken to be equal. We choose copolymers with $Z_c = 400$ which is the same as in model calculations of the previous chapter and close to the value used in the experimental work reviewed in section 4.4. Here, again, the overall scale of the values of χ is chosen close to 0.0263 as in section 4.1. As already stated in the Introduction and section 2.4, for each blend we neglect its dependence on overall concentrations, and do not need to relate it directly to either temperature or degrees of polymerization. The other important system characteristics are the composition of the copolymers, i.e., Z_{cA}/Z_c, and the degrees of polymerization of each homopolymer relative to the copolymers, related to parameter α of Broseta and Fredrickson and mentioned in section 5.1. [87].

Our first three sets of calculations are for a symmetric system, containing copolymers with $Z_{cA} = Z_{cB} = Z_c/2$, and homopolymers with equal degrees of polymerization, $Z_{hA} = Z_{hB} \equiv Z_h$. Figure 5.1 shows four phase diagrams for the case of relatively low homopolymer molecular weight, $Z_h = Z_c/8$, which is $Z_h = 50$ in this case. For $\chi Z_c < 10.5$, (not shown) the system is in a single homogeneous phase for all concentrations. As χ is increased beyond this value, e.g. the temperature is lowered, the first feature which appears is microphase separation of the pure copolymer. This is illustrated in the first panel of figure 5.1, for which $\chi Z_c = 12$. Addition of these low molecular weight homopolymers in any proportion tends to dissolve the microphase, but there is no macrophase separation anywhere on the diagram which is consistent with the results for binary blends [29]. In principle, there is a small two phase region between the M and H regions which vanishes in this approach. Thus there are only a single microphase region, M, and a single homogeneous phase region, H, on this diagram. As the value of χ is further increased

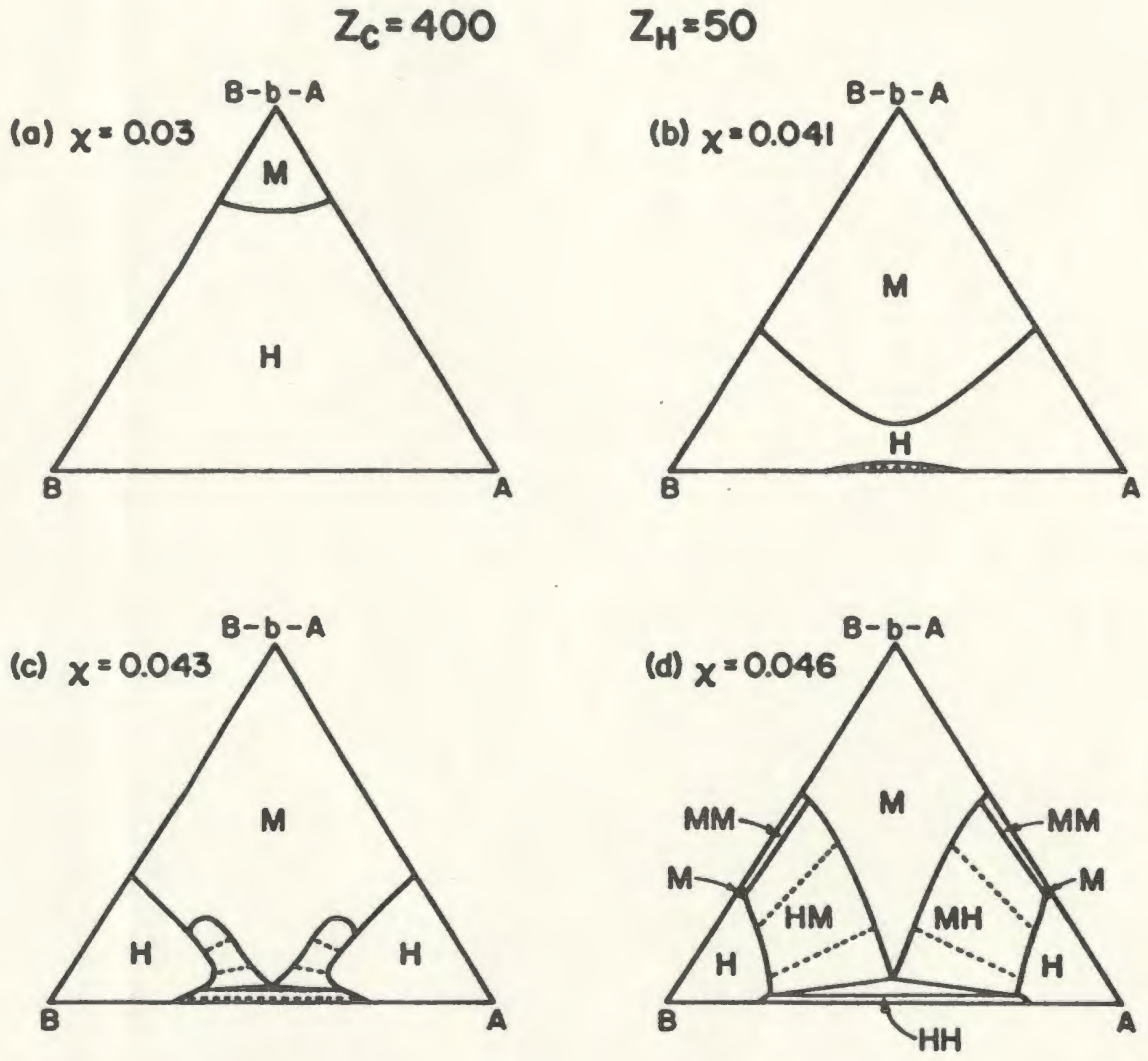

Figure 5.1: Calculated phase diagrams for a model symmetric ternary *A-b-B/A/B* blend with copolymer degree of polymerization $Z_c = 400$, ($Z_{cA} = Z_{cB} = Z_c/2$), homopolymer degrees of polymerization $Z_{hA} = Z_{hB} = 50$, and four values of the Flory interaction parameter as indicated. All reference volumes ρ_{op} and Kuhn statistical lengths b_p are taken to be equal. In each of these diagrams, the apex of the triangle represents pure copolymers, and each of the other vertices represents pure *A* or *B* homopolymers. Each edge represents a binary blend, and each interior point represents a ternary blend. Regions where a single homogeneous phase is stable are labeled *H*, and those where a single microphase is stable are labeled *M*. Two phase regions are indicated by explicit labels, such as *HH* or *MH*, and/or by the presence of the straight tie lines. In these cases the two coexisting phases are indicated by the two phases in which the tie lines terminate. There is a triangular three phase region in each of panels (c) and (d), (very small in (c)), bounded by 3, two phase regions.

up to the point where $\chi Z_h = 2$, the only change is an increase in size of the *M* region. Beyond this, the binary homopolymer blend phase separates, creating a two phase *HH* region near the base of the phase diagram. The second panel of figure 5.1 corresponds to the case where this has begun. It is also apparent from this panel that the microphase is relatively stable near the isopleth, i.e., along the vertical line on the phase diagram from the apex of the triangle to the base, along which the overall *A:B* composition ratio is 50:50. Along the isopleth, in this case the microphase persists to copolymer volume fractions as low as about 15%. By contrast, in each binary copolymer/homopolymer blend it persists only to about 40% copolymer content. With a further increase in χ, the regions of microphase and macrophase separation overlap, as indicated in the third panel of figure 5.1, for which $\chi = 0.043$. At this point the phase diagram has become quite rich, exhibiting single phase *M* and *H* regions, a two phase *HH* region at the base of the triangle, two phase *MH* "fingers", and a very small three phase region. It also indicates tiny two phase *MM* regions at the tip of each "finger", but the reliability of such details is almost certainly beyond the capabilities of the current approach. In the final panel of figure 5.1, χ is further increased so that the binary copolymer/homopolymer blends macrophase separate. For each such binary blend, there is an *MM* region, but it gives way to an *MH* region if there is even a small amount of the other homopolymer present. It should also be pointed out that there is probably even further structure to these diagrams because of the possibility of other morphologies, i.e., cylinders, spheres or "double diamond".

Perhaps the most interesting feature of figure 5.1 is the predicted relative stability of the single *M* phase near the isopleth. It persists to very large homopolymer content, but is destabilized by disparate amounts of *A* and *B* homopolymers. This can be understood physically by considering horizontal "slices" of the free energy surface, shown in figure 5.2 which is for $\chi = 0.045$, which corresponds qualitatively to panel (c) of figure

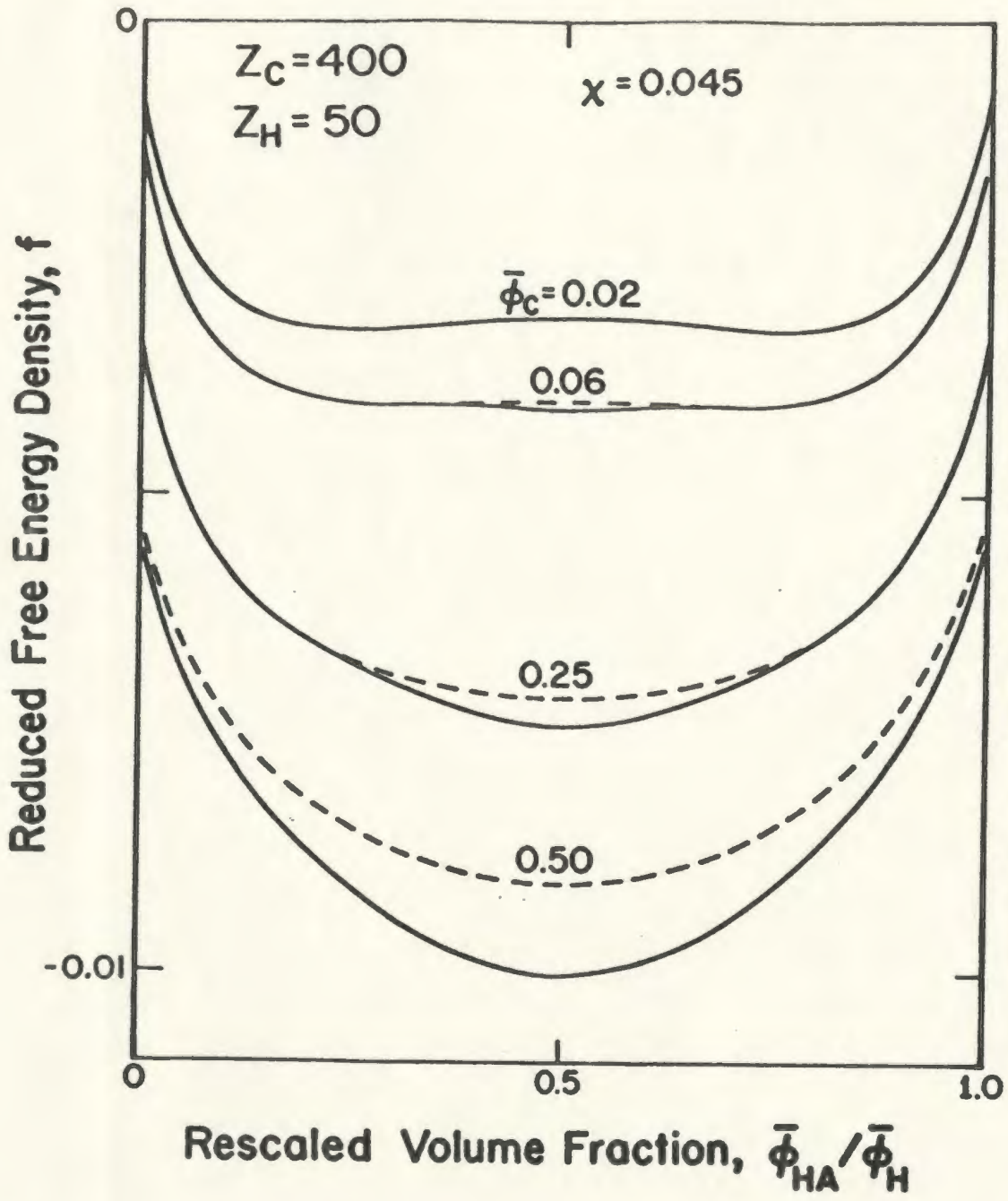

Figure 5.2: Slices of the free energy surface as a function of homopolymer A contents, for the blend of figure 5.1 with $\chi = 0.045$, and different copolymer volume fractions $\bar{\phi}_c$ as indicated. In each case, the solid line is the full free energy density, the dashed line is f_{hom}, and the difference is Δf. For each curve the horizontal axis is rescaled by a factor equal to the total homopolymer content, $\bar{\phi}_h = \bar{\phi}_{hA} + \bar{\phi}_{hB}$.

5.1. These slices do not represent the phase separation quantitatively, because not all the tie lines are horizontal, but they illustrate the controlling features. The top curve shows the free energy for near zero copolymer content, $\overline{\phi}_c = 0.02$, which corresponds to a horizontal line very near to the base of the associated phase diagram. There is a region of negative curvature near the centre of this curve, which causes macrophase separation to two homogeneous phases, consistent with figure 5.1(c) or (d). In this case the binodal points correspond to the two minima in the free energy. The other sets of curves, which correspond to progressively more copolymer content, illustrate that there is a competition between the Flory-Huggins free energy of mixing which tends to induce macrophase separation and the free energy of the microphase which tends to stabilize the microphase, with maximum effect near the isopleth. For very small copolymer content, Δf is too small to have an effect and the system continues to separate to two homogeneous phases. However, further increasing the copolymer content (second set of curves) both increases the magnitude of Δf at the isopleth, and reduces the tendency towards macrophase separation. This stabilizes the microphase near the isopleth, but there are still unstable regions on either side of the central minimum, which induce macrophase separation. Following this curve across from left to right would indicate a sequence of phases of $H \rightarrow HM \rightarrow M \rightarrow MH \rightarrow H$. This corresponds qualitatively to horizontally traversing figure 5.1(c) or (d) from a single H region, through an HM "finger", through the central M region, and so on to the other side. With a further increase in copolymer content (third set of curves) the regions of negative curvature shrink and then disappear, implying a sequence $H \rightarrow M \rightarrow H$, and the microphase persists over more of the"slice". This corresponds qualitatively to a traverse of figure 5.1(c), passing just above the MH "fingers". Finally, for large enough copolymer content (last set of curves) the microphase M persists over the entire slice, as in the uppermost regions of figures 5.1(c) and (d).

As discussed in section 2.4 the elastic scattering intensity, $I(k)$, for *A-b-B/A/B* copolymer homopolymer blends, can have its maximum either for $k^* = 0$ or $k^* \neq 0$, indicating onset of macrophase or microphase separation, respectively. This provides a complementary perspective on the system. The stability limits for macrophase separation can be calculated [82, 90] from the following condition of $I(k)$ divergence:

$$I^{-1}(k = 0) = 0, \tag{5.10}$$

and similarly the condition for the stability limits of microphase separation is:

$$I^{-1}(k = k^*) = 0. \tag{5.11}$$

In this section we calculate $f^{(2)}(k, -k)$ and use eq. 2.111, which relates it to $\tilde{S}(\ k, -\ k\ ) \sim I(k)$, to determine the stability limits by solving the equations 5.10 and 5.11. Figure 5.3 shows the stability limits for macrophase and microphase separation along the isopleth, i.e., $\overline{\phi}_{hA} = \overline{\phi}_{hB}$, with $\overline{\phi}_c$ varying from 0 to 1. The horizontal lines indicate the values of χ used in figure 5.1. The slopes of the phase boundaries, both of which are monotonic in this case, indicate that these copolymers tend to stabilize microphase separation but reduce the tendency towards macrophase separation. Moving down the isopleth from the apex to the base of the triangle of figure 5.1(a) corresponds to moving from right to left along the lower horizontal line of figure 5.3. In both cases, the phase changes from *M* to *H* at $\overline{\phi}_c \simeq 0.7$. Moving down the isopleth in figure 5.1(b) corresponds to moving along the second line in figure 5.3, with the sequence of phases $M \rightarrow H \rightarrow HH$. Finally, the isopleths in figure 5.1(c) and (d) correspond to the two top lines of figure 5.3, with the implied sequence of phases being *M* to a macrophase separated system, without an intervening single phase *H* region.

Figure 5.4 is for a system which is the same as that discussed in figures 5.1 to 5.3 except that the homopolymer degrees of polymerization are increased to $Z_h = Z_c/4$, so

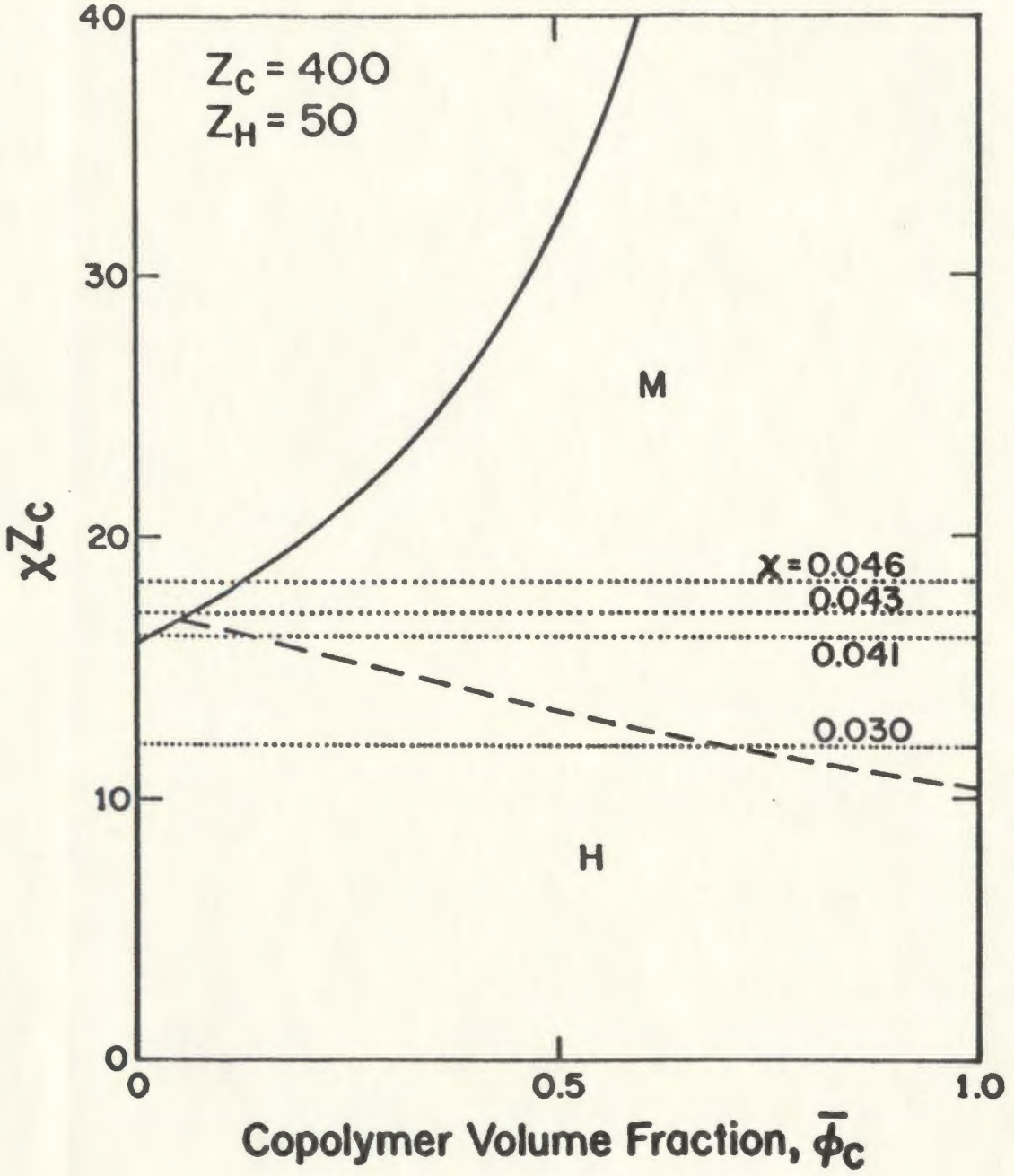

Figure 5.3: Stability limits for the macrophase (—) and microphase (- - -) transitions for the copolymer/homopolymer blend used in figures 5.1 and 5.2, along the isopleth. The horizontal lines correspond to the values of χ used in figure 5.1.

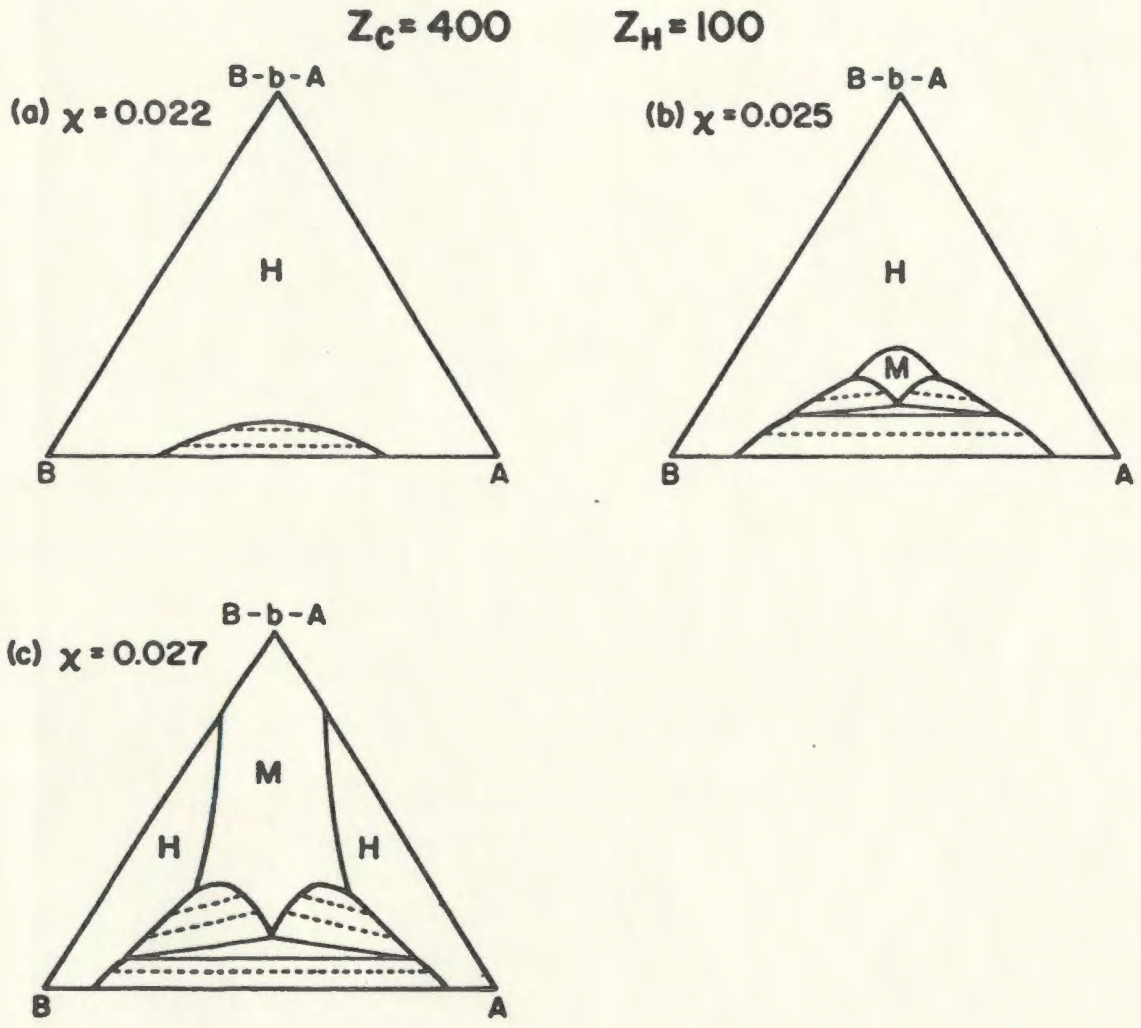

Figure 5.4: Calculated phase diagrams for a model symmetric *A-b-B/A/B* blend for a copolymer with $Z_c = 400$ as in figure 5.1, homopolymer degrees of polymerization increased to $Z_{hA} = Z_{hB} = 100$, and three values of χ as indicated. The notation is as in figure 5.1.

that the molecular weight of each homopolymer is one half that of the corresponding block of the copolymer. In this case, for $\chi < 0.02$ there is no structure to the phase diagram. As χ is increased the first feature to appear is the macrophase separation of the two homopolymers; the first panel shows this for $\chi = 0.022$. The next panel is for the case $\chi = 0.025$. In this case $\chi Z_c = 10$, and so the copolymer does not microphase separate. Furthermore, adding *either* A or B homopolymers to the copolymer (binary blends) induces neither microphase nor macrophase separation. This is consistent with earlier results for binary systems [29]. However, addition of *A and B* homopolymers in nearly equal proportions, i.e., near the isopleth, induces both, resulting in a new feature for the phase diagram. Starting at the top of the isopleth, adding homopolymers induces microphase separation at about 70% homopolymer. Further additional homopolymer induces macrophase separation, and in this region of the phase diagram there are two phase *MH* regions as well as a three phase region. Below this is an *HH* region. Larger values of χ increase the tendencies towards both kinds of phase separation. Figure 5.4(c) is for the case in which it is increased slightly, enough so that the neat copolymer microphase separates, but not enough to induce binary copolymer/homopolymer blends to macrophase separate.

As illustrated in figure 5.5, for this system the slopes of the two stability limits along the isopleth have again the same sign. For larger values of Z_h/Z_c, (not shown) the slopes of both lines increase in magnitude. The case illustrated is, in fact, very near the one in which the microphase stability limit is nearly horizontal as $\overline{\phi}_c \rightarrow 1$. A horizontal boundary in this limit would imply that small amounts of homopolymer tend to neither stabilize nor destabilize the microphase. This implies in turn that, as for binary copolymer/homopolymer blends [29], there is a threshold such that if Z_h exceeds this threshold, then small amounts of homopolymer tend to induce microphase separation, but lower molecular weight homopolymers tend to destabilize it. In both cases, for these

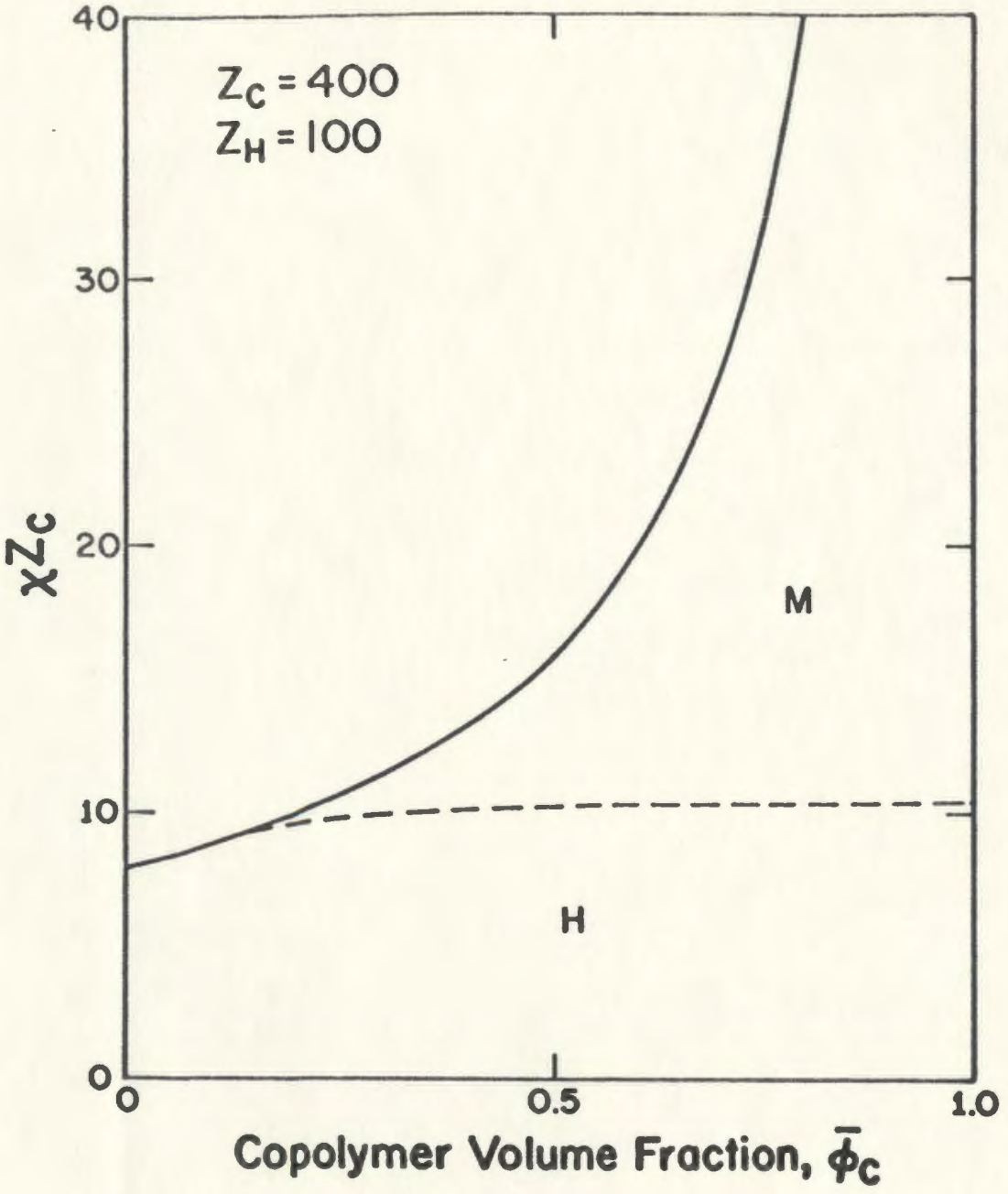

Figure 5.5: Stability limits for the macrophase (—) and microphase (- - -) transitions for the copolymer/homopolymer blend used in figure 5.4, along the isopleth.

model systems with symmetric copolymers, we find that this threshold is very close to $Z_h = Z_c/4$.

Finally, figure 5.6 contains phase diagrams for the intermediate case $Z_h = 75 \simeq Z_c/5.3$. In this case, for $\chi \lesssim 0.0263$ the phase diagram is featureless. Copolymer microphase separation and homopolymer macrophase separation both appear at $\chi \simeq 0.0265$, as illustrated in the first panel for which $\chi = 0.028$. In this case small amounts of these relatively low molecular weight homopolymers tend to destabilize the microphase. However, as seen in figure 5.6(b), the theory predicts a new effect for this system. Although small amounts of homopolymer destabilize the microphase, additional homopolymer can then restabilize it. The sequence of phases along the isopleth is $M \rightarrow H \rightarrow M \rightarrow$ macrophase separation. This is, however, a very delicate effect; a slight further increase in χ, such as to a value of 0.032 as in the last panel of this figure, causes it to disappear, and furthermore the phenomenon might well be eliminated by other effects such as a composition dependent χ or fluctuation effects.

The predicted existence of two distinct M regions in figure 5.6(b) can be related to the stability limits, shown in figure 5.7. The important point is that the stability limit of the microphase in this case is non-monotonic. Initially, addition of homopolymer destabilizes the microphase, but this tendency reaches a maximum near $\overline{\phi}_c \simeq 0.2$ and for greater amounts of homopolymer this phase boundary turns downwards for a short interval before macrophase separation occurs.

This phenomenon could also be explored by small angle X-ray scattering, SAXS, from the homogeneous phase [15, 11]. The intensity of such scattering, as discussed in section 2.4, is proportional to the inverse of the coefficient of the second term in the free energy expansion, $f^{(2)}$ of eq. 2.105. The scattering from a fully symmetric system with

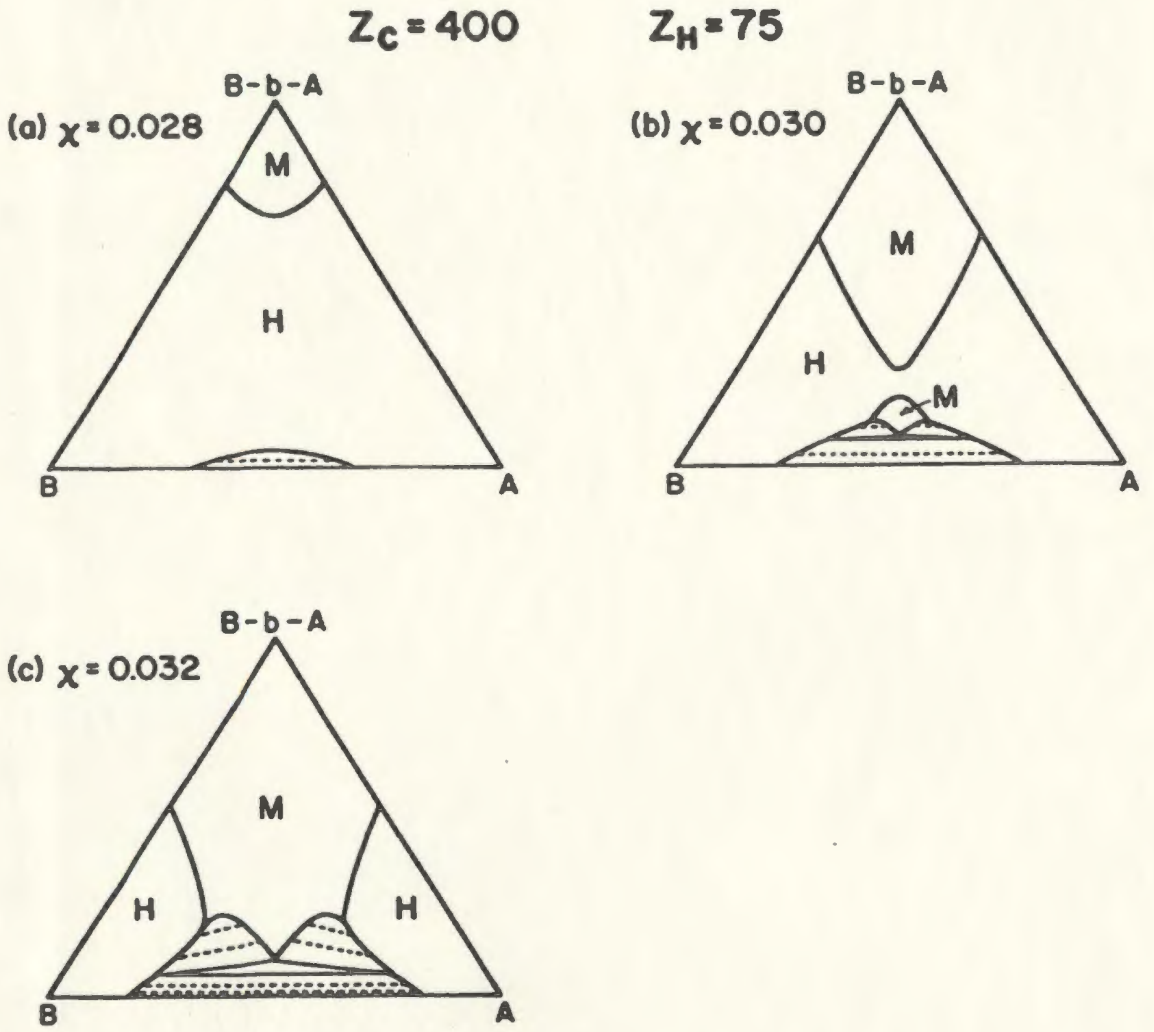

Figure 5.6: Calculated phase diagrams for a model symmetric *A-b-B/A/B* blend for a copolymer with $Z_c = 400$ as in figure 5.1, homopolymer degrees of polymerization $Z_{hA} = Z_{hB} = 75$, and three values of χ as indicated. The notation is as in figure 5.1.

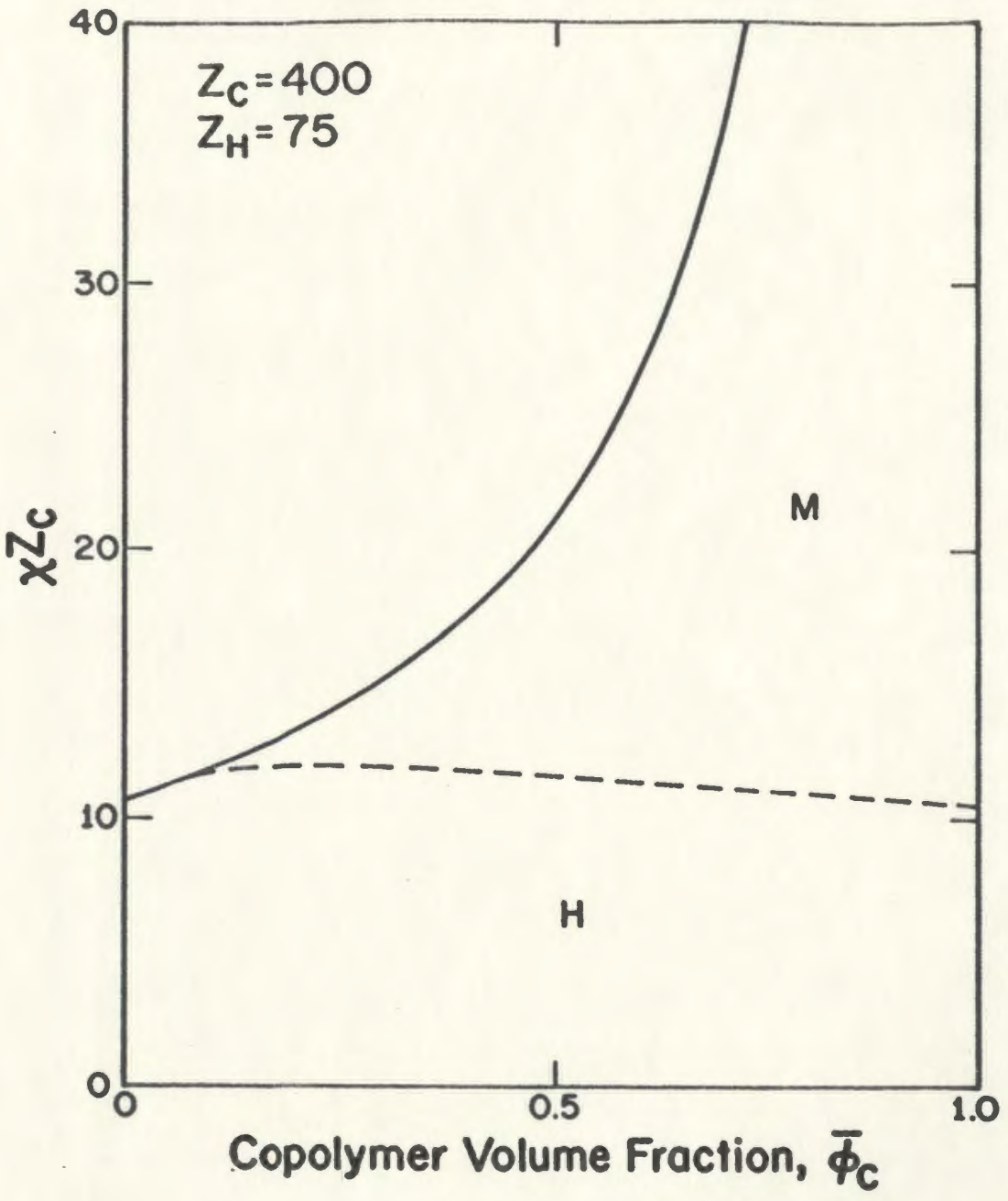

Figure 5.7: Stability limits for the macrophase (—) and microphase (- - -) transitions for the copolymer/homopolymer blend used in figure 5.6, along the isopleth.

concentrations which place it on the isopleth can be expressed [15] by eq. 2.115, with

$$\frac{S(k)}{W(k)} = [\bar{\phi}_c \frac{r_c}{8}[g_{cA}^{(2)}(\boldsymbol{k}, -\boldsymbol{k}) - g_{cA}^{(1)}(\boldsymbol{k})^2] + \bar{\phi}_h \frac{r_h}{4} g_h^{(2)}(\boldsymbol{k}, -\boldsymbol{k})]^{-1}, \tag{5.12}$$

where $\bar{\phi}_h$ is the total homopolymer volume fraction, and $g_h^{(2)}$ could refer to either homopolymer. For the special case $\chi = 0$, this reduces to

$$I(\boldsymbol{k}) \propto \bar{\phi}_c \frac{r_c}{8}[g_{cA}^{(2)}(\boldsymbol{k}, -\boldsymbol{k}) - g_{cA}^{(1)}(\boldsymbol{k})^2] + \bar{\phi}_h \frac{r_h}{4} g_h^{(2)}(\boldsymbol{k}, -\boldsymbol{k}). \tag{5.13}$$

There are two terms in eq. 5.13, proportional to the copolymer and homopolymer volume fractions respectively. The first peaks at a finite wavenumber, whereas the second peaks at $k = 0$. In general, as homopolymer is substituted for copolymer, the peak in $I(k)$ moves towards zero wavenumber, but the value at maximum can either increase, which signals the case in which the homopolymer tends to stabilize the microphase, or decrease, which signals the homopolymer tending to destabilize it.

The scattering profiles for $\chi = 0$, i.e., eq. 5.13, for the system used in figures 5.6 and 5.7 are shown in figure 5.8. They are presented as a function of $R_g k$ where R_g is the unperturbed radius of gyration of the copolymers, ${R_g}^2 = Z_c b^2/6$. The first panel is for pure copolymer; the peak occurs at $R_g k^* = 1.95$, which is equivalent to $Z_c(k^* b)^2 = 22.7$, and has the value $I(k^*) = Z_c/21$. The second panel is for $\bar{\phi}_c = 0.5$, which shows the copolymer and homopolymer contributions as well as the total. The resultant peak has moved towards $k = 0$, and in this case has decreased in value. This is consistent with figures 5.6 and 5.7, in which addition of homopolymer initially destabilizes the microphase. The third panel, which is for $\bar{\phi}_c = 0.2$, is similar. However, for the case $\bar{\phi}_c = 0.15$, shown in the last panel, the peak value has increased slightly, consistent with the reappearance of the M phase region in figure 5.6(b).

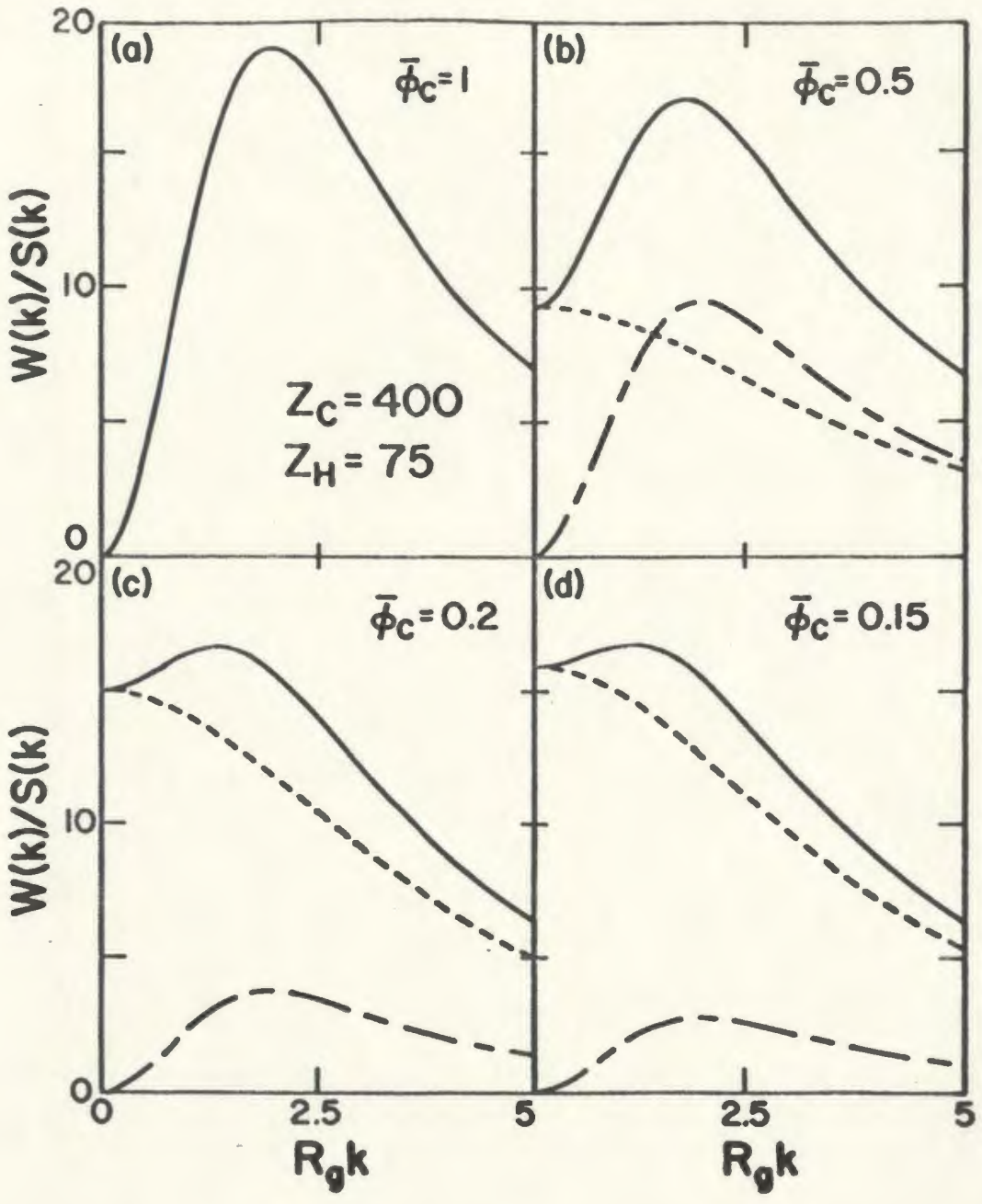

Figure 5.8: Calculated scattering curves for the ternary system of figures 5.6 and 5.7, for four different compositions $\bar{\phi}_c$ as indicated, along the isopleth. Each figure shows the total curve (—), the contribution proportional to $\bar{\phi}_c$ (- - -), and the contribution proportional to $\bar{\phi}_h$ (– – –).

5.3.2 Asymmetric Model Systems

We consider next two model systems in which the reference densities and Kuhn lengths are again equal, but the degrees of polymerization are not. In the first, we use symmetric copolymers but choose different homopolymers, $Z_{hA} \neq Z_{hB}$, and in the second case choose asymmetric copolymers, but $Z_{hA} = Z_{hB}$.

Figure 5.9 shows phase diagrams for the symmetric copolymer, $Z_c = 400$, but $Z_{hA} = 50$ and $Z_{hB} = 200$. In this case the first feature to appear is homopolymer phase separation, occurring for $\chi \geq 0.0225$; the first panel of figure 5.9 is for $\chi = 0.024$, where this phase separation is seen. Increasing the value of χ to 0.026 produces the diagram of the second panel. In this case $\chi Z_c = 10.4$, just below the threshold for pure copolymer microphase separation. Addition of the relatively high molecular weight B homopolymer (binary blend) induces microphase separation but not macrophase separation, whereas the relatively low molecular weight A homopolymer induces neither. In the ternary blend, both types of phase separation occur.

The relative stability of the single M phase appears here as well. In this case it falls primarily within the region of the phase diagram where there is more homopolymer B than homopolymer A, corresponding to an overall excess of B type monomer in the system. This is consistent with the tendencies of the relatively high molecular B homopolymers to stabilize the microphase, and the low molecular weight A homopolymers to destabilize it.

Figure 5.10 shows calculated phase diagrams for a system with $Z_{cA} = 240$ and $Z_{cB} = 160$, and $Z_{hA} = Z_{hB} = Z_h = 50$ as in figure 5.1. The effects of asymmetry in the copolymer can be observed by comparing figure 5.10 with 5.1. In this case, the copolymer composition is 40:60, and so is probably very close to the lamellae-cylinders boundary. The first feature to appear is copolymer microphase separation, occurring for $\chi \geq 0.0284$;

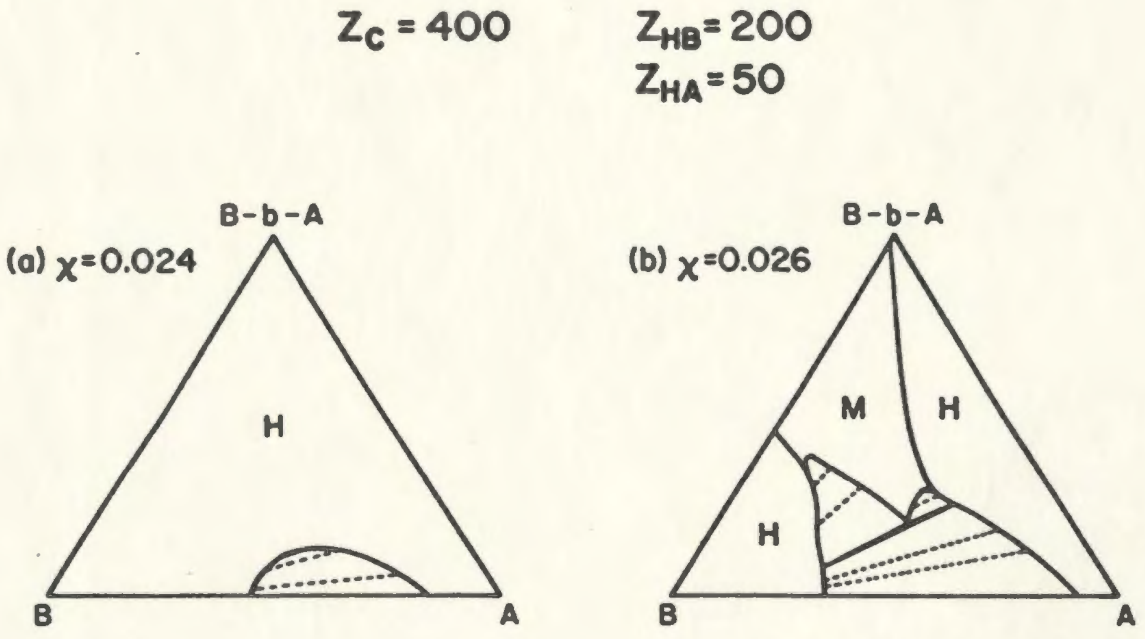

Figure 5.9: Calculated phase diagrams for a model *A-b-B/A/B* blend with a symmetric copolymer with $Z_c = 400$ as in figures 5.1 to 5.8, but with homopolymer degrees of polymerization $Z_{hA} = 50$ and $Z_{hB} = 200$, and two values of χ as indicated. The notation is as in figure 5.1.

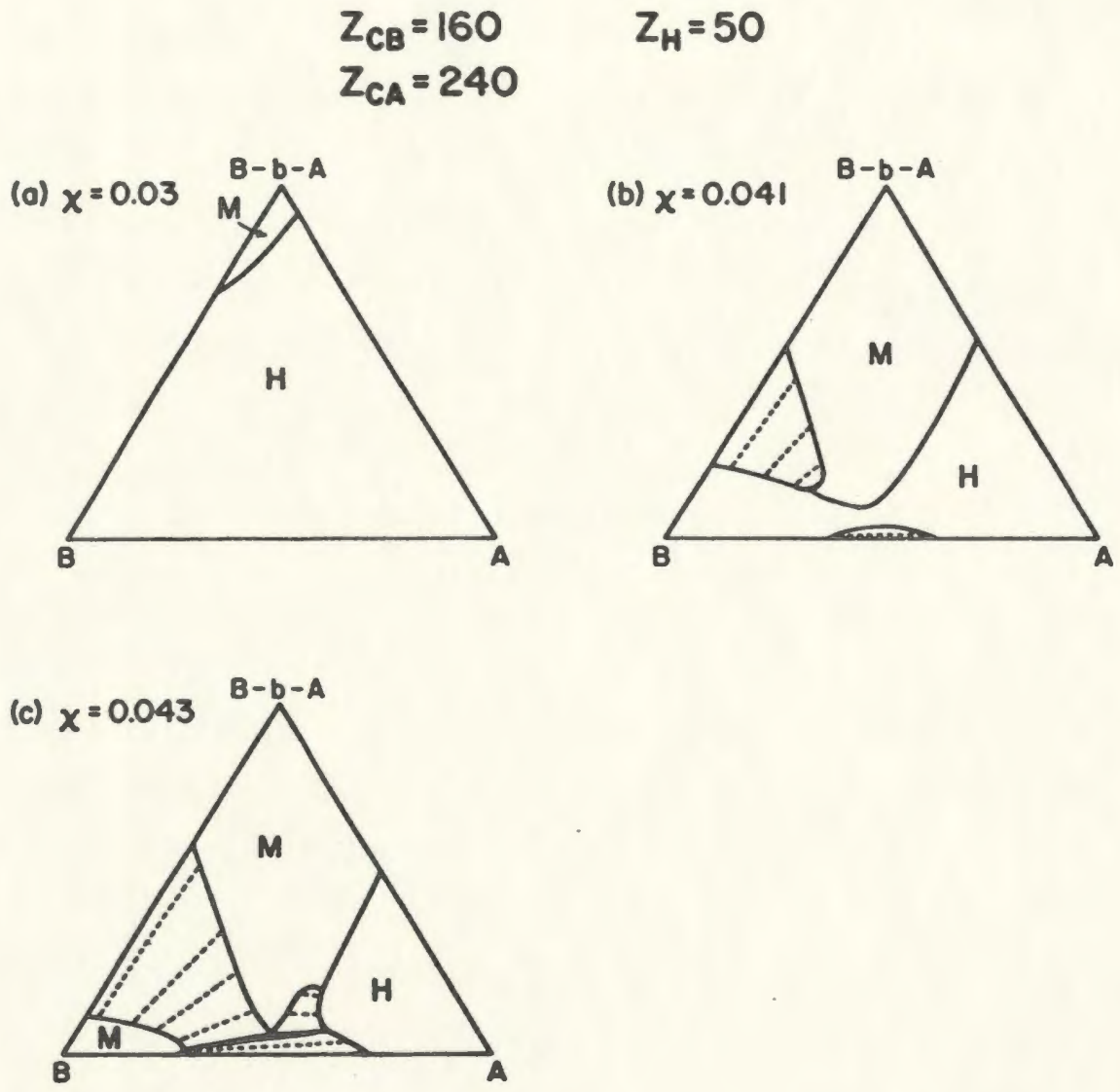

Figure 5.10: Calculated phase diagrams for a model *A-b-B/A/B* blend with $Z_c = 400$ as in figures 5.1 to 5.9, but with asymmetric copolymers with $Z_{cA} = 240$ and $Z_{cB} = 160$, and homopolymer degrees of polymerization $Z_{hA} = Z_{hB} = 50$. The three panels correspond to three values of χ, as indicated. The notation is as in figure 5.1.

the first panel is for $\chi = 0.030$. Either homopolymer tends to destabilize the microphase, but the A homopolymer sooner than the B homopolymer. This is reasonable since additional A homopolymers drive the overall composition ratio even further from 50:50, whereas additional B homopolymers drive it towards 50:50. Increasing the value of χ to 0.039 causes the binary copolymer/B-homopolymer blend to phase separate, and then at $\chi = 0.04$ the homopolymers also phase separate. Both these features are present in the second panel of figure 5.10, for which $\chi = 0.041$. With further increases in χ, the phase separated regions further overlap, resulting in an asymmetric phase diagram such as that of the third panel, for which $\chi = 0.043$.

5.3.3 Real Systems: Polystyrene/Polyisoprene

As a final application, figure 5.11 shows a calculated phase diagram for a ternary *PS-b-PI/PS/PI* mixture. These copolymers and copolymer blends have been studied extensively experimentally, for example by Hashimoto and coworkers [10], [13]–[15], [79], [82], [91]–[93], and theoretically in chapter 4 of this dissertation. For this calculation, we specified the copolymers to have $Z_{cPS} = 145$ and $Z_{cPI} = 240$, corresponding to samples used in a number of experiments [79, 82, 13, 14] and labeled *HY-8*, as discussed in chapter 4. The volume fractions for the neat copolymer system are $\phi_{PS} \simeq 0.45$ and $\phi_{PI} \simeq 0.55$. In order to obtain an interesting phase diagram, for the homopolymers we chose $Z_{hPS} = 80$ and $Z_{hPI} = 160$, which are about 55% and 66% of the corresponding blocks of the copolymers.

We use independently determined Kuhn statistical lengths and reference densities [82, 83] cited in the previous chapter. Furthermore in order to keep the entire blend in the weak segregation regime, we chose $\chi = 0.029$, which is close to measured values for neat copolymers, (especially to the "effective" interaction parameters for systems diluted with non-selective solvent) [14] and is the same as the χ parameter used in chapter 4 for

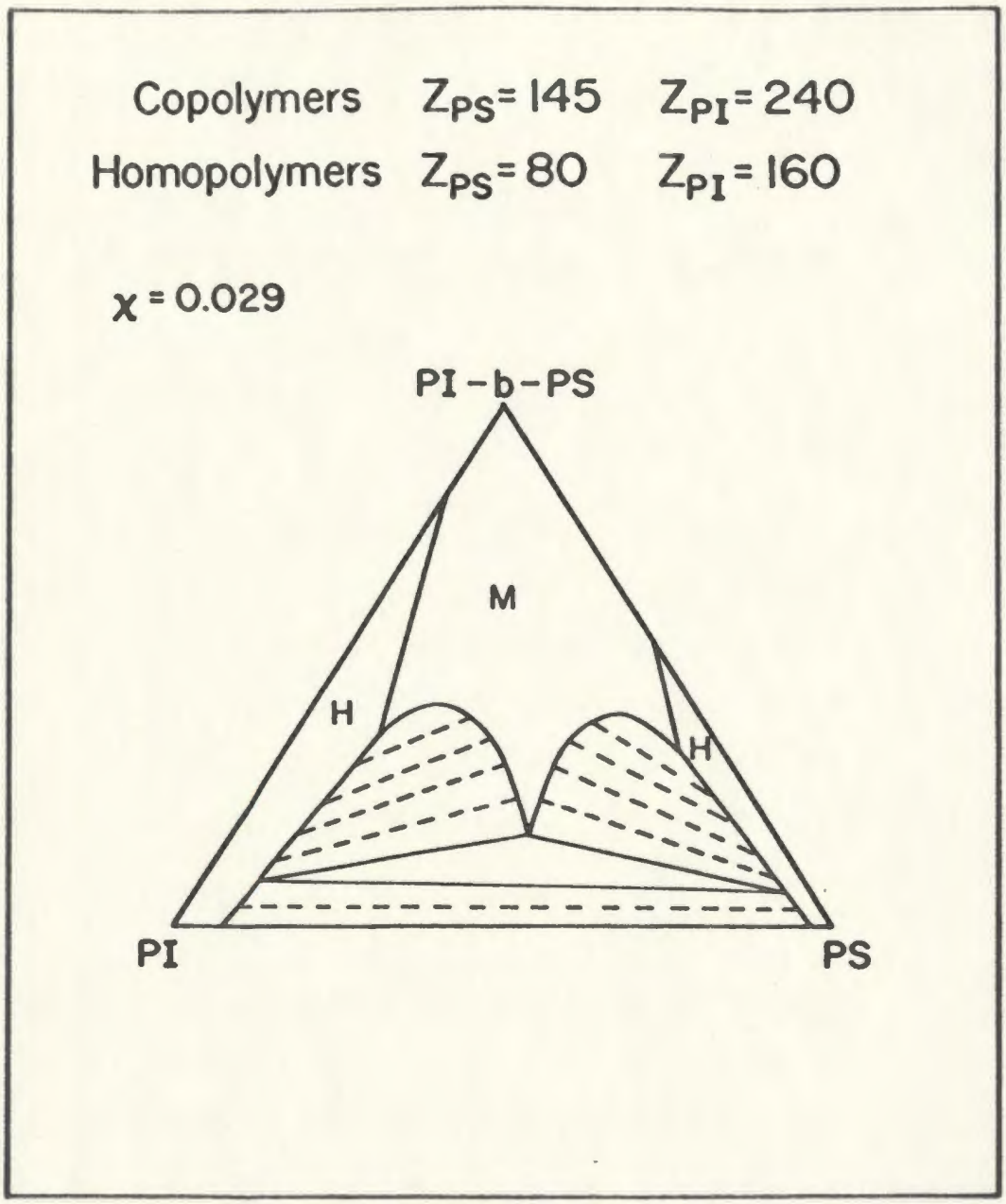

Figure 5.11: Calculated phase diagram for *PS-b-PI/PS/PI*, using measured values of the Kuhn statistical lengths and monomer volumes, degrees of polymerization as indicated, and $\chi = 0.029$.

polystyrene-polyisoprene interactions.

As seen in the figure 5.11, for these choices the theory indicates that the pure copolymer is microphase separated. Addition of either homopolymer PI or PS dissolves the microphase, but more PS (about 50%) than PI (about 15%) is required. This is consistent with the fact that as homopolymer PS is initially added to the copolymer, the overall *PS:PI* composition ratio changes from 45:55 towards 50:50, an effect which would tend to stabilize the microphase relative to the homogeneous phase. However, it is perhaps surprising because the homopolymer PS has the lower molecular weight, both in absolute terms and relative to the corresponding copolymer block, which would of itself indicate that the PS would have the greater tendency to destabilize the microphase. The actual behaviour is governed by a competition between these two effects.

The binary homopolymer blend exhibits macrophase separation, but neither one of the binary copolymer/homopolymer blends does. The single phase is predicted to be relatively stable near the isopleth, as in the earlier cases. In fact, the topology of this diagram is most like that of figure 5.4(c); the differences are due primarily to the asymmetry of the components.

To summarize this chapter we repeat the main results. We have developed a procedure for calculating ternary phase diagrams and presented a series of results for model systems, and one for *PS-b-PI/PS/PI*, showing a variety of topologies. We also examined the phenomenon of induced microphase separation for ternary copolymer/homopolymer blends. For a fully symmetric model system, $Z_{cA} = Z_{cB} \equiv Z_c/2$, $Z_{hA} = Z_{hB} \equiv Z_h$, a small amount of homopolymer tended to stabilize a microphase in the ternary blend under the same conditions as in the binary blend, i.e., if $Z_h \geq Z_c/4$. However, the theory predicted two additional effects. First, for some cases homopolymers could induce the microphase in the ternary blend when they did not in either corresponding binary blend,

i.e., an M region appeared near the centre of the phase diagram. Second, homopolymers of relatively low molecular weight, namely that for $Z_h \simeq Z_c/5.3$, tended to first destabilize the microphase, and then to restabilize it. One feature which appeared in a number of cases was the relative stability of the microphase for blends with overall A:B concentrations near 50:50. This was particularly noticeable for those cases in which both microphase and macrophase separation occurred. It is worth noticing that the *PS-b-PI/PS/PI* blend presented by Hashimoto et al. [13, 14] maintained a lamellar structure with long range order for copolymer volume fractions as low as 10%, discussed in section 4.4.

Chapter 6

Conclusions

In this chapter we summarize and draw conclusions from all the work presented in this thesis. In particular, we intend to stress the relations between our three projects and theories which we have applied or developed for them. An overall motif of this thesis has been the microscopic description of the lamellar morphology of copolymer blends, and the interplay of microphase and macrophase separation in those blends. The theories, presented in preceding chapters, are based on the Hong and Noolandi formalism and the same general assumptions, which we subsequently name. We model polymers as continuous flexible chains, with Wiener measure as statistical weight. Mean field theory has been consistently applied, so that, except in the discussion of SAXS from the disordered phase in section 2.4, the fluctuations have been ignored. This is the main limitation in the close proximity of the MST, where the fluctuations can be particularly significant. All blends are either in the concentrated or semi-dilute regimes.

Despite the same underlying assumptions we have used different ways of applying and modifying the formalism, depending on the complexity of the problem, computer speed and time resources. The least complicated case of copolymer/solvent blends has been treated by the numerical self-consistent procedure, which is the most accurate of the mean field theories presented in this dissertation. The principal deficiency of this method is the long time needed to complete the numerical calculations, particularly close to the MST. For the other two projects, i.e., for copolymer/homopolymer blends, a fourth order expansion of the free energy has been developed. This approach, on the

other hand, is both numerically efficient and fairly accurate in the weak segregation regime, as we have found in subsection 4.3.1. The drawback of this approach is its limitation to regions close to the MST. We have used our fourth order expansion in two different versions, i.e., the many wavenumber and the one wavenumber approximation, for the second and the third projects, respectively. The many wavenumber approach has been developed for systematic studies of lamellar structure of *A-b-B/A/B* copolymer blends. It allowed us to determine some equilibrium properties of these blends which are beyond range of the one wavenumber approximation, i.e., χ parameter dependence of d, d_A, d_B and a_I, distribution of homopolymers within the subdomains, and the existence of thresholds as discussed in chapter 4. In calculating ternary phase diagrams of these blends, the one wavenumber approximation has been used, nonetheless. This further approximation has been justified by relatively small differences between the free energies, Δf, in the many wavenumber and the one wavenumber cases. The other motivation for this simplification was the need for speedy numerical calculations which facilitate the construction of numerous ternary phase diagrams in a relatively short time.

In the first two projects, using different approaches, we have investigated the lamellar morphology of copolymer blends, assuming that these systems do not macrophase separate. To verify this requirement, we have constructed the appropriate phase diagrams using the methods developed and described in chapter 5 (the third project). The accuracy of the fourth order expansion near the MST was tested by performing model numerical self-consistent calculations for the copolymer/selective solvent case, covering a range of blend concentrations, and comparing these two approaches. We found that the results of the two calculations agreed very well for values of χ within about 10% of its value at the MST. For example, expressing the dependence of d on χ as $d \propto \chi^p$, for the series of calculations which we used for the comparison, we found $p = 0.50 \pm 0.01$ (self-consistent calculations) or $p = 0.51 \pm 0.01$ (approximate calculations). This comparison did not,

of course, give any information on the validity of mean field theory itself, which neglects the fluctuation effects.

Both in section 2.4 and 4.4, the temperature dependence of χ parameter has been discussed. If the mean field theory were perfectly adequate for description of copolymer blends, we would expect a linear dependence on T^{-1}. Tanaka and Hashimoto [15] have, indeed, found this kind of dependence for individual blends. But as the volume fractions and the degrees of polymerization of components have been varied, the χ parameter has changed as well. This indicates that mean field theory, despite its numerous successes, has some deficiencies. One of the possible methods to "cure" this problem has been presented by Dudowicz and Freed [94]. They have dropped the assumption of incompressibility and have obtained composition dependent effective χ parameters. It is also possible that taking the fluctuations into account might shed some light on the microscopic origin of the interaction parameter.

For model numerical self-consistent calculations of chapter 3, we have found that the scaling behaviour of domain thickness for copolymer/selective solvent is, virtually, the same as one for the copolymer/nonselective solvent blend. The differences of exponents in the weak segregation regime are due to the development of an improved version of the computer programme. When we performed calculations near the MST, we assumed the lamellar structure throughout. This assumption might not be always satisfied. Real system self-consistent calculations for *PS-b-PBD/S* blend, unlike the nonselective solvent case [30], clearly show that the dilution approximation is not valid for these cases, i.e., the product $r_c\chi\overline{\phi}_c$ does not play the role analogous to that of $r_c\chi$ for pure copolymer. In particular, for $r_c\chi\overline{\phi}_c \simeq 5$, with $f_{PS} = 0.5$ and $\overline{\phi}_c = 0.2$, we have predicted a stable equilibrium lamellar structure. A further difference with the nonselective case is the absence of maxima in the solvent density at interfaces. Selective solvent is preferentially localized in PBD subdomains, with the maximum density variation of about 4%. Otherwise, the

real system calculations show quantitative agreement with model calculations for both selective and nonselective cases.

In chapters 4 and 5, we presented an approximate treatment of the lamellar microphase of binary *A-b-B/A* and ternary *A-b-B/A/B* block copolymer/homopolymer blends. Included in the approach was the assumption that there is only one Flory interaction parameter which represented the effective *A-B* interactions, irrespective of whether the monomers belonged to copolymers or homopolymers. The method calculated the polymer distribution functions via perturbative solutions to the modified diffusion equations, and these were used to express the free energy density as an expansion in terms of the local density of A (or alternatively B) monomers, with contributions from both homopolymers and copolymers, and its range of validity was restricted to the weak segregation regime. This approach did not include fluctuation effects [61], numerical solutions to the self-consistent field equations [30, 33] or equation of state effects. Because of these limitations, we made no attempt to discriminate between different structures (lamellae, cylinders, spheres). Instead we explicitly assumed the lamellar structure, and restricted our attention to systems in which the copolymer block degrees of polymerization Z_{cA} and Z_{cB} were chosen so that A and B volume fractions in each copolymer satisfied $f_A \simeq f_B \simeq 0.5$.

In chapter 4, using summations over many wavenumbers in the fourth order expansion of Δf, we included a model for the density profiles which allowed for some indication of the effects of concentrations, χ, and the degrees of polymerization of the homopolymers and each block of the copolymers. Our focus had been on the domain thickness d, the two subdomain thicknesses d_A and d_B, the lateral swelling of copolymers by homopolymers as characterized by the average lateral distance between joints, the related localization of the homopolymers, and the density profiles of each component. We carried out model calculations for binary and ternary blends to explore how these quantities depend on the

system characteristics, and in section 4.3, we compared the calculations with three sets of experiments, all of which were done in the strong segregation regime. We also carried out a series of calculations for binary styrene-isoprene blends with characteristics similar to the those of the experimental systems.

We found that, for constant χ, the addition of homopolymers with relatively high degrees of polymerization, Z_h, caused an increase in the layer thickness, and the size of the increase was an increasing function of Z_h. Homopolymers with relatively small Z_h lead to a decrease in d, and so there was a threshold value Z_h^{th} such that if $Z_h < Z_h^{th}$, then d decreased, but otherwise it increased. The value of Z_h^{th} depended on the total degree of polymerization of the copolymer and the relative degrees of polymerization of each block. For ternary blends, it could depend on the proportions of the added homopolymers. However, in all cases considered, it was on the order of $Z_h^{th} \simeq Z_c/5$. This was comparable to the threshold value for the phenomenon of induced microphase formation. A picture emerged in which added homopolymers with $Z_h \lesssim Z_h^{th}$ tended to destabilize the microphase and reduce the domain thickness, whereas if $Z_h \gtrsim Z_h^{th}$ then they tended to stabilize the microphase and increase d.

When the content of selective solvent in the copolymer blend is increased, the layer thickness of the ordered structure is decreased and the microphase is destabilized, as discussed in chapter 3. This is, therefore, consistent with the behaviour of "short" homopolymers (hA or hB) added to the A-b-$B/A/B$ blend.

The variation in the thickness of each subdomain was more complicated. In binary blends with symmetric copolymers, we found that adding hA homopolymers always induced a lateral swelling of the copolymers, and a consequent reduction in the thickness of the B subdomain. However, the extent of the swelling and the qualitative behaviour of d_A depended on the molecular weight of the homopolymers. For very low Z_{hA} the swelling was relatively extensive, and all of d, d_A and d_B decreased. For intermediate

values of Z_{hA}, approximately $Z_h^{th}/2 \lesssim Z_{hA} \lesssim Z_h^{th}$, d and d_B decreased but d_A increased, and for larger Z_{hA}, d and d_A increased while d_B decreased. We also investigated the addition of hA homopolymers to asymmetric copolymers with $Z_{cA} < Z_{cB}$. In these blends, the behaviour was more complicated: d_A virtually always increased, but d_B could either increase or decrease. In all these blends in this regime there was another factor as well. If the system approached the MST as homopolymers were added, then both d_A and d_B tended towards $d/2$ in this limit, irrespective of whether they initially increase or decrease.

The behaviour of d, d_A and d_B was qualitatively similar in ternary blends. The quantitative behaviour depended on the relative degrees of polymerization and composition.

Following Tanaka et al. [14], we also expressed our results in terms of the changes in the square root of the average cross sectional area per copolymer molecule in each layer, a_J/a_{J_o}. We found that this always increased as homopolymers were added, and that the size of the change increased with decreasing Z_h. All this was consistent with the picture that low molecular weight homopolymers were relatively uniformly solubilized in the subdomains, but that homopolymers of higher molecular weight were progressively more localized towards the subdomain centre. This was illustrated by calculated density profiles in the weak segregation regime. In agreement with experiments, we found that for symmetric copolymers, a_J/a_{J_o} was virtually the same for binary and ternary blends [14].

As discussed in section 4.3, these predictions for the weak segregation regime were generally consistent with the experimental results for the strong segregation regime. It is possible that those qualitative differences which did appear are due to the differences between the strong and weak segregation regimes, or due to variations of χ with the homopolymer and copolymer degrees of polymerization and volume fraction, as well as

temperature.

In chapter 5, we calculated phase diagrams for ternary *A-b-B/A/B* copolymer/homopolymer blends in the weak segregation regime. The total free energy for those blends was calculated by adding two terms:

- the free energy of mixing expressed by eq 2.87,
- the fourth order expansion of the free energy, using only one wavenumber.

In the first two projects the free energy of mixing was not directly involved in the formalism, but it has to be borne in mind that we had to verify whether the blends formed a single phase, before starting calculations in chapters 3 and 4. The microphase separation transition was approximated as the condition for the homogeneous phase to be unstable relative to the lamellar microphase. As in chapter 4, we restricted, again, our attention to copolymers with similar A and B volume fractions, $f_A \simeq f_B \simeq 0.5$. Even for these systems there was probably more structure to these diagrams than we exhibit due to the existence of other structures throughout the phase diagram. The approach could be thought of as the simplest treatment of these systems which incorporates microphase and macrophase separation, and the results should be considered primarily as guides to behaviour which could occur. The method was a modification of earlier treatments of binary copolymer/homopolymer blends [27, 29].

When modeling the blend we assumed that each phase was either homogeneous or an ordered microphase. We used a model of micelle formation developed earlier to identify and thereby avoid systems in which disordered micellar phases formed [29], and we assumed that at equilibrium only an insignificant fraction of the copolymers migrated to interfaces, (for those cases where macrophase separation occurs).

Most of our results of chapter 5 were presented as phase diagrams for symmetric and asymmetric model systems in which we chose the Kuhn statistical lengths and the

monomer volumes to be equal for all components. We found that even for simple systems a variety of topologies occurs. One feature which appeared in a number of cases was the relative stability of the microphase for blends with overall *A:B* compositions near 50:50. This was particularly noticeable for those cases in which both microphase and macrophase separation occurred. It is worth noticing that the *PS-b-PI/PS/PI* blend presented by Hashimoto et al. [13, 14] maintained a lamellar structure with long range order for copolymer volume fractions as low as 10%, as discussed in section 4.4.

We also examined the phenomenon of induced microphase formation. For a fully symmetric model system, $Z_{cA} = Z_{cB} \equiv Z_c/2$, $Z_{hA} = Z_{hB} \equiv Z_h$, a small amount of homopolymer tended to stabilize a microphase in the ternary blend under the same conditions as in the binary blend, i.e., if $Z_h \geq Z_c/4$. However, the theory predicted two additional effects. First, for some cases homopolymers could induce the microphase in the ternary blend when they did not in either corresponding binary blend, i.e., an *M* region appeared near the center of the phase diagram. Second, homopolymers of relatively low molecular weight, namely that for $Z_h \simeq Z_c/5.3$, tended to first destabilize the microphase, and then to restabilize it. This phenomenon would likely be very hard to observe directly, but it might be possible to explore it using small angle X-ray scattering from the homogeneous phase.

We also considered model systems in which the reference densities and Kuhn lengths were equal, as before, but the degrees of polymerization were not. In one case we used symmetric copolymers mixed with homopolymers which had unequal degrees of polymerization, and in the other we used asymmetric copolymers mixed with homopolymers with equal degrees of polymerization. We ended with a calculation for *PS-b-PI/PS/PI*, using appropriate monomer volumes and Kuhn statistical lengths and a reasonable value for the interaction parameter. Such calculations allowed one to explore some of the competition between the effects of overall *A:B* composition and individual degrees of polymerization

on the compatability and structures of these blends. For example, in the case studied, addition of homopolymer PI had more of a tendency to destabilize the microphase than did addition of homopolymer PS, despite the fact that it had the higher molecular weight.

The theories presented in this thesis can be further tested experimentally. Subsequently, we propose some possible experiments:

1. The domain thickness of copolymer blends can be determined by the position of the first order "peak" in the scattering intensity of SAXS, as in experiments discussed in section 4.4. The dependencies of d on Z_c, $\overline{\phi}_c$ and χ could be determined by this method for both copolymer/homopolymer and copolymer/solvent blends in the weak segregation regime. Similarly, the existence of the calculated thresholds can be explored.

2. By using methods, e.g. Transmission Electron Microscopy, which allow to distinguish between ordered and disordered, as well as single phase and two (three) phase regions, ternary phase diagrams for A-b-$B/A/B$ blends can be constructed and compared with the calculated ones.

3. Localization of homopolymers within the microdomains of copolymer/homopolymer blends, A-b-B/A and A-b-$B/A/B$, can be probably investigated by deuterating the homopolymer chains.

4. As already mentioned, homopolymers of relatively low molecular weight, namely that for $Z_h \simeq Z_c/5.3$, tended to first destabilize the microphase, and then to restabilize it. It might be possible to explore this phenomenon using small angle X-ray scattering from the homogeneous phase.

The work of this thesis can be extended in many different directions. One of the possibilities is development of numerical self-consistent procedure for *A-b-B/A/B* copolymer/homopolymer blends, analogous to that for copolymer/solvent case presented in chapter 3. The calculations would, most likely, require more computer time, but they would not be restricted to the weak segregation regime as they were in chapters 4 and 5. The other possibility to explore would be to generalize the fourth order expansion of the free energy, which has been applied only to the lamellar structure, to cylindrical, spherical (for pure copolymer it was done by Leibler [11]) and, maybe even, "double diamond" cases. One might also consider extending the fourth order expansion from *A-b-B/A/B* blends into more general case of *A-b-B/H/D* blends, which would require at least three independent components in the free energy expansion. In one wavenumber approximation, it can be done in a quite straightforward, but approximate, way by generalizing the work of Hong, Noolandi and Whitmore [27, 29]. To date, there is no theory of copolymer blends which would exceed the mean field approximation. Creation of such a theory, which would include fluctuations in a way analogous to Fredrickson and Helfand's approach [61], would pose, in our opinion, the most challenging possibility.

These are only some examples of the possible future projects. Theory of copolymer/homopolymer blends is a fascinating and expanding field of research which is far from being closed. Finally, again, we express our hope that this dissertation has somehow contributed to this field.

Bibliography

[1] Cowie, J.M.G. *Polymers: Chemistry and Physics of Modern Materials*; Intertext Books: Aylesbury, 1973.

[2] Olvera de la Cruz, M.; Sanchez, I. C. *Macromolecules* **19**, *2501* (1986).

[3] Hashimoto, T.; Ijichi, Y; Fetters, J.L. *J. Chem. Phys.* **89**, *2463* (1988).

[4] Ijichi, Y; Hashimoto, T.; Fetters, J.L. *Macromolecules* **22**, *2817* (1989).

[5] Kavassalis, T.A.; Whitmore M.D (*Macromolecules*, in press).

[6] Thomas, E.L.; Alward, D.B.; Kinning, D.L.; Martin, D.L.; Handlin, D.L.,Jr.; Fetters, L.J. *Macromolecules* **19**, *2197* (1986).

[7] Thomas E.L.; Anderson D.M.; Henkee C.S.; Hoffman D. *Nature* **334**, *598* (1988).

[8] Hasegawa, H.; Tanaka, H.; Yamasaki, K.; Hashimoto, T. *Macromolecules* **20**, *1651* (1987).

[9] Flory, P.J. *Principles of Polymer Chemistry*; Cornell University Press: Ithaca, 1953.

[10] Hashimoto, T.; Tanaka, H.; Iizuka, N. In *Space-Time Organization in Macromolecular Fluids, Springer Series in Chemical Physics*; Tanaka, F., Doi, M. and Ohta, T., Ed.; Springer-Verlag: Berlin, 1989, Vol. 51.

[11] Leibler, L. *Macromolecules* **13**, *1602* (1980).

[12] de Gennes, P.-G. *Scaling Concepts in Polymer Physics*; Cornell University Press: Ithaca, NY, 1979.

[13] Hashimoto, T.; Tanaka, T.; Hasegawa, H. *Macromolecules* **23**, *4378* (1990).

[14] Tanaka, H.; Hasegawa, H.; Hashimoto, T. *Macromolecules* **24**, *240* (1991).

[15] Tanaka, H.; Hashimoto, T. *Macromolecules* (submitted for publication).

[16] Winey, K.I. *Ph. D. Thesis*, University of Massachusetts, 1991.

[17] Kinning, D.J.; Winey, K.I.; Thomas, E.L. *Macromolecules* **21**, *3502* (1988).

[18] Quan, X.; Gancarz, I.; Koberstein, J.T.; Wignall, G.D. *Macromolecules* **20**, *1431* (1987).

[19] Owens, J.N. *Ph. D. Thesis*, Princeton University, 1986.

[20] Owens, J.N.; Gancarz, I.; Koberstein, J.T.; Russel, T.P. *Macromolecules* **22**, *3380* (1989).

[21] Owens, J.N.; Gancarz, I.; Koberstein, J.T.; Russel, T.P. *Macromolecules* **22**, *3388* (1989).

[22] Koberstein, J.T.; Russel, T.P.; Walsh, D.J.; Pottick, L. *Macromolecules* **23**, *877* (1990).

[23] Russel, T.P.; Hjelm, R.P.; Seeger, P.A. *Macromolecules* **23**, *890* (1990).

[24] Anastasiadis, S.H.; Russel, T.P.; Satija S.K.; Majkrzak C.F. *J. Chem. Phys.* **92**, *5677* (1990).

[25] Han, C.D.; Kim, J; Kim, J.K. *Macromolecules* **22**, *383* (1989).

[26] Han, C.D.; Baek, D.M.; Kim, J.K. *Macromolecules* **23**, *561* (1990).

[27] Hong, K.M.; Noolandi, J. *Macromolecules* **16**, *1083* (1983).

[28] Noolandi, J.; Hong, K.M. *Macromolecules* **15**, *482* (1982).

[29] Whitmore, M.D.; Noolandi, J. *Macromolecules* **18**, *2486* (1985).

[30] Whitmore, M.D.; Noolandi, J. *J. Chem. Phys.* **93**, *2946* (1990).

[31] Whitmore, M.D.; Noolandi, J. *Macromolecules* **18**, *657* (1985).

[32] Vilgis, T.A.; Noolandi, J. *Macromolecules* **23**, *2941* (1990).

[33] Noolandi, J.; Hong, K.M. *Ferroelectrics* **30**, *117* (1980).

[34] Shibayama, M.; Hashimoto, T.; Kawai, H.; *Macromolecules* **16**, *16* (1983).

[35] Zin, W.-C.; Roe, R.-J. *Macromolecules* **17**, *183* (1984).

[36] Roe, R.-J.; Zin, W.-C. *Macromolecules* **17**, *189* (1984).

[37] Almdal, K.; Rosedale, J.H.; Bates, F.S.; Wignall, G.D.; Fredrickson, G.H. *Phys. Rev. Lett.* **65**, *1112* (1990).

[38] Cohen, R.E.; Ramos, A.R. *Macromolecules* **12**, *131* (1979).

[39] Gaillard, P.; Ossenbach-Sauter, M.; Riess, G.; *Macromol. Chem. Rapid Commun.* **1**, *171* (1980).

[40] Ohta, T.; Kawasaki, K. *Macromolecules* **19**, *2621* (1986).

[41] Edwards, S.F. *Proc. Phys. Soc. London* **85**, *613* (1965).

[42] Edwards, S.F. *Proc. Phys. Soc. London* **88**, *265* (1966).

[43] Dolan, A.K.; Edwards, S.F. *Proc. R. Soc. London. A.* **337** *509* (1973).

[44] Dolan, A.K.; Edwards, S.F. *Proc. R. Soc. London. A.* **343** *427* (1974).

[45] Helfand, E. In *Recent Advances in Polymer Blends, Grafts and Blocks*; Sperling, L.H., Ed.; Plenum: New York, 1974.

[46] Helfand, E. *Macromolecules* **8**, *552* (1975).

[47] Helfand, E. *J. Chem. Phys.* **62**, *999* (1975).

[48] Helfand, E.; Wassermann, Z.R. *Macromolecules* **9**, *879* (1976).

[49] Helfand, E.; Wassermann, Z.R. *Macromolecules* **13**, *994* (1980).

[50] Helfand, E.; Wassermann, Z.R. *Macromolecules* **11**, *960* (1978).

[51] Helfand, E.; Wassermann, Z.R. In *Developments in Block Copolymers;* Goodman, I., Ed.; Elsevier: New York, 1982; Vol. 1.

[52] Hong, K.M.; Noolandi, J. *Macromolecules* **14**, *727* (1981).

[53] Meier, D.J. *J. Polym. Sci.* **26** *81* (1969).

[54] Meier, D.J.; In *Thermoplastic Elatomers: A Comprehensive Review*; Legge, R.R., Holden, G. and Schroeder, H.E, Ed.; Hanser, Münich, 1987.

[55] Freed, K.F. *Renormalization Group Theory of Macromolecules*; Wiley-Interscience: New York, 1987.

[56] Oono, Y.; Freed, K.J. *J. Chem. Phys.* **75**, *993* (1981).

[57] Oono, Y.; Freed, K.J. *J. Phys. A* **15**, *1931* (1982).

[58] Kholodenko, A.L.; Freed, K.J. *J. Chem. Phys.* **78**, *7390* (1983).

[59] Landau, L.D. *Phys. Z. Sowjet.* **11**, *26,545* (1937).

[60] Amit, D.; *Field Theory, the Group Renormalization, and Critical Phenomena*; World Scientific: Singapore, 1987.

[61] Fredrickson, G.H.; Helfand, E. *J. Chem. Phys.* **87**, *697* (1987).

[62] Brazovskii, S.A. Zh. Eksp. Teor. Fiz. **68** 175 (1975).

[63] Whitmore, M.D; Vavasour, J. *Macromolecules* (submitted for publication)

[64] Olvera de la Cruz, M. *Phys. Rev. Lett.* **67**, *85* (1991).

[65] Banaszak M.; Whitmore, M.D *Macromolecules* (submitted for publication).

[66] Banaszak M.; Whitmore, M.D *Macromolecules* (accepted for publication).

[67] Kawasaki, K.; Ohta, T. Kohrogui, M. *Macromolecules* **21**, *2972* (1988).

[68] Kawasaki, K.; Kawakatsu, T. *Macromolecules* **23**, *4006* (1990).

[69] Shull, K.R.; Kramer, E.J. *Macromolecules* **23**, *4769* (1990).

[70] Shull, K.R.; Kramer, E.J.; Hadziioannou, G; Tang, W. *Macromolecules* **23**, *4779* (1990).

[71] Leibler, L.; Benoit H. *Polymer* **22**, *195* (1981).

[72] Bates, F.S.; Rosedale, J.H.; Fredrickson, G.H.; Glinka C.J. *Phys. Rev. Lett.* **65**, *2229* (1988).

[73] Whitmore, M.D.; Noolandi, J. *Macromolecules* **21**, *1482* (1988).

[74] Hong, K.M.; Noolandi, J. *Macromolecules* **14**, *736* (1981).

[75] Press, W.H.; Flannery, B.P.; Teukolsky, S.A.; Vetterling, W.T. *Numerical Recipes*; Cambridge University Press: Cambridge, 1989.

[76] Kruse, R.L. In *Copolymers, Polyblends and Composites*; Platzer, N.A.J., Ed.; American Chemical Society: Washington, D.C., 1975, p. 141.

[77] Cahn, J.W.; Hilliard, J.E. *J. Chem. Phys.* **28**, *258* (1957).

[78] Helfand, E.; Tagami, Y. *J. Chem. Phys.* **56**, *3592* (1972).

[79] Hasegawa, H.; Tanaka, H.; Yamasaki, K.; Hashimoto, T. *Macromolecules* **20**, *1651* (1987).

[80] Shibayama, M.; Hashimoto, T. *Macromolecules* **19**, *740* (1986).

[81] Tanaka, H.; Sakurai, S.; Hashimoto, T.; Whitmore, M.D. *Polymer* (in press).

[82] Mori, K.; Tanaka, H.; Hasegawa, H.; Hashimoto, T. *Polymer* **30**, *1389* (1989).

[83] Brandrup, J.; Immergut, E.H., Eds. *Polymer Handbook,* 2nd ed.; Wiley-Interscience: New York, 1975.

[84] Tanaka, H.; Hashimoto, T. *Macromolecules* (submitted for publication).

[85] Knobler, C.M.; Scott, R.L. In *Phase Transitions and Critical Phenomena*; Domb, C. and Lebowitz, J.L., Ed.; Academic Press: London, 1984, Vol. 9.

[86] Whitmore, M.D *private communication*

[87] Broseta, D.; Fredrickson, G.H. *J. Chem. Phys.* **93**, *2927* (1990).

[88] Furman, S.; Dattagupta, S.; Griffiths, R.B. *Phys. Rev. B.* **15**, *441* (1977).

[89] Hsu, C.C.; Prausnitz, J.M. *Macromolecules* **7**, *320* (1974).

[90] Tanaka, H.; Hashimoto, T. *Polymer* **29**, *212* (1988).

[91] Inoue, T.; Soen, T.; Hashimoto, T.; Kawai, H. *Macromolecules* **3**, *87* (1970).

[92] Hashimoto, H.; Fujimura, M.; Hashimoto, T.; Kawai, H. *Macromolecules* **14**, *844* (1981).

[93] Koizumi, S.; Hasegawa, H.; Hashimoto, T. *Macromolecules* **23**, *2955* (1990).

[94] Dudowicz, J.; Freed, K.F. *Macromolecules* **23**, *1519* (1990).

Appendix A

Calculation of the Expansion Coefficients

The modified diffusion equation (2.79) is

$$[-\frac{\hat{b}_p^2}{6}\nabla^2 + \tilde{\omega}_p(\boldsymbol{r})]Q_p(\boldsymbol{r},\tau|\boldsymbol{r}') = -\frac{1}{r_p}\frac{\partial}{\partial\tau}Q_p(\boldsymbol{r},\tau|\boldsymbol{r}'), \tag{A.1}$$

with

$$Q_p(\boldsymbol{r},0|\boldsymbol{r}') = \delta(\boldsymbol{r}-\boldsymbol{r}'). \tag{A.2}$$

Since we expect the periodic structures to occur it is more convenient to work in Fourier space. Let us define

$$Q_p(\boldsymbol{k},\tau|\boldsymbol{k}') = \int d\boldsymbol{r}d\boldsymbol{r}'Q_p(\boldsymbol{r},\tau|\boldsymbol{r}')\exp[-i(\boldsymbol{k}\boldsymbol{r}-\boldsymbol{k}'\boldsymbol{r}')], \tag{A.3}$$

and

$$\tilde{\omega}_p(\boldsymbol{k}) = \int d\boldsymbol{r}\hat{\omega}_p(\boldsymbol{r})\exp[-i\boldsymbol{k}\boldsymbol{r}], \tag{A.4}$$

with $p = hA$, hB, cA and cB.

It is easy to show that the functionals Q_c, Q_{hA} and Q_{hB}, defined by (2.13) and (2.14), can be written as

$$Q_{hA} = Q_{hA}(\boldsymbol{0},1|\boldsymbol{0}), \tag{A.5}$$

$$Q_{hB} = Q_{hB}(\boldsymbol{0},1|\boldsymbol{0}), \tag{A.6}$$

$$Q_c = \int \frac{d\boldsymbol{k}}{(2\pi)^3}Q_{cA}(\boldsymbol{0},1|\boldsymbol{k})Q_{cB}(\boldsymbol{k},1|\boldsymbol{0}). \tag{A.7}$$

It can be shown [27] that, by solving the diffusion equation perturbatively, an expansion for $Q_p(\boldsymbol{k},\tau|\boldsymbol{k}')$ in powers of $\tilde{\omega}_p(\boldsymbol{k})$ can be obtained in the following form:

$$\begin{aligned} Q_p(\boldsymbol{k},\tau|\boldsymbol{k}') &= \sum_{n=0}^{\infty}\frac{(-\tau_p)^n}{n!}\int\frac{d\boldsymbol{k}_1}{(2\pi)^3}\cdots\frac{d\boldsymbol{k}_{n+1}}{(2\pi)^3}\times \\ &\quad (2\pi)^3\delta(\boldsymbol{k}+\sum_{i=1}^{n+1}\boldsymbol{k}_i)(2\pi)^3\delta(\boldsymbol{k}_0+\boldsymbol{k}_{n+1})\times \\ &\quad G_p^{(n)}(\sum_{i=1}^{n+1}\boldsymbol{k}_i,\sum_{i=2}^{n+1}\boldsymbol{k}_i,\cdots,\boldsymbol{k}_{n+1};\tau)\tilde{\omega}_p(-\boldsymbol{k}_1)\cdots\tilde{\omega}_p(-\boldsymbol{k}_n), \end{aligned} \tag{A.8}$$

where

$$G_p^{(n)}(\boldsymbol{q}_1,\cdots,\boldsymbol{q}_{n+1};\tau) = n!\sum_{i=1}^{n+1}{}'\frac{\exp[-x_i\tau]}{\prod_{j=1}^{n+1}(x_j-x_i)}, \tag{A.9}$$

with $x_i = r_p\hat{b}_p^2q_i^2/6$ and the prime in front of the product sign indicates that the $(j=i)$ factor is to be omitted. This leads to the following expression for Q_κ/V:

$$\begin{aligned} \frac{Q_\kappa}{V} &= 1+\frac{(-\tau_\kappa)^2}{2!V}g^\kappa_{ij}\tilde{\omega}_i\tilde{\omega}_j + \\ &\quad \frac{(-\tau_\kappa)^3}{3!V}g^\kappa_{ijk}\tilde{\omega}_i\tilde{\omega}_j\tilde{\omega}_k + \\ &\quad \frac{(-\tau_\kappa)^4}{4!V}g^\kappa_{ijkl}\tilde{\omega}_i\tilde{\omega}_j\tilde{\omega}_k\tilde{\omega}_l + \\ &\quad \frac{(-\tau_\kappa)^5}{5!V}g^\kappa_{ijklm}\tilde{\omega}_i\tilde{\omega}_j\tilde{\omega}_k\tilde{\omega}_l\tilde{\omega}_m+\cdots, \end{aligned} \tag{A.10}$$

where $i\equiv(i,\boldsymbol{k}_i)$, and summation over subscripts and integration over wavevectors are implied by repeated indices. Functions $g^\kappa_{ijk\cdots l}$ have the following form:

$$g^{(n)}_{\kappa,ijk\cdots l} = (2\pi)^3\delta(\boldsymbol{k}_i+\boldsymbol{k}_j+\boldsymbol{k}_k+\cdots+\boldsymbol{k}_l)g^\kappa_{ijk\cdots l}(\boldsymbol{k}_i,\boldsymbol{k}_j,\boldsymbol{k}_k,\cdots,\boldsymbol{k}_l),$$

with $\kappa = hA, hB$ or c, and $i = hA, hB, cA$, and cB,

$g^{(n)}_{hA,ijk\cdots l}$ may be different from zero if $i=j=k=\cdots=l=hA$,

$g^{(n)}_{hB,ijk\cdots l}$ may be different from zero if $i=j=k=\cdots=l=hB$,

$g^{(n)}_{c,ijk\cdots l}$ may be different from zero if $i = cA$ or $i = cB$,

$j = cA$ or $j = cB$,

$k = cA$ or $k = cB$,

$\cdots$

$j = cA$ or $j = cB$.

The explicit expressions for $g^{\kappa}_{i\cdots j}$(n subscripts) are

$$g^{hA}_{i\cdots j} = (2\pi)^3\delta(\boldsymbol{k}_i + \cdots + \boldsymbol{k}_j)g^{(n)}_{hA}(\boldsymbol{k}_i, \cdots, \boldsymbol{k}_j), \tag{A.11}$$

$$g^{hB}_{i\cdots j} = (2\pi)^3\delta(\boldsymbol{k}_i + \cdots + \boldsymbol{k}_j)g^{(n)}_{hB}(\boldsymbol{k}_i, \cdots, \boldsymbol{k}_j), \tag{A.12}$$

$$\begin{aligned} g^{c}_{i\cdots lp\cdots j} &= (2\pi)^3\delta(\boldsymbol{k}_i + \cdots + \boldsymbol{k}_j){f_A}^m {f_B}^{n-m} \\ & g^{(m)}_{cA}(\boldsymbol{k}_i + \cdots + \boldsymbol{k}_l)g^{(n-m)}_{cB}(\boldsymbol{k}_p + \cdots + \boldsymbol{k}_j), \end{aligned} \tag{A.13}$$

where $g^{(n)}_p$ is defined as the full symmetrization of $\hat{G}^{(n)}_p$ over its arguments

$$g^{(n)}_p(\boldsymbol{k}_1, \boldsymbol{k}_2, \cdots, \boldsymbol{k}_n) = \frac{1}{n!}\sum_{\sigma\in\,\mathrm{S}_n}\hat{G}^{(n)}_p(\boldsymbol{k}_{\sigma(1)}, \boldsymbol{k}_{\sigma(2)}, \cdots, \boldsymbol{k}_{\sigma(n)}), \tag{A.14}$$

with S_n denoting the permutation group of n objects. The function $\hat{G}^{(n)}_p(\boldsymbol{k}_1, \boldsymbol{k}_2, \cdots, \boldsymbol{k}_n)$ is defined as

$$\hat{G}^{(n)}_p(\boldsymbol{k}_1, \boldsymbol{k}_2, \cdots, \boldsymbol{k}_n) = G^{(n)}_p(\boldsymbol{0}, \boldsymbol{k}_1, \boldsymbol{k}_1 + \boldsymbol{k}_2, \cdots, \sum_{i=1}^{n}\boldsymbol{k}_i; 1). \tag{A.15}$$

In particular we have

$$g^{(1)}_p(\boldsymbol{k}) = \frac{1 - \exp[-x]}{x}, \tag{A.16}$$

and

$$g^{(2)}_p(\boldsymbol{k}, -\boldsymbol{k}) = \frac{2(x - 1 + \exp[-x])}{x^2}, \tag{A.17}$$

with $x = Z_p b^2_p k^2/6$.

We transformed eq. 2.92, as described in section 2.3, to obtain a new expression for Δf

$$\begin{aligned}\Delta f \cong\ & \frac{1}{V}\int' \frac{d\boldsymbol{k}}{(2\pi)^3}\chi\phi_\alpha(\boldsymbol{k})\phi_\beta(\boldsymbol{k}) - \\ & \frac{1}{V}\int' \frac{d\boldsymbol{k}}{(2\pi)^3}[\phi_\alpha(\boldsymbol{k})\omega_\alpha(-\boldsymbol{k}) + \phi_\beta(\boldsymbol{k})\omega_\beta(-\boldsymbol{k})] - \\ & \frac{1}{2V}\mathcal{G}_{ij}\tilde{\omega}_i\tilde{\omega}_j + \\ & \frac{1}{6V}\mathcal{G}_{ijk}\tilde{\omega}_i\tilde{\omega}_j\tilde{\omega}_k - \\ & \frac{1}{24V}\mathcal{G}_{ijkl}\tilde{\omega}_i\tilde{\omega}_j\tilde{\omega}_k\tilde{\omega}_l, \end{aligned} \tag{A.18}$$

where we defined and calculated $\mathcal{G}$'s as

$$\mathcal{G}_{ij} = r_{hP}\overline{\phi}_{hP}g_{ij}^{hP} + r_c\overline{\phi}_c g_{ij}^c, \tag{A.19}$$

$$\mathcal{G}_{ijk} = r_{hP}^2\overline{\phi}_{hP}g_{ijk}^{hP} + r_c\overline{\phi}_c^2 g_{ijk}^c, \tag{A.20}$$

$$\mathcal{G}_{ijkl} = r_{hP}^3\overline{\phi}_{hA}(g_{ijk}^{hP} - \frac{3}{V}g_{ij}^{hP}g_{kl}^{hP}\delta_{ik}) + r_c\overline{\phi}_c^3(g_{ijkl}^c - \frac{3}{V}g_{ij}^c g_{kl}^c), \tag{A.21}$$

with i, j, k, and $l = \alpha$ or β, and HP denotes the homopolymer indicated by i, e.g.,

$$g_{ij}^{hP} = \delta_{i,\alpha}g_{ij}^{hA} + \delta_{i,\beta}g_{ij}^{hB}, \tag{A.22}$$

$$r_{hP}\overline{\phi}_{hP}g_{ij}^{hP} = \delta_{i,\alpha}r_{hA}\overline{\phi}_{hA}g_{ij}^{hA} + \delta_{i,\beta}r_{hB}\overline{\phi}_{hB}g_{ij}^{hB}, \tag{A.23}$$

etc.. The $\mathcal{G}$'s are also used in eq. 2.101 and 2.102.

The coefficients of eq. 2.103 and 2.104, which arise from inverting eq. 2.101 and 2.102, involve the inverses of the $\mathcal{G}$'s:

$$\Gamma_{ij} = -[\mathcal{G}]_{ij}^{-1} \tag{A.24}$$

$$\Gamma_{ijk} = \frac{1}{2}[\mathcal{G}]_{is}^{-1}[\mathcal{G}]_{jp}^{-1}[\mathcal{G}]_{kq}^{-1}\mathcal{G}_{spq} \tag{A.25}$$

$$\begin{aligned}\Gamma_{ijkl} = & \frac{1}{2}[\mathcal{G}]_{ip}^{-1}[\mathcal{G}]_{jq}^{-1}\mathcal{G}_{pqs}[\mathcal{G}]_{sr}^{-1}\mathcal{G}_{rvt}[\mathcal{G}]_{vk}^{-1}[\mathcal{G}]_{tl}^{-1} - \\ & \frac{1}{6}[\mathcal{G}]_{ip}^{-1}[\mathcal{G}]_{jv}^{-1}[\mathcal{G}]_{ks}^{-1}[\mathcal{G}]_{lt}^{-1}\mathcal{G}_{pvst}. \end{aligned} \tag{A.26}$$

For the final expression for the free energy, eq. 2.105, it is convenient to introduce first the related quantities $\hat{f}^{(n)}_{ij\ldots}$. Listing the four second order ones explicitly and the rest more generally:

$$\hat{f}^{(2)}_{\alpha\alpha}(\boldsymbol{k}_1,-\boldsymbol{k}_1) = \frac{1}{2}[\mathcal{G}]^{-1}_{\alpha\alpha}(\boldsymbol{k}_1,-\boldsymbol{k}_1), \tag{A.27}$$

$$\hat{f}^{(2)}_{\beta\beta}(\boldsymbol{k}_1,-\boldsymbol{k}_1) = \frac{1}{2}[\mathcal{G}]^{-1}_{\beta\beta}(\boldsymbol{k}_1,-\boldsymbol{k}_1), \tag{A.28}$$

$$\hat{f}^{(2)}_{\alpha\beta}(\boldsymbol{k}_1,-\boldsymbol{k}_1) = \frac{1}{2}\left(\chi + [\mathcal{G}]^{-1}_{\alpha\beta}(\boldsymbol{k}_1,-\boldsymbol{k}_1)\right), \tag{A.29}$$

$$\hat{f}^{(2)}_{\beta\alpha}(\boldsymbol{k}_1,-\boldsymbol{k}_1) = \hat{f}^{(2)}_{\alpha\beta}(\boldsymbol{k}_1,-\boldsymbol{k}_1), \tag{A.30}$$

$$\begin{aligned}\hat{f}^{(3)}_{ijk}(\boldsymbol{k}_1,\boldsymbol{k}_2,\boldsymbol{k}_3) = &-\frac{1}{6}\sum_{spq}\times[\mathcal{G}]^{-1}_{is}(\boldsymbol{k}_1,-\boldsymbol{k}_1)[\mathcal{G}]^{-1}_{jp}(\boldsymbol{k}_2,-\boldsymbol{k}_2)\\ &[\mathcal{G}]^{-1}_{kq}(\boldsymbol{k}_3,-\boldsymbol{k}_3)\mathcal{G}_{spq}(\boldsymbol{k}_1,\boldsymbol{k}_2,\boldsymbol{k}_3),\end{aligned} \tag{A.31}$$

$$\begin{aligned}\hat{f}^{(4)}_{ijkl}(\boldsymbol{k}_1,\boldsymbol{k}_2,\boldsymbol{k}_3,\boldsymbol{k}_4) = &-\frac{1}{24}\sum_{spqt}[\mathcal{G}]^{-1}_{is}(\boldsymbol{k}_1,-\boldsymbol{k}_1)[\mathcal{G}]^{-1}_{jp}(\boldsymbol{k}_2,-\boldsymbol{k}_2)\times\\ &[\mathcal{G}]^{-1}_{kq}(\boldsymbol{k}_3,-\boldsymbol{k}_3)[\mathcal{G}]^{-1}_{lt}(\boldsymbol{k}_4,-\boldsymbol{k}_4)\mathcal{G}_{spqt}(\boldsymbol{k}_1,\boldsymbol{k}_2,\boldsymbol{k}_3,\boldsymbol{k}_4)+\\ &\frac{1}{8}\sum_{pqsrvt}[\mathcal{G}]^{-1}_{ip}(\boldsymbol{k}_1,-\boldsymbol{k}_1)\times\\ &[\mathcal{G}]^{-1}_{jq}(\boldsymbol{k}_2,-\boldsymbol{k}_2)\mathcal{G}_{pqs}(\boldsymbol{k}_1,\boldsymbol{k}_2,-\boldsymbol{k}_1-\boldsymbol{k}_2)\times\\ &[\mathcal{G}]^{-1}_{sr}(\boldsymbol{k}_1+\boldsymbol{k}_2,-\boldsymbol{k}_1-\boldsymbol{k}_2)\times\\ &\mathcal{G}_{rvt}(\boldsymbol{k}_1+\boldsymbol{k}_2,\boldsymbol{k}_3,\boldsymbol{k}_4)[\mathcal{G}]^{-1}_{vk}(\boldsymbol{k}_3,-\boldsymbol{k}_3)\times\\ &[\mathcal{G}]^{-1}_{tl}(\boldsymbol{k}_4,-\boldsymbol{k}_4).\end{aligned} \tag{A.32}$$

Now let us define

$$\Delta_i = \begin{cases} 1 & \text{if } i=\alpha \\ -1 & \text{if } i=\beta \end{cases} \tag{A.33}$$

then

$$f^{(2)}(\boldsymbol{k}_1,-\boldsymbol{k}_1) = \sum_{ij}\hat{f}^{(2)}_{ij}(\boldsymbol{k}_1,-\boldsymbol{k}_1)\Delta_i\Delta_j, \tag{A.34}$$

$$f^{(3)}(\boldsymbol{k}_1,\boldsymbol{k}_2,\boldsymbol{k}_3) = \sum_{ijk}\hat{f}^{(3)}_{ijk}(\boldsymbol{k}_1,\boldsymbol{k}_2,\boldsymbol{k}_3)\Delta_i\Delta_j\Delta_k, \tag{A.35}$$

$$f^{(4)}(\boldsymbol{k}_1, \boldsymbol{k}_2, \boldsymbol{k}_3, \boldsymbol{k}_4) = \sum_{ijkl} \hat{f}^{(4)}_{ijkl}(\boldsymbol{k}_1, \boldsymbol{k}_2, \boldsymbol{k}_3, \boldsymbol{k}_4)\Delta_i\Delta_j\Delta_k\Delta_l. \quad \text{(A.36)}$$

Appendix B

Model Density Profiles

In order to evaluate Δf, and subsequently the four density profiles $\phi_p(x)$, we need a model for $\phi_a(x)$, in particular the function $u(x;d,p,q)$ appearing in eq. 4.4. We express u as the convolution of two functions:

$$u(x) = C\int_{-\infty}^{+\infty} dy v(x-y)w(y), \tag{B.1}$$

The first function v, is a periodic step function, chosen to be symmetric about the origin:

$$v(x) = \begin{cases} 1 & \text{for} \quad |x| \leq p/2, \\ p/(d-p) & \text{for} \quad p/2 < |x| \leq d, \end{cases} \tag{B.2}$$

The period d corresponds to the lamellar thickness. The second function w, is a symmetric, bell shaped smoothing function,

$$w(x) = \frac{1}{2q\cosh^2(x/q)}. \tag{B.3}$$

This function has maximum value $w(0) = 1/2q$ and width proportional to q, and the area under it is unity. Finally, the constant "C" in eq. B.1 is chosen so that $u(0) = 1$.

The resultant function, $u(x)$, is periodic with period d. It can be expressed conveniently as a Fourier sum

$$u(x) = \sum_{n=1}^{\infty} u_n \cos(\frac{2\pi n}{d}x), \tag{B.4}$$

with coefficients

$$u_n = 2\pi C \frac{q}{(d-p)} \frac{\sin(n\pi p/d)}{\sinh(n\pi^2 q/d)}. \tag{B.5}$$

There are two convenient limits to this function. The first is $q/d >> 1$. In this case, the $n = 1$ term dominates, and $u(x)$ reduces to the single term

$$u(x) = \cos(\frac{2\pi n}{d}x), \tag{B.6}$$

with "C" chosen appropriately. This is the one wave number form expected for the weak segregation limit. In this case the two subdomain thicknesses are $d_A = d_B = d/2$. The other limit is $q/p << 1$ and $q/(p-q) << 1$, i.e. the smoothing function is much narrower than either plateau in $v(x)$. Its effect is to smooth each step-like interface to a hyperbolic tangent shape. For example, a step function of unit height centered at the origin, $v(x) = \theta(x)$, is smoothed to:

$$u(x) = \frac{1}{2}[1 + \tanh(\frac{x}{q})]. \tag{B.7}$$

In this limit the density profile would be flat within each subdomain, and be given by a hyperbolic tangent in each interphase. The subdomain thicknesses would be $d_A = p$ and $d_B = d - p$.

Once we have calculated $\phi_\alpha(x)$ and $\phi_\beta(x)$, we characterize the result by domain thickness d, the two subdomain thicknesses d_A and d_B, and the interfacial thickness. We identify the centre of the interface as the point of inflection in $\phi_\alpha(x)$, which divides d into d_A and d_B. The width of the interface, a_I, is taken the distance between the two points where the line is tangent to $\phi_\alpha(x)$ at the inflection point intersects with the values of $\phi_\alpha(x)$ at the centres of the adjoining subdomains.

In the numerical work of the chapter 4, the values of d, p and q are not predetermined, but instead in each case are calculated through the minimization of Δf. Because the systems are in the weak segregation regime, only a few terms make significant contributions to the summations. In all cases, keeping 12 terms caused the truncation error to be on the order of 10^{-14}.

Appendix C

Calculation of the Homopolymer Density Profiles

Subsequently we show how to calculate the potentials $\omega_\alpha(\boldsymbol{k})$ and $\omega_\beta(\boldsymbol{k})$ from the profile $\phi_\alpha(\boldsymbol{k})$, and next the profiles $\phi_{hA}(\boldsymbol{k})$, $\phi_{hB}(\boldsymbol{k})$, $\phi_{cA}(\boldsymbol{k})$ and $\phi_{cB}(\boldsymbol{k})$.

Equations (2.103,2.104) can be written to the second order, as

$$\omega_\alpha(\boldsymbol{k}) \cong \Gamma^2_{\alpha i}\phi_i + \Gamma^3_{\alpha ij}\phi_i\phi_j, \tag{C.1}$$

$$\omega_\beta(\boldsymbol{k}) \cong \Gamma^2_{\beta i}\phi_i + \Gamma^3_{\beta ij}\phi_i\phi_j, \tag{C.2}$$

where $i, j, k = \alpha$ or β, and $\phi_\beta = -\phi_\alpha$,

$$\Gamma_{ij} = -[\mathcal{G}]^{-1}_{ij} \tag{C.3}$$

$$\Gamma_{ijk} = \frac{1}{2}[\mathcal{G}]^{-1}_{is}[\mathcal{G}]^{-1}_{jp}[\mathcal{G}]^{-1}_{kq}\mathcal{G}_{spq}. \tag{C.4}$$

Let us define

$$\omega_\alpha{}^{(1)}(\boldsymbol{k}) = \Gamma^2_{\alpha i}\phi_i, \tag{C.5}$$

$$\omega_\alpha{}^{(2)}(\boldsymbol{k}) = \Gamma^3_{\alpha ij}\phi_i\phi_j, \tag{C.6}$$

$$\omega_\beta{}^{(1)}(\boldsymbol{k}) = \Gamma^2_{\beta i}\phi_i, \tag{C.7}$$

$$\omega_\beta{}^{(2)}(\boldsymbol{k}) = \Gamma^3_{\beta ij}\phi_i\phi_j. \tag{C.8}$$

Thus

$$\omega_\alpha(\boldsymbol{k}) \cong \omega_\alpha{}^{(1)}(\boldsymbol{k}) + \omega_\alpha{}^{(2)}(\boldsymbol{k}), \tag{C.9}$$

$$\omega_\beta(\boldsymbol{k}) \cong \omega_\beta{}^{(1)}(\boldsymbol{k}) + \omega_\beta{}^{(2)}(\boldsymbol{k}). \tag{C.10}$$

Equation (2.98,2.99,2.100) can be expressed, to the second order, as

$$\begin{aligned}
\phi_{hA}(\boldsymbol{k}) \cong\ & -r_{hA}\overline{\phi}_{hA}g_{hA}^{(2)}(\boldsymbol{k})\omega_{\alpha}(\boldsymbol{k}) + \\
& \frac{1}{2}r_{hA}^{2}\overline{\phi}_{hA}\int\frac{(2\pi)^{3}}{V}d\boldsymbol{q}g_{hA}^{(3)}(\boldsymbol{k},\boldsymbol{q},-\boldsymbol{k}-\boldsymbol{q})\omega_{\alpha}{}^{(1)}(\boldsymbol{q})\omega_{\alpha}{}^{(1)}(-\boldsymbol{k}-\boldsymbol{q}) \\
& \text{for } \boldsymbol{k}\neq 0, \qquad \text{(C.11)} \\
\phi_{cA}(\boldsymbol{k}) \cong\ & -r_{c}\overline{\phi}_{c}f_{A}^{2}g_{cA}^{(2)}(\boldsymbol{k})\omega_{\alpha}(\boldsymbol{k}) - \\
& r_{c}\overline{\phi}_{c}f_{A}f_{B}g_{cA}^{(1)}(\boldsymbol{k})g_{cB}^{(1)}(\boldsymbol{k})\omega_{\beta}(\boldsymbol{k}) + \\
& \frac{1}{2}r_{c}^{2}\overline{\phi}_{c}\int\frac{(2\pi)^{3}}{V}d\boldsymbol{q}f_{A}^{3}g_{cA}^{(3)}(\boldsymbol{k},\boldsymbol{q},-\boldsymbol{k}-\boldsymbol{q})\omega_{\alpha}{}^{(1)}(\boldsymbol{q}),\omega_{\alpha}{}^{(1)}(-\boldsymbol{k}-\boldsymbol{q}) + \\
& \frac{1}{2}r_{c}^{2}\overline{\phi}_{c}\int\frac{(2\pi)^{3}}{V}d\boldsymbol{q}f_{A}^{2}f_{B}g_{cA}^{(2)}(\boldsymbol{k},\boldsymbol{q})g_{cB}^{(1)}(-\boldsymbol{k}-\boldsymbol{q})\omega_{\alpha}{}^{(1)}(\boldsymbol{q})\omega_{\beta}{}^{(1)}(-\boldsymbol{k}-\boldsymbol{q}) + \\
& \frac{1}{2}r_{c}^{2}\overline{\phi}_{c}\int\frac{(2\pi)^{3}}{V}d\boldsymbol{q}f_{A}^{2}f_{B}g_{cA}^{(2)}(\boldsymbol{k},-\boldsymbol{k}-\boldsymbol{q})g_{cB}^{(1)}(\boldsymbol{q})\omega_{\beta}{}^{(1)}(\boldsymbol{q})\omega_{\alpha}{}^{(1)}(-\boldsymbol{k}-\boldsymbol{q}) + \\
& \frac{1}{2}r_{c}^{2}\overline{\phi}_{c}\int\frac{(2\pi)^{3}}{V}d\boldsymbol{q}f_{A}f_{B}^{2}g_{cA}^{(1)}(\boldsymbol{k})g_{cB}^{(2)}(\boldsymbol{q},-\boldsymbol{k}-\boldsymbol{q})\omega_{\beta}{}^{(1)}(\boldsymbol{q})\omega_{\beta}{}^{(1)}(-\boldsymbol{k}-\boldsymbol{q}), \\
& \text{for } \boldsymbol{k}\neq 0, \qquad \text{(C.12)} \\
\phi_{hB}(\boldsymbol{k}) \cong\ & -r_{hB}\overline{\phi}_{hB}g_{hB}^{(2)}(\boldsymbol{k})\omega_{\beta}(\boldsymbol{k}) + \\
& \frac{1}{2}r_{hB}^{2}\overline{\phi}_{hB}\int\frac{(2\pi)^{3}}{V}d\boldsymbol{q}g_{hB}^{(3)}(\boldsymbol{k},\boldsymbol{q},-\boldsymbol{k}-\boldsymbol{q})\omega_{\beta}{}^{(1)}(\boldsymbol{q})\omega_{\beta}(-\boldsymbol{k}-\boldsymbol{q}), \\
& \text{for } \boldsymbol{k}\neq 0, \qquad \text{(C.13)} \\
\phi_{cB}(\boldsymbol{k}) \cong\ & -r_{c}\overline{\phi}_{c}f_{B}^{2}g_{cB}^{(2)}(\boldsymbol{k})\omega_{\beta}(\boldsymbol{k}) - \\
& r_{c}\overline{\phi}_{c}f_{B}f_{A}g_{cB}^{(1)}(\boldsymbol{k})g_{cA}^{(1)}(\boldsymbol{k})\omega_{\alpha}(\boldsymbol{k}) + \\
& \frac{1}{2}r_{c}^{2}\overline{\phi}_{c}\int\frac{(2\pi)^{3}}{V}d\boldsymbol{q}f_{B}^{3}g_{cB}^{(3)}(\boldsymbol{k},\boldsymbol{q},-\boldsymbol{k}-\boldsymbol{q})\omega_{\beta}{}^{(1)}(\boldsymbol{q})\omega_{\beta}{}^{(1)}(-\boldsymbol{k}-\boldsymbol{q}) + \\
& \frac{1}{2}r_{c}^{2}\overline{\phi}_{c}\int\frac{(2\pi)^{3}}{V}d\boldsymbol{q}f_{B}^{2}f_{A}g_{cB}^{(2)}(\boldsymbol{k},\boldsymbol{q})g_{cA}^{(1)}(-\boldsymbol{k}-\boldsymbol{q})\omega_{\beta}{}^{(1)}(\boldsymbol{q})\omega_{\alpha}{}^{(1)}(-\boldsymbol{k}-\boldsymbol{q}) + \\
& \frac{1}{2}r_{c}^{2}\overline{\phi}_{c}\int\frac{(2\pi)^{3}}{V}d\boldsymbol{q}f_{B}^{2}f_{A}g_{cB}^{(2)}(\boldsymbol{k},-\boldsymbol{k}-\boldsymbol{q})g_{cA}^{(1)}(\boldsymbol{q})\omega_{\alpha}{}^{(1)}(\boldsymbol{q})\omega_{\beta}{}^{(1)}(-\boldsymbol{k}-\boldsymbol{q}) + \\
& \frac{1}{2}r_{c}^{2}\overline{\phi}_{c}\int\frac{(2\pi)^{3}}{V}d\boldsymbol{q}f_{B}f_{A}^{2}g_{cB}^{(1)}(\boldsymbol{k})g_{cA}^{(2)}(\boldsymbol{q},-\boldsymbol{k}-\boldsymbol{q})\omega_{\alpha}{}^{(1)}(\boldsymbol{q})\omega_{\alpha}{}^{(1)}(-\boldsymbol{k}-\boldsymbol{q}), \\
& \text{for } \boldsymbol{k}\neq 0. \qquad \text{(C.14)}
\end{aligned}$$

For $\boldsymbol{k}=0$ eq. (2.83) holds.